Title
Characterizing the Mitochondrial Redox Relay System

Author
Zhang, Danyun

Publication Date
2021

Peer reviewed|Thesis/dissertation

UNIVERSITY OF CALIFORNIA

Los Angeles

Characterizing the Mitochondrial Redox Relay System

A dissertation submitted in partial satisfaction of the

requirements for the degree Doctor of Philosophy

in Biochemistry, Molecular and Structural Biology

by

Danyun Zhang

2021

ABSTRACT OF THE DISSERTATION

Characterizing the Mitochondrial Redox Relay System

by

Danyun Zhang

Doctor of Philosophy in Biochemistry, Molecular and Structural Biology

University of California, Los Angeles, 2021

Professor Carla Marie Koehler, Chair

The biogenesis of mitochondria depends on sophisticated import machineries to correctly target and fold cytosolically synthesized mitochondrial proteins. The mitochondrial import and assembly (MIA) pathway is a redox relay system that is essential for protein import into the intermembrane space (IMS) of mitochondria. It is unique that protein oxidation is tightly coupled to protein translocation. Given that the intermembrane space is highly relevant to a broad spectrum of diseases including apoptosis and neurodegeneration, additional research is needed to understand the underlying mechanism and new roles of regulation by the redox relay system.

We have identified a novel protein, Aim32 that is dually localized in matrix and IMS. Aim32 is a thioredoxin-like [2Fe-2S] ferredoxin protein and binds with Erv1. Deletion of Aim32

or mutation of conserved cysteine residues resulted in an increased accumulation of proteins with aberrant disulfide linkages. In addition, the steady-state level of assembled mitochondrial protein import complexes was decreased, and a subset of the complexes showed disassembly. Aim32 also bound to several mitochondrial proteins through disulfide linkages, suggesting a function in maintaining the redox status of proteins by potentially targeting cysteine residues. These studies suggest that Aim32 may be poised as a sensor or regulator in quality control in a broad range of mitochondrial proteins.

In addition to the function of ALR/Erv1 in protein translocation, it plays critical roles in various cellular pathways. We found ALR/Erv1 has an unexpected pro-survival role in hPSCs. A small molecule inhibitor that is specific for ALR/Erv1 was applied to investigate the hPSCs apoptosis and differentiation, which has the potential in hPSCs therapeutics.

The dissertation of Danyun Zhang is approved.

Catherine F. Clarke

Joseph A. Loo

Michael A. Teitell

Carla Marie Koehler, Committee Chair

University of California, Los Angeles

2021

DEDICATION

To my family, friends, and mentors for all the encouragement and support.

TABLE OF CONTENTS

LIST OF FIGURES

LIST OF TABLES

APPENDICES

ACKNOWLEDGEMENTS

It has been a challenging but rewarding journey. I am always grateful and honored to dedicate to the field of science research, and I would like to acknowledge people who helped me along this way. First, I would like to express my gratitude to my advisor, Dr. Carla Koehler. I have been very fortunate to work with Carla. Over the years she has provided me guidance, support, and knowledge that I needed not only in my research career but also made me who I am today. I am truly thankful for her understanding and always being so supportive when I was struggling.

I am also very grateful to my thesis committee, Dr. Catherine Clark, Dr. Joseph Loo, and Dr. Michael Teitell for their advice and guidance. Cathy has always been so kind and supportive. I also had amazing opportunity to collaborate on the stem cell project with Mike. I am always thankful for all the valuable ideas and knowledge.

I particularly want to thank Dr. Deepa Dabir. Thank you for being a great mentor, collaborator, and friend. Deepa has helped me on my multiple projects with excellent advice and mentor. I extremely appreciate her time and dedication to keep me on track and I am not sure how I would have fared without her.

I would also like to express my appreciation to my fellow colleagues. To the past and present members of the Koehler lab, including Janos Steffen, Matthew Maland, Eriko Shimada, Jesmine Cheung, Eric Torres, Michael Conti, Sean Atamdede, Melania Abrahamian, Matt Krieger, Jordan Whatley, Lucas Vincenzi, Jenny Ngo, Gary Shmorgon, and our many undergraduate students. I must thank my mentor, Matt for my first year in the Koehler lab for all the guidance. I

particularly want to thank Jesmine and Eric being such amazing friends. Thank you for all the advice, thank you for our good times and thank you for always being there for me. I am also grateful to Hui Su Tsui for being such a kind and amazing mentor during my first-year rotation. I would like to thank Charles Wang for all the advices on science and bunny. Last but not least, I am very fortunate to have such an amazing friend Jenny that I cherish the time we spend together that makes me feel not alone in graduate school.

Finally, I want to thank to the people who helped me outside lab. Thanks to my parents for rising me up and being supportive of my career choice.

Chapter 1 is an introduction to mitochondrial protein import pathways. Published small molecule probe for mitochondrial redox pathway is highlighted.

Chapter 2 is a version of submitted manuscript authored by myself, Owen R. Dailey, Mikayla R. Sweitzer, Daniel J. Simon, Yasaman Jami-Alahmadi, James A. Wolfschlegel, Carla M. Koehler and Deepa V. Dabir. The title is "Aim32, a dual-localized 2Fe-2S mitochondrial protein that functions in redox quality control". I would like to thank Dr. Deepa Dabir for the collaboration on this project. Thank you to Yasaman Jami-Alahmadi for performing the mass spectrometry analysis. Also thank you to Dr. James Wolfschlegel for collaboration. I would like to thank Dr. Steven Claypool and Dr. Keriann Bachus for critical discussions. I would also like to thank Dr. Keriann Bachus and Dr. Rosemary Stuart for provision of key reagents.

Chapter 3 summarizes further investigation of Aim32 disulfide interactions and assessment of role of Aim32 within two compartments of mitochondria. I would like to thank Dr. Deepa Dabir for the collaboration on this project. Thank you to Yasaman Jami-Alahmadi for performing the mass spectrometry analysis. Also thank you to Dr. James Wolfschlegel for collaboration. I would like to thank Angela Bui for helping with the immunoprecipitation experiment.

Chapter 4 characterizes mitochondrial protein Cmc4. The initial identifications of Cmc4 interaction were done by Matt Maland. Thank you the Chanfreau lab for provision of the BY4742 and mutant strains.

Chapter 5 summarizes a collaboration project between the Dr. Carla Koehler lab and Dr. Michael Teitell lab on the project of using a small molecule to investigate mitochondrial

disulfide relay system in human pluripotent stem cells. The apoptosis assays, generation of ALR-KD cell lines, and seahorse measurements are performed by Stephanie Kennedy from Teitell lab (Figure 5-1 to 5-4, 5-6, and 5-7). I would like to thank Dr. Deepa Dabir for the collaboration in biochemical assays and analyses. I would like to thank Nate Miller from Dr. Orian Shrihai lab for performing and analyzing DHE staining for ROS examination (Figure 5-5). I would also like to thank Anton Petcherski from Dr. Orian Shrihai lab helping with fluorescence confocal microscopy and mitochondrial morphology analysis (Figure S5-1).

VITA

2013	Research Assistant Fuli Institute of Food Science Zhejiang University, China
2013-2015	Research Assistant Department of Nutritional Sciences & Toxicology University of California, Berkeley
2015	B.S. in Chemical Biology University of California, Berkeley
2015-2018	UCLA University Fellowships for Graduate Studies Department of Chemistry and Biochemistry University of California, Los Angeles
2015-2020	Teaching Assistant Department of Chemistry and Biochemistry University of California, Los Angeles
2015-2021	Graduate Student Researcher Department of Chemistry and Biochemistry University of California, Los Angeles

PRESENTATIONS AND PUBLICATIONS

Zhang D, Dailey OR, Sweitzerb MR, Jami-Alahmadic Y, Wohlschlagel JA, Koehler CM, and Dabir DV, Aim32 is a dual-localized [2Fe-2S] protein that functions in mitochondrial redox quality control. 2021. (Submitted manuscript)

Zhang D, Dabir D.V, Kennedy S.A.L, Koehler C.M, Teitell M.A. (2018) Poster: Investigating the Mitochondrial Disulfide Relay System in Human Pluripotent Stem Cells. UCLA Mitochondria Symposium, Los Angeles, CA

Zhang D, Dabir D.V, Kennedy S.A.L, Torres A.Jr, Koehler C.M, Malone C.S, Teitell M.A.(2018) Poster: Investigating the Mitochondrial Disulfide Relay System in Human Pluripotent Stem Cells. Mitochondrial Medicine, Cambridge, UK

Zhang D, Dabir D.V, Koehler C.M. (2017) Poster: Using a small molecule to characterize mitochondrial intermembrane space proteins CHCHD2 and CHCHD10.

UCLA Mitochondria Symposium, Los Angeles, CA

Kuo T, Chen TZ, Lee RA, Nguyen N, Broughton AE, **Zhang D**, and Wang JC, Pik3r1 is Required for Glucocorticoid-induced Perilipin 1 Phosphorylation in Lipid droplet for Adipocyte Lipolysis. Diabetes, 2017, 66(6) 1601-1610. PMID:28292967

Kuo T, Liu PH, Chen TZ, Lee RA, New J, **Zhang D**, and Wang JC, Transcriptional Regulation of FoxO3 Gene by Glucocorticoids in Murine Myotubes. Am J Physiol Endocrinol Metab, 2016, 310:572-585. PMID:24565756

Chapter 1: Mitochondrial Biogenesis and Health

1.1 The Importance of Mitochondria

The mitochondrion is a dual membrane-bound intercellular organelle found in most eukaryotic cells. It is presumably originated as a prokaryotic cell engulfed by early eukaryotes and became endosymbionts living inside the eukaryotes[1]. The prominent role of mitochondria is the powerhouse of the cell, generating metabolic energy in the form of ATP to support essential cellular activities and functions. In addition to supplying cellular energy, the mitochondria have been characterized many other functions that include cell signaling, apoptosis, heme and iron-sulfur biosynthesis, and steroid synthesis[2].

Because mitochondria play import roles in maintaining cellular homeostasis and many essential processes, it is no surprise that maintaining mitochondria health is vital. Defects in mitochondrial homeostasis not only take parts in metabolic disease such as diabetes[3], but recent evidences have shown mitochondrial dysfunction in cancer and neurodegenerative diseases including Parkinson's disease, Alzheimer's disease, amyotrophic lateral sclerosis (ALS), and Huntington's disease affecting millions people worldwide[4,5]. Parkinson's disease, for instance, is a well-known long-lasting neurodegenerative disorder. Patients suffer from uncontrolled trembling as a result of dysfunctional mitochondrial turnover. It was reported that in 2015, Parkinson's disease affected 6.2 million people and resulted in roughly 117,400 deaths globally[6]. However, many mitochondria associated diseases are still not well characterized in regard to how dysfunction leads to pathological consequences. Clearly, in order to develop

therapeutic treatment, it is important to study the mechanism of mitochondrial dysfunction that eventually results in degenerative disorders. As research continues in diverse fields, studies on mitochondria biogenesis and function will enable further understanding of how mitochondria contribute to human health and disease.

1.2 Protein Trafficking at Mitochondria

Mitochondria contains its own genome that encodes for 13 proteins, which only make-up 1% of the proteins that are found in the mitochondrion[7]. The mitochondrial encoded genes primarily include components of the electron transport chain as well as mitochondria rRNAs and tRNAs[8]. The other 99% of the mitochondrial proteome is encoded by the nucleus genome and translated in the cytosol, thus requiring a transport mechanism that both properly targets and transports select proteins to the mitochondria to perform their normal function. Because of the duel-membrane nature, precursor proteins that are translated in cytosol are destined to one of four areas of mitochondria, which include the outer membrane (OM), intermembrane space (IMS), inner membrane (IM), or the matrix[9] (Figure 1.1). Precursor proteins typically contain targeting sequences (MTS) that direct nascent peptides to the correct compartment. The most common targeting sequence is a cleavable N-terminal amphipathic alpha helix, but many proteins, particularly those of the outer and inner membrane, contain targeting and sorting information within the mature part of the protein[10].

The mitochondrial outer membrane is a phospholipid bilayer that separates the IMS from cytosol. Nearly all precursors enter mitochondria via the translocase on the outer membrane or the TOM complex[9]. The central component of TOM is the channel-forming protein Tom40,

which interacts with a variety of receptors with precursor protein recognition sites to direct nascent proteins to translocate[11]. Other TOM complex components including receptors Tom20, Tom22, and Tom70 recognize the precursor targeting sequence and guide the precursors to the TOM channel[11,12]. After translocation through the TOM complex, the importing precursor proteins will follow different sorting pathways. Proteins destined for the outer membrane such as beta barrels Tom40 and Por1 (VDAC) and alpha-helical anchored protein Tom22, are mediated by the sorting and assembly machinery or SAM complex[9].

Protein import into the intermembrane space use different approaches[13]. Most IMS proteins are small and shuttled via the Mitochondrial Import and Assembly (MIA) pathway after entering the Tom40 complex (Fig 1.2). The MIA pathway represents the oxidative folding pathway of IMS[14–17]. It delivers proteins with conserved cysteine motifs, including the small Tim proteins Tim8, Tim9, Tim10, Tim 12 and Tim13 with the twin CX_3C motif[18,19] and proteins with a twin CX_9C motif, such as Cox17 and Cox19[20,21]. The machinery responsible for mediating the oxidative folding of these substrates are the receptor Mia40 and the sulfhydryl oxidase Erv1. Electrons shuttle from Erv1 to a variety of electron acceptors, including oxygen and cytochrome *c*. Thus, the mitochondrial intermembrane space supports the assembly of disulfide bonds in proteins. Other intermembrane space proteins that contain a bipartite N-terminal, including cytochrome *b2* and cytochrome *c* peroxidase, targeting sequence interact with Tim23 translocon on the inner membrane and arrested in IMS by the “stop-transfer” domain in the targeting sequence[22,23]. Thus, the translocation depends on membrane potential. The presequence is cleaved by processing peptidases in both the matrix and intermembrane space[24].

The mitochondrial inner membrane is compartmentalized into numerous cristae, which greatly expand the surface area to enhance the ability to produce ATP[25]. The inner membrane is permeable to O_2, H_2O, and CO_2, but not as permeable to ions and small molecules as the outer membrane. This provides a barrier to build a proton gradient and membrane potential that is used to drive ATP production. A large family of proteins function as metabolite carriers, most of which are embedded in the inner membrane. Carrier proteins often contain targeting sequences located internally and are inserted into the inner membrane via the TIM22 complex in a membrane potential dependent manner[26]. This complex contains small Tim proteins (Tim8, Tim9, Tim10, Tim12 and Tim13), and the membrane components of Tim54, Tim22, and Tim18[27,28]. The small Tim complexes of Tim9-10 and Tim8-13 acts as chaperons facilitating membrane carrier proteins traveling through IMS[19,29]. Tim22 is the channel-forming protein. Tim54 acts as the receptor for the complex and directly binds the small Tim complex[30].

The translocase of the inner membrane (TIM23 complex) sorts proteins into the inner membrane or into the matrix with the assistance of the ATP-dependent presequence associated motor (PAM) [10,31,32]. TIM23 complex guides presequences into the matrix in a membrane potential dependent manner. The main components of the complex include Tim23, Tim50, Tim17, and Tim21. Two homodimers of Tim23 and Tim17 form the core of the channel, also known as the TIM23 core complex[33]. Tim17 contains a pair of highly conserved cysteine residues that form a structural disulfide bond exposed to the IMS which is critical for efficient protein translocation through the TIM23 complex[34]. Tim50 closely associates with Tim23 in the inner membrane and is responsible for recognizing nascent precursors from the TOM channel

and mediating Tim23 channel gating[35,36]. For the matrix-targeted protein, targeting sequence is cleaved by the matrix processing protease (MPP) once it is translocated into the matrix[24,37]. For laterally inserted precursors, a second cleavage occurs by inner membrane peptidase (IMP) for removal of the hydrophobic sorting sequence. Presequence protease (PreP) degrades the resulting peptides[38].

1.3 Mitochondrial disulfide relay system- MIA pathway

The MIA (mitochondrial import and assembly) pathway in the IMS of mitochondria is unique; protein oxidation is tightly coupled to protein translocation, which is heavily dictated by thiol-disulfide exchange reactions[39]. These proteins take part in several important mitochondrial processes, including assembly of the respiratory chain, lipid homeostasis, mitochondrial dynamics, and metal ion homeostasis[40,41,15]. However, as our knowledge of the mitochondrial proteome expands, it is evident that a wide spectrum of substrates traffic through this pathway, thus connecting it to other extramitochondrial processes within the cell. Consequently, the oxidative folding pathway is highly relevant to a broad spectrum of diseases including, but not limited to myopathy, Huntington's disease, and Parkinson's disease.

The major player of the MIA pathway, Mia40 (human as CHCHD4), acts like a receptor for the import of cysteine-rich IMS proteins. Precursors are imported across the TOM complex in an unfolded and reduced state[42,43]. Mia40 then forms a transient disulfide bonds with the imported substrates after they cross the TOM complex[15,44,45]. Mia40 contains six conserved cysteine residues constituting a -CPC-CX_9C-CX_9C- motif[39]. The CPC motif of Mia40 functions as a redox active site that forms a transient disulfide bond with the importing precursors,

resulting in a mixed disulfide bond formation between conserved cysteine motif in substrate and CPC motif of Mia40. Indeed, Mia40 can acquire up to six electrons when oxidizing substrates such as Tim13 that acquire two disulfide bonds simultaneously[46]. The precursor is eventually released in its folded and oxidized form from Mia40 and the newly formed disulfide bond within the substrate prevents retro-translocation, leaving Mia40 in the reduced form[47,48]. The MIA import pathway is well conserved between yeast and humans with some noteworthy differences[49]. The human homolog CHCHD4 shares high sequence identity with its eukaryotic homologs in the central part of its sequence including the cysteine motif but lacks a large N-terminal extension including a transmembrane region with respect to the yeast homologs, thus being completely soluble in the IMS[50]. The N-terminal targeting sequence of yeast Mia40 appears dispensable for function. While CHCHD4 is a substrate for its own pathway to the IMS, yeast Mia40 contains targeting sequences for both presequence (TIM) and MIA pathways. This suggests the import of Mia40 with evolutionary transition from lower eukaryotes relying on the presequence pathway to the MIA pathway[51].

The other major player of the MIA pathway, sulfhydryl oxidase Erv1, which is essential for respiration and viability, re-oxidizes Mia40[52,53]. Electrons are shuttled from Erv1 to either cytochrome *c* to be used in the electron transport chain, or molecular oxygen[14,20], and the electron acceptor may depend upon growth conditions[54]. Erv1 forms a 1:1 complex with cytochrome *c* and the electron transport chain then serves as an electron acceptor to reoxidize cytochrome *c*[41,54]. When Erv1 passes electron to molecular oxygen and generates hydrogen peroxide which is subsequently reduced to water by cytochrome *c* peroxidase (Ccp1)[47,55]. Then

Ccp1 reoxidize cytochrome *c* that cytochrome *c* and Ccp1 function efficiently as Erv1 electron acceptors. In yeast, the MIA pathway functions under anaerobic conditions and one such electron acceptor couple identified to date is Osm1/fumarate[56]. However, yeast seems to have additional terminal electron acceptors because yeast lacking OSM1 and CYC1 were still viable under anaerobic conditions. ALR, the human homolog of Erv1, also belongs to the sulfhydryl oxidase family[57,58]. It was originally identified as an augmenter of liver regenerating[59]. ALR is ubiquitously expressed, however the functions in other organs are not clear yet. It has been speculated that serum ALR levels can serve as a biomarker for regenerating or injured liver. Understanding ALR's role in pathology would allow for better development of diagnostic tools. Purified ALR, same as Erv1, was found to contain the core sulfhydryl oxidase a FAD-binding site and a conserved proximal CXXC motif[60]. Current evidence indicates the enzymatic activities of mitochondrial ALR in reduction of cytochrome *c*, regulation of the activities of certain proteins by its sulfhydryl oxidase activity and inducing Fe/S maturation of cellular proteins[57,40]. Further work has to be done to better understand the multiple roles of ALR in mitochondrial biogenesis, which is essential in both studying the MIA pathway and the overall behavior of IMS proteins in disease pathology.

Yeast has served as an important model for MIA pathway and for elucidating the overall IMS function, which is highly relevant to human pathology and disease. For instance, a point mutation in ALR causes an autosomal recessive myopathy, with patients developing congenital cataract, sensorineural hearing loss and developmental delay[61]. ALR downregulation in mouse embryonic cells decreases their pluripotency along with increased mitochondrial fragmentation,

and mitophagy[62]. A role for CHCHD4 has been proposed in hypoxia signaling via Hypoxia-Inducing Factor 1α (HIF1α)[63], and in mitochondrial calcium uptake[64]. Finally, an interaction between Apoptosis-inducing factor (AIF) and CHCHD4 was shown to regulate respiratory chain biogenesis[65]. Interestingly, several non-classical substrates connect the MIA pathway with other extramitochondrial cellular processes. However, insights into the molecular mechanisms that connect the MIA pathway with these processes is still lacking and needs to be addressed. Moreover, many diseases and disorders are consequences of mitochondrial biogenesis dysfunction related with proteins associated with the MIA pathway. Mutations of the genes for mitochondrial twin CX_9C proteins, CHCHD2 and CHCHD10, are associated with a variety of neurodegenerative diseases including the pathogenesis of Parkinson's diseases (PD)[66], amyotrophic lateral sclerosis (ALS) and frontotemporal lobe dementia (FTD)[67]. Furthermore, the MIA pathway has insight into cancer biology. It is reported that Mia40 expression can modulate the localization of tumor suppressor protein p53[68]. In addition, overexpression of CHCHD2 has been reported in many different cancers[69,70]. Although there are numerous mitochondrial diseases affecting huge population, it has been difficult to study mitochondrial protein and import machineries due to lack inadequate of tools and approaches.

1.4 Probing mitochondrial import mechanisms with small molecule inhibitors

Although mitochondrial biogenesis has been studied extensively using genetic and biochemical analysis, Mia40/Erv1 mediated protein import pathway is essential for cell viability. Traditional methods such as gene knockout and RNA-interference are not suitable in this case. Thus, novel approaches are needed for elucidating the roles of IMS proteins while limiting off-

target consequences in order to shed light on how dysfunction can lead to diseases.

Small molecules, MitoBloCK-6 (MB6)[71], identified by Carla Koehler's laboratory, is a selective inhibitor of the Mia40/Erv1 redox-mediated import pathway in mitochondria (Figure 1-3). MB6 does not alter mitochondrial function or disrupt mitochondrial integrity but is specific to Erv1 oxidase activity. MB6 inhibits Erv1 by interfering with the binding or electron transfer between Mia40 and cytochrome *c*. MB6 also inhibits Erv1 human homolog, ALR activity. The small molecule MB6 allow for specific and rapid manipulations that will allow investigating mechanisms that were previously too difficult. MB6 will be an excellent tool to study the MIA pathway and mitochondrial biogenesis of IMS proteins. Furthermore, this versatile small molecule can be potentially used in therapeutic treatment for IMS protein associated diseases.

Interestingly, MB6 selectively kills unwanted undifferentiated human pluripotent stem cells (hPSCs), suggesting a distinct role for ALR in hPSCs homeostasis (Figure 1-3). hPSCs have the potential in regenerative therapeutics because of the ability to self-renew and to differentiate into many cell types of the body[72]. However, the feasibility of using stem cell for clinical purposes remains controversial. Because the differentiation process is rarely complete with some undifferentiated hPSCs remaining among the differentiated derivatives, the potential detrimental result is the human embryonal carcinoma cell lines, which are pluripotent cell lines derived from the undifferentiated stem cell components of spontaneously arising germ cell tumors[73]. The risk of teratoma formation needs to be eliminated before hPSCs-based therapies for treatment. Because MB6 selectively kills undifferentiated hPSCs, MB6 is particularly attractive as an agent to remove hPSCs that fail-to-differentiate in transplantation studies. The small molecule can be

directly added to the media without any genetic manipulation of cells. MB6 can be washed away from the media before cells are applied to patients, thus rendering the compound quite safe. Therefore, MB6 can be used to enhance transplantation therapeutics. In addition, MB6 is an excellent tool for mechanistic studies to develop stem cell differentiation protocols for a broad range of cell types. MB6 can be used to understand the contribution of mitochondrial to hPSCs function and differentiation and the distinct of ALR in hPSCs.

Defects in mitochondria function impact human health greatly and result in a wide range of different issues that spam from degenerative diseases to cancer. Utilizing small molecule tools in mitochondrial research is a novel approach that will help understanding of mitochondrial biogenesis and how dysfunction leads to disease as well as characterizing additional roles of mitochondrial proteins in mitochondrial homeostasis.

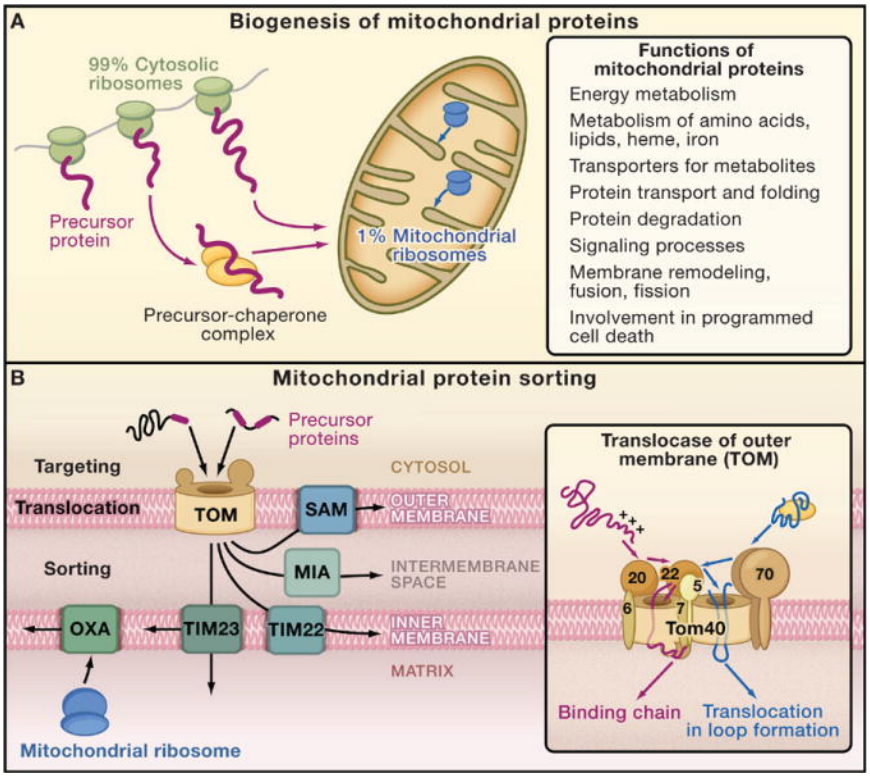

Figure 1-1 General Mitochondrial Protein Translocation[9]. (A) Cytosolic and mitochondrial protein synthesis. Most mitochondrial proteins are synthesized on cytosolic ribosomes and are imported into the organelle. About 1% of mitochondrial proteins are synthesized inside the organelle. (B) Sorting pathways of mitochondria. The translocase of the outer membrane (TOM complex) is the main entry gate into mitochondria. Subsequently, the precursor proteins follow different sorting pathways. MIA, mitochondrial intermembrane space assembly; OXA, insertase/export machinery of the inner membrane; SAM, sorting and assembly machinery; TIM22 complex, carrier translocase of the inner membrane; TIM23 complex, presequence translocase of the inner membrane. (Inset) The TOM complex consists of seven different subunits. The receptors Tom20, Tom22, and Tom70 recognize precursor proteins and transfer them to the central component, the channel-forming Tom40. Three small Tom proteins, Tom5,

Tom6, and Tom7, are involved in the assembly and dynamics of the TOM complex. (Presequence-carrying precursor proteins, red; hydrophobic precursors with internal targeting signals, blue.

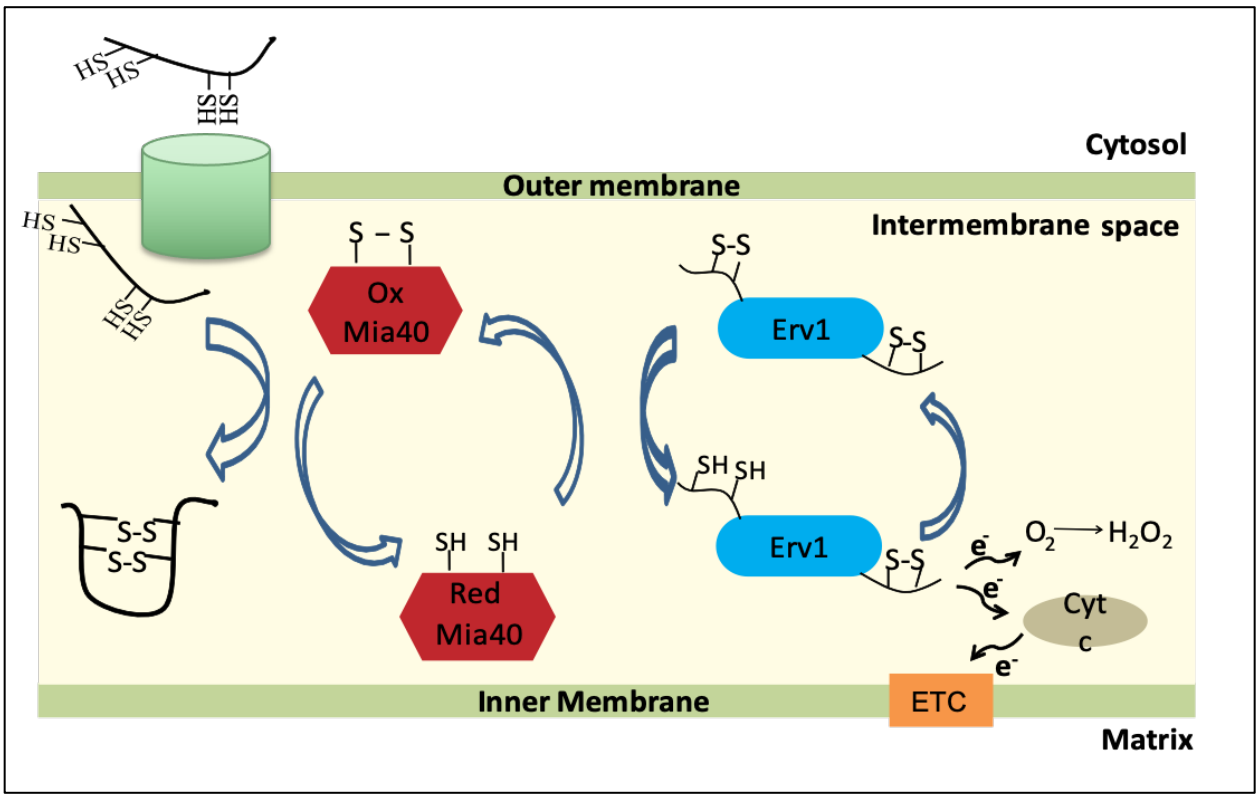

Figure 1-2 MIA import pathway. Usually small, cysteine rich substrates, such as small Tim chaperones, are imported through the Translocon of the Outer Membrane (TOM40) complex and form a mixed disulfide bond with Mia40. The substrate is oxidized, locking it in the intermembrane space. Mia40 is subsequently re-oxidized by the sulfhydryl oxidase, Erv1. Erv1 passes the acquired electrons to cytochrome c (and eventually the electron transport chain), or molecular oxygen.

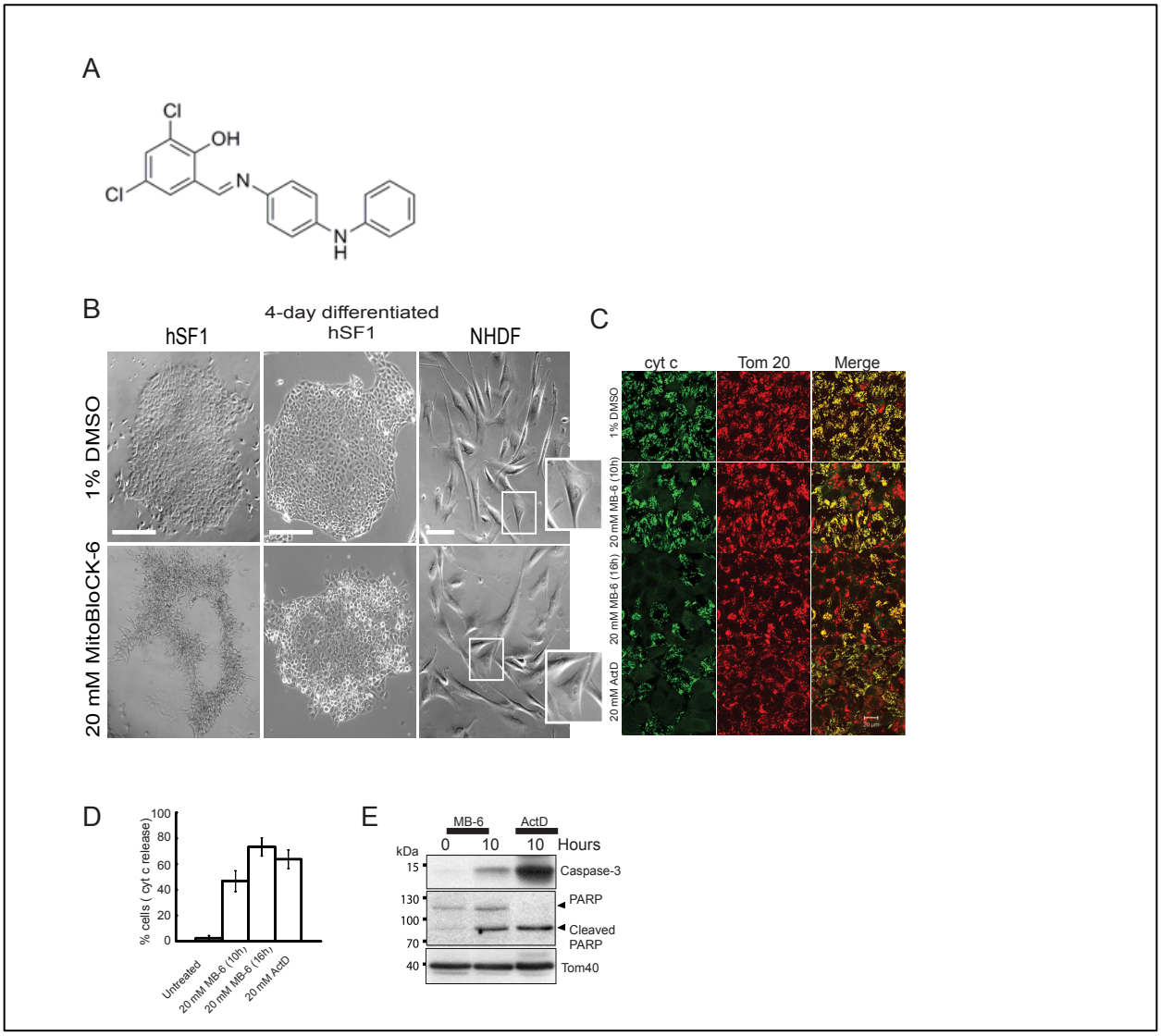

Figure 1-3 MitoBloCK-6 inhibits growth and induces apoptosis in stem cells, but not differentiated cells[71]**.** (A) MitoBloCK-6 (MB6) structure. (B)Brightfield images of hSF1 cells, retinoic acid differentiated 4-day hSF1 cells, and NHDF cells treated with 20 µM MitoBloCK-6 or 1% DMSO for 16 hr. (C) HSF1 cells were treated with 20 µM MitoBloCK-6 or 1% DMSO. As a positive control, apoptosis was induced in cells by treatment with 20 µM actinomycin D (ActD) and 100 µM z-VAD-fmk for 16 hours. Cells were fixed and analyzed by immunofluorescence microscopy using antibodies against cyt *c* (green) and Tom20 (Red).

Merged images are also depicted in panels. (D) Quantification of data obtained in (C) and represented as % of cells that lost the mitochondrial cyt c staining but retained Tom20 staining. Data was collected from three independent experiments. Error bars represent standard deviation. (E) As in 'B', HSF1 cells were treated with 20 μM MitoBloCK-6 or 20 μM actinomycin D for the indicated time. Whole cell extracts were analyzed by SDS-PAGE and immunoblotted with antibodies for caspase-3 fragment and PARP. Tom40 was included as a loading control.

References

1. Dyall, S. D., Brown, M. T. & Johnson, P. J. Ancient Invasions: From Endosymbionts to Organelles. *Science* vol. 304 253–257 (2004).
2. McBride, H. M., Neuspiel, M. & Wasiak, S. Mitochondria: More Than Just a Powerhouse. *Current Biology* vol. 16 (2006).
3. Sivitz, W. I. & Yorek, M. A. Mitochondrial dysfunction in diabetes: From molecular mechanisms to functional significance and therapeutic opportunities. *Antioxidants and Redox Signaling* vol. 12 537–577 (2010).
4. Lezi, E. & Swerdlow, R. H. Mitochondria in neurodegeneration. *Adv. Exp. Med. Biol.* **942**, 269–286 (2012).
5. Lin, M. T. & Beal, M. F. Mitochondrial dysfunction and oxidative stress in neurodegenerative diseases. *Nature* vol. 443 787–795 (2006).
6. Vos, T. *et al.* Global, regional, and national incidence, prevalence, and years lived with disability for 310 diseases and injuries, 1990–2015: a systematic analysis for the Global Burden of Disease Study 2015. *Lancet* **388**, 1545–1602 (2016).
7. Andersson, S. G. E. *et al.* On the origin of mitochondria: A genomics perspective. in *Philosophical Transactions of the Royal Society B: Biological Sciences* vol. 358 165–179 (Royal Society, 2003).
8. Borst, P. & Grivell, L. A. The mitochondrial genome of yeast. *Cell* vol. 15 705–723 (1978).
9. Chacinska, A., Koehler, C. M., Milenkovic, D., Lithgow, T. & Pfanner, N. Importing Mitochondrial Proteins: Machineries and Mechanisms. *Cell* vol. 138 628–644 (2009).

10. Koehler, C. M. Protein translocation pathways of the mitochondrion. *FEBS Letters* vol. 476 27–31 (2000).

11. Ahting, U. *et al.* Tom40, the pore-forming component of the protein-conducting TOM channel in the outer membrane of mitochondria. *J. Cell Biol.* **153**, 1151–1160 (2001).

12. Yamano, K. *et al.* Tom20 and Tom22 share the common signal recognition pathway in mitochondrial protein import. *J. Biol. Chem.* **283**, 3799–3807 (2008).

13. Herrmann, J. M. & Hell, K. Chopped, trapped or tacked - Protein translocation into the IMS of mitochondria. *Trends in Biochemical Sciences* vol. 30 205–212 (2005).

14. Koehler, C. M., Beverly, K. N. & Leverich, E. P. Redox pathways of the mitochondrion. *Antioxidants and Redox Signaling* vol. 8 813–822 (2006).

15. Chacinska, A. *et al.* Essential role of Mia40 in import and assembly of mitochondrial intermembrane space proteins. *EMBO J.* **23**, 3735–3746 (2004).

16. Mesecke, N. *et al.* A disulfide relay system in the intermembrane space of mitochondria that mediates protein import. *Cell* **121**, 1059–1069 (2005).

17. Sideris, D. P. & Tokatlidis, K. Oxidative protein folding in the mitochondrial intermembrane space. *Antioxidants and Redox Signaling* vol. 13 1189–1204 (2010).

18. Webb, C. T., Gorman, M. A., Lazarou, M., Ryan, M. T. & Gulbis, J. M. Crystal structure of the mitochondrial chaperone TIM9•10 reveals a six-bladed α-propeller. *Mol. Cell* **21**, 123–133 (2006).

19. Curran, S. P., Leuenberger, D., Schmidt, E. & Koehler, C. M. The role of the Tim8p-Tim13p complex in a conserved import pathway for mitochondrial polytopic inner membrane proteins. *J. Cell Biol.* **158**, 1017–1027 (2002).

20. Tienson, H. L. *et al.* Reconstitution of the Mia40-Erv1 oxidative folding pathway for the small tim proteins. *Mol. Biol. Cell* **20**, 3481–3490 (2009).

21. Fraga, H. *et al.* The mitochondrial intermembrane space oxireductase mia40 funnels the oxidative folding pathway of the cytochrome c oxidase assembly protein cox19. *J. Biol. Chem.* **289**, 9852–9864 (2014).

22. Gabriel, K. *et al.* Novel Mitochondrial Intermembrane Space Proteins as Substrates of the MIA Import Pathway. *J. Mol. Biol.* **365**, 612–620 (2007).

23. Glick, B. S. *et al.* Cytochromes c1 and b2 are sorted to the intermembrane space of yeast mitochondria by a stop-transfer mechanism. *Cell* **69**, 809–822 (1992).

24. Hawlitschek, G. *et al.* Mitochondrial protein import: Identification of processing peptidase and of PEP, a processing enhancing protein. *Cell* **53**, 795–806 (1988).

25. Mannella, C. A. Structure and dynamics of the mitochondrial inner membrane cristae.

Biochimica et Biophysica Acta - Molecular Cell Research vol. 1763 542–548 (2006).

26. Rehling, P. *et al.* Protein insertion into the mitochondrial inner membrane by a twin-pore translocase. *Science (80-.).* **299**, 1747–1751 (2003).

27. Wagner, K. *et al.* The Assembly Pathway of the Mitochondrial Carrier Translocase Involves Four Preprotein Translocases. *Mol. Cell. Biol.* **28**, 4251–4260 (2008).

28. Gebert, N. *et al.* Assembly of the three small Tim proteins precedes docking to the mitochondrial carrier translocase. *EMBO Rep.* **9**, 548–554 (2008).

29. Endres, M., Neupert, W. & Brunner, M. Transport of the ADP/ATP carrier of mitochondria from the TOM complex to the TIM22.54 complex. *EMBO J.* **18**, 3214–3221 (1999).

30. Kerscher, O., Holder, J., Srinivasan, M., Leung, R. S. & Jensen, R. E. The Tim54p-Tim22p complex mediates insertion of proteins into the mitochondrial inner membrane. *J. Cell Biol.* **139**, 1663–1675 (1997).

31. Hell, K., Herrmann, J. M., Pratje, E., Neupert, W. & Stuart, R. A. Oxa1p, an essential component of the N-tail protein export machinery in mitochondria. *Proc. Natl. Acad. Sci. U. S. A.* **95**, 2250–2255 (1998).

32. Mokranjac, D. & Neupert, W. The many faces of the mitochondrial TIM23 complex. *Biochimica et Biophysica Acta - Bioenergetics* vol. 1797 1045–1054 (2010).

33. Ting, S. Y., Schilke, B. A., Hayashi, M. & Craig, E. A. Architecture of the TIM23 inner mitochondrial translocon and interactions with the matrix import motor. *J. Biol. Chem.* **289**, 28689–28696 (2014).

34. Ramesh, A. *et al.* A disulfide bond in the TIM23 complex is crucial for voltage gating and mitochondrial protein import. *J. Cell Biol.* **214**, 417–431 (2016).

35. Tamura, Y. *et al.* Tim23 - Tim50 pair coordinates functions of translocators and motor proteins in mitochondrial protein import. *J. Cell Biol.* **184**, 129–141 (2009).

36. Gevorkyan-Airapetov, L. *et al.* Interaction of Tim23 with Tim50 is essential for protein translocation by the mitochondrial TIM23 complex. *J. Biol. Chem.* **284**, 4865–4872 (2009).

37. Mossmann, D., Meisinger, C. & Vögtle, F. N. Processing of mitochondrial presequences. *Biochimica et Biophysica Acta - Gene Regulatory Mechanisms* vol. 1819 1098–1106 (2012).

38. Johnson, K. A. *et al.* The closed structure of presequence protease PreP forms a unique 10 000 Å3 chamber for proteolysis. *EMBO J.* **25**, 1977–1986 (2006).

39. Banci, L. *et al.* MIA40 is an oxidoreductase that catalyzes oxidative protein folding in mitochondria. *Nat. Struct. Mol. Biol.* **16**, 198–206 (2009).

40. Lange, H. *et al.* An essential function of the mitochondrial sulfhydryl oxidase Erv1p/ALR in the maturation of cytosolic Fe/S proteins. *EMBO Rep.* **2**, 715–720 (2001).

41. Bihlmaier, K. *et al.* The disulfide relay system of mitochondria is connected to the respiratory chain. *J. Cell Biol.* **179**, 389–395 (2007).

42. Lu, H., Allen, S., Wardleworth, L., Savory, P. & Tokatlidis, K. Functional TIM10 Chaperone Assembly Is Redox-regulated in Vivo. *J. Biol. Chem.* **279**, 18952–18958 (2004).

43. Lutz, T., Neupert, W. & Herrmann, J. M. Import of small Tim proteins into the mitochondrial intermembrane space. *EMBO J.* **22**, 4400–4408 (2003).

44. Tokatlidis, K. A disulfide relay system in mitochondria. *Cell* vol. 121 965–967 (2005).

45. Naoé, M. *et al.* Identification of Tim40 that mediates protein sorting to the mitochondrial intermembrane space. *J. Biol. Chem.* **279**, 47815–47821 (2004).

46. Neal, S. E. *et al.* Mia40 protein serves as an electron sink in the Mia40-Erv1 import pathway. *J. Biol. Chem.* **290**, 20804–20814 (2015).

47. Stojanovski, D., Bragoszewski, P. & Chacinska, A. The MIA pathway: A tight bond between protein transport and oxidative folding in mitochondria. *Biochimica et Biophysica Acta - Molecular Cell Research* vol. 1823 1142–1150 (2012).

48. Böttinger, L. *et al.* In vivo evidence for cooperation of Mia40 and Erv1 in the oxidation of mitochondrial proteins. *Mol. Biol. Cell* **23**, 3957–3969 (2012).

49. Fischer, M. *et al.* Protein import and oxidative folding in the mitochondrial intermembrane space of intact mammalian cells. *Mol. Biol. Cell* **24**, 2160–2170 (2013).

50. Hofmann, S. *et al.* Functional and mutational characterization of human MIA40 acting during import into the mitochondrial intermembrane space. *J. Mol. Biol.* **353**, 517–528 (2005).

51. Chacinska, A. *et al.* Mitochondrial biogenesis, switching the sorting pathway of the intermembrane space receptor Mia40. *J. Biol. Chem.* **283**, 29723–29729 (2008).

52. Ang, S. K., Zhang, M., Lodi, T. & Lu, H. Mitochondrial thiol oxidase Erv1: Both shuttle cysteine residues are required for its function with distinct roles. *Biochem. J.* **460**, 199–210 (2014).

53. Allen, S., Balabanidou, V., Sideris, D. P., Lisowsky, T. & Tokatlidis, K. Erv1 mediates the Mia40-dependent protein import pathway and provides a functional link to the respiratory chain by shuttling electrons to cytochrome c. *J. Mol. Biol.* **353**, 937–944 (2005).

54. Dabir, D. V. *et al.* A role for cytochrome c and cytochrome c peroxidase in electron shuttling from Erv1. *EMBO J.* **26**, 4801–4811 (2007).

55. Erman, J. E. & Vitello, L. B. Yeast cytochrome c peroxidase: Mechanistic studies via protein engineering. *Biochimica et Biophysica Acta - Protein Structure and Molecular Enzymology* vol. 1597 193–220 (2002).

56. Neal, S. E., Dabir, D. V., Wijaya, J., Boon, C. & Koehler, C. M. Osm1 facilitates the transfer of electrons from Erv1 to fumarate in the redox-regulated import pathway in the mitochondrial intermembrane space. *Mol. Biol. Cell* **28**, 2773–2785 (2017).

57. Nalesnik, M. A., Gandhi, C. R. & Starzl, T. E. Augmenter of liver regeneration: A fundamental life protein. *Hepatology* vol. 66 266–270 (2017).

58. Farrell, S. R. & Thorpe, C. Augmenter of liver regeneration: A flavin-dependent sulfhydryl oxidase with cytochrome c reductase activity. *Biochemistry* **44**, 1532–1541 (2005).

59. Hagiya, M. *et al.* Cloning and sequence analysis of the rat augmenter of liver regeneration (ALR) gene: Expression of biologically active recombinant ALR and demonstration of tissue distribution. *Proc. Natl. Acad. Sci. U. S. A.* **91**, 8142–8146 (1994).

60. Wu, C.-K., Dailey, T. A., Dailey, H. A., Wang, B.-C. & Rose, J. P. The crystal structure of augmenter of liver regeneration: A mammalian FAD-dependent sulfhydryl oxidase. *Protein Sci.* **12**, 1109–1118 (2003).

61. Di Fonzo, A. *et al.* The Mitochondrial Disulfide Relay System Protein GFER Is Mutated in Autosomal-Recessive Myopathy with Cataract and Combined Respiratory-Chain Deficiency. *Am. J. Hum. Genet.* **84**, 594–604 (2009).

62. Todd, L. R. *et al.* Growth Factor ero1-like Modulates Drp1 to Preserve Mitochondrial Dynamics and Function in Mouse Embryonic Stem Cells. *Mol. Biol. Cell* **21**, 1225–1236 (2010).

63. Thomas, L. W., Staples, O., Turmaine, M. & Ashcroft, M. Chchd4 regulates intracellular oxygenation and perinuclear distribution of mitochondria. *Front. Oncol.* **7**, 71 (2017).

64. Petrungaro, C. *et al.* The Ca2+-dependent release of the Mia40-induced MICU1-MICU2 dimer from MCU regulates mitochondrial Ca2+ uptake. *Cell Metab.* **22**, 721–733 (2015).

65. Modjtahedi, N. & Kroemer, G. CHCHD4 links AIF to the biogenesis of respiratory chain complex I. *Mol. Cell. Oncol.* **3**, (2016).

66. Funayama, M. *et al.* CHCHD2 mutations in autosomal dominant late-onset Parkinson's disease: A genome-wide linkage and sequencing study. *Lancet Neurol.* **14**, 274–282 (2015).

67. Bannwarth, S. *et al.* A mitochondrial origin for frontotemporal dementia and amyotrophic lateral sclerosis through CHCHD10 involvement. *Brain* **137**, 2329–2345 (2014).

68. Zhuang, J. *et al.* Mitochondrial disulfide relay mediates translocation of p53 and partitions its subcellular activity. *Proc. Natl. Acad. Sci. U. S. A.* **110**, 17356–17361 (2013).

69. Liu, Y. & Zhang, Y. CHCHD2 connects mitochondrial metabolism to apoptosis. *Mol. Cell. Oncol.* **2**, (2015).

70. Wei, Y. *et al.* CHCHD2 is coamplified with EGFR in NSCLC and regulates mitochondrial function and cell migration. *Mol. Cancer Res.* **13**, 1119–1129 (2015).

71. Dabir, D. V. *et al.* A small molecule inhibitor of redox-regulated protein translocation into mitochondria. *Dev. Cell* **25**, 81–92 (2013).

72. Thomson, J. A. Embryonic stem cell lines derived from human blastocysts. *Science (80-.).* **282**, 1145–1147 (1998).

73. Fujikawa, T. *et al.* Teratoma formation leads to failure of treatment for type I diabetes using embryonic stem cell-derived insulin-producing cells. *Am. J. Pathol.* **166**, 1781–1791 (2005).

Chapter 2: Aim32, a dual-localized 2Fe-2S mitochondrial protein that functions in redox quality control

2.1 Abstract

Yeast is a facultative anaerobe and uses diverse electron acceptors to maintain redox-regulated import in the mitochondrial intermembrane space assembly (MIA) pathway. We used mass spectrometry to identify additional proteins that interacted with the sulfhydryl oxidase Erv1 of the MIA pathway. Aim32, a thioredoxin-like [2Fe-2S] ferredoxin protein, was identified as an Erv1 binding protein. Detailed localization studies showed that Aim32 resided in both the mitochondrial matrix and intermembrane space, placing it in a rare group that is dual-localized within mitochondria. Aim32 interacted with additional proteins including redox protein Osm1 and protein import components Tim17, Tim23, and Tim22. Deletion of Aim32 or mutation of conserved cysteine residues that coordinate the Fe-S center in Aim32 resulted in an increased accumulation of proteins with aberrant disulfide linkages. In addition, the steady-state level of assembled TIM22, TIM23, and Oxa1 protein import complexes was decreased, and a subset of the import complexes showed misassembly, among other phenotypes. Aim32 also bound to several mitochondrial proteins under nonreducing conditions, suggesting a function in maintaining the redox status of proteins by potentially targeting cysteine residues that may be sensitive to oxidation. Finally, Aim32 was essential for growth in the presence of ethidium bromide and in conditions of stress such as elevated temperature and hydroxyurea (HU). These studies suggest that Aim32 is likely not a direct participant in the MIA pathway. Instead, the Fe-S

protein Aim32 has a potential role in general redox homeostasis in the matrix and intermembrane space. Thus, Aim32 may be poised as a sensor or regulator in quality control for a broad range of mitochondrial proteins.

2.2 Introduction

Mitochondrial biogenesis depends on coordinated translocation machineries to correctly target and fold imported cytosolic proteins. In the intermembrane space (IMS), a subset of proteins acquires disulfide bonds in an oxidative folding pathway[1–4]. The mitochondrial intermembrane space import and assembly (MIA) pathway consists of the oxidoreductase Mia40 and sulfhydryl oxidase Erv1 that coordinate the insertion of disulfide bonds into substrate proteins[3–7]. Substrates typically have a CX3C (i.e., the small Tim proteins) or CX9C (i.e., proteins such as Cox19 that may have a role in Complex IV assembly) motif and cross the membrane in a reduced and unfolded state. Mia40 serves as an import receptor and mediates disulfide bond insertion[8,9]. Erv1 then reoxidizes Mia40[9], and the electrons are passed to a variety of terminal electron acceptors including O2 and cytochrome (cyt) *c*[10,11]. In yeast, the MIA pathway functions under anaerobic conditions with the fumarate/Osm1 couple[12]. However, *S. cerevisiae* seems to have additional terminal electron acceptors because strains deleted for *OSM1* and *CYC1* were still viable under anaerobic conditions [12].

In contrast to the endoplasmic reticulum (ER), the MIA pathway lacks a bonafide disulfide isomerase. With model substrate Cox19, Mia40 is necessary and sufficient to introduce both disulfide bonds in a coordinated process[13]. However, Mia40 is a peculiar oxidoreductase in that it has no isomerase activity[14]. Within the IMS, glutathione may have proofreading capacity,

preventing the formation of non-productive intermediates[15]; however, these studies were done in vitro and may not reflect the scenario *in vivo*[9,16]. Because yeast is a facultative anaerobe, it may employ different electron acceptors, such as thioredoxins, glutaredoxins, iron-sulfur (Fe/S) cluster proteins and possibly varied editing elements to sustain oxidative folding across diverse environmental conditions.

Redox control within the mitochondrion is essential for the proper functioning of the organelle. The thiol-disulfide balance in the matrix and IMS is quite different; the mitochondrial matrix is considerably more reducing than the mitochondrial IMS to facilitate proper protein folding and activity[17]. Redox homeostasis in the matrix and IMS are maintained independently [18,19]. In the matrix, glutathione reductase and the mitochondrial thioredoxin reductase are key regulator[20]. Sod2 is a matrix antioxidant that prevents oxidative damage to proteins by neutralizing reactive oxygen species (ROS)[21]. Any changes in redox state in one compartment may affect the other as has been shown for the ER where inhibiting protein folding has a major effect on overall cellular redox due to the operation of the refolding pathway [22].

Aim32 (Altered Inheritance of Mitochondria 32) was first reported in a study that assessed the mode of action of the antimalarial drug (primaquine) and demonstrated to counteract primaquine-induced oxidative stress in the absence of *SOD2*[23]. More recently, it was shown by Stegmaier et al. that Aim32 is a soluble mitochondrial matrix protein, and a prototype of the widely distributed class of Fe/S proteins bearing a thioredoxin-like ferredoxin (TLF) domain with a bis-histidinyl coordinated [2Fe-2S] cluster[24]. They further postulated a general role for Aim32 in the degradation of allelochemicals, such as flavonoids and phenolic compounds.

However, a specific mitochondrial function for Aim32 was not assigned.

The thioredoxin fold of Aim32 is commonly found in oxidoreductases and chaperones[25]. Proteins with a TLF domain may function as a thiol-based molecular switch by modulating disulfide bond formation in target proteins[26–28]. Depending on the structure around the redox-active cysteine pair, the redox potential of thioredoxins can differ considerably. Moreover, mutagenesis of cysteine residues within the characteristic CXXC motif of thioredoxin proteins considerably changes the redox potential, modulating the properties of such proteins freely between reducing and oxidizing activities[29–31]. Thus, Fe-S proteins are unique in that they have the potential of playing multiple roles in redox sensing and electron transfer within a particular system, and versatile in their adaptability to the redox status of the cell. Despite this, the exact biological function(s) of Aim32, and thioredoxin-like [2Fe-2S] ferredoxins in general are not well understood.

In this study, we characterize the biological function of the thioredoxin-like ferredoxin protein, Aim32 within the mitochondria. Using several complementary approaches, we first demonstrate that Aim32 is dually localized to the matrix and IMS of the mitochondria where it is essential for anaerobiosis. Aim32 has several binding partners within the IMS, inner membrane, and the matrix. In the IMS, interactions with Erv1 and Osm1 may support a role in import, whereas additional interactions with translocon proteins including the TIM22 and TIM23 complexes suggest a role in protein stabilization or assembly of protein import complexes. Herein, we show that Aim32 may have a quality control function to maintain the assembly of protein complexes in which components may have thiols that are sensitive to damage.

2.3 Aim32, Osm1, and Erv1 form a functional complex

Yeast must have other terminal electron acceptors in addition to cyt *c* and the Osm1/fumarate couple, because *Δcyc3Δosm1* cells were viable under anaerobic conditions[12]. Since Erv1 assembles in several distinct complexes, we sought to identify additional partner proteins of Erv1. Briefly, a 2-micron plasmid for Erv1 with a tandem affinity tag technique (termed CNAP for consecutive nondenaturing affinity purification) was constructed[32]. The HISPC tag consists of a Protein-C epitope tag separated from a His10 tag by a 5-amino acid linker; two-step purification was achieved with a Ni^{2+}-column followed by elution with an imidazole buffer and subsequent purification with an antibody column against the Protein-C epitope. The HISPC tag was integrated in frame at the C-terminus of Erv1 in plasmids that expressed *ERV1* or the *erv1-12* allele from the endogenous promoter. The tagged proteins were designated as Erv1-HISPC and *erv1*-12-HISPC. The plasmids were introduced into a strain deleted for ERV1 by plasmid shuffling[10]. Addition of the tag did not alter growth properties or Erv1 localization, supporting that Erv1 function was not impaired (data not shown). A preparative scale pull-down was performed with the aforementioned columns. The final concentrated eluates were resolved by 10-15% SDS-PAGE. Compared with the negative control (WT+Vec), the proteins (highlighted by arrows) co-affinity purified strongly with Erv1-HISPC and *erv1*-12-HISPC extracts (Figure S2-1). The bands were excised from the gel, digested with trypsin, and the proteins were identified by mass spectrometry. Specifically, a new partner protein, Aim32, was enriched in the mitochondrial lysates from the *erv1*-12-HISPC and Erv1-HISPC yeast strains compared to the control, untagged WT strain (Figure S2-1).

We confirmed the interaction between Erv1 and Aim32 using a strain in which Erv1 was tagged with a C-terminal histidine tag (Erv1-His) [10]. Similar to cyt *c* and Mia40, a fraction (~10%) of Aim32 co-purified with Erv1; as a control, the tested proteins were not detected in the untagged WT strain (Figure 2-1A). Because we have identified Osm1 as a new partner protein of Erv1[12], we performed a similar analysis to determine if Aim32 co-purified with a C-terminal His-tagged Osm1 (Figure 2-1B). We utilized the Osm1-His strain and found that a fraction (~5%) of Aim32 co-purified with Osm1. Using 2-dimensional (2D) gel analysis (BN-PAGE followed by reducing SDS-PAGE), Aim32 was present in several complexes ranging between 70 and 230 kDa and co-migrated with complexes that contained Erv1 (~100 to 200 kDa) and Osm1 (~100 to 200 kDa) (Figure 2-1C). In sum, we demonstrate that a subset of Aim32 interacts with Erv1 and Osm1 and migrates in similar-sized complexes.

2.4 Aim32 is dual localized to the IMS and matrix of the mitochondria

To confirm a function in mitochondria, we localized Aim32 (Figure 2-2A). Lysates from spheroplasts were subjected to differential centrifugation and fractions from the 13K pellet (mitochondria) and the 40K supernatant (cytosol) and 40K pellet (microsomes) were separated by SDS-PAGE. Immunoblotting with appropriate markers, Erv1 and Ccp1 for mitochondria, hexokinase for cytosol, and protein disulfide isomerase (PDI) and Sec62 for ER, verified integrity of the fractionation. Aim32 purified with the mitochondrial fraction.

The sub-mitochondrial localization of Aim32 was determined using osmotic shock in the presence of proteinase K (Figure 2-2B). OM marker Tom70 was degraded immediately, whereas matrix marker Tim44 was inaccessible to protease, even in low sorbitol concentration. IMS

markers cyt *b2* and Erv1 were degraded as the sorbitol concentration decreased. Aim32 showed a similar degradation pattern to the IMS markers. As a control, the addition of detergent resulted in degradation of all proteins. Of note, a small fraction of Aim32 remained protease resistant at 0 to 0.1 M sorbitol; this may indicate that osmotic shock did not lyse the mitochondrial OM or a fraction of Aim32 may be localized to the matrix.

We employed an alternative strategy with *in vitro* import of radiolabeled Aim32 followed by osmotic shock to confirm mitochondrial localization (Figure 2-2C). Imported Mia40 and Aim32 were cleaved by proteinase K, but matrix-localized Su9-DHFR was protected from protease. The addition of detergent also resulted in degradation of Aim32 and Mia40; DHFR was not efficiently degraded because it was tightly folded[12]. The imported form of Aim32 was slightly smaller than the translated standard, which suggests that the N-terminal targeting sequence may be cleaved (Figure 2-2C). To confirm this, using recombinant matrix processing peptidase (MPP) or the presequencing processing peptidase (Cym1), cleavage of radiolabeled Aim32 was tested[33]. Based on a putative cleavage site at the 13th amino acid [predicted using MitoFates[34]], MPP likely cleaved Aim32 at the N-terminus (Figure 2-2D), resulting in a ~1 kDa shift. In contrast, MPP that was inactivated by the addition of EDTA and *o*-phenanthroline[35] as well as Cym1 failed to cleave Aim32. MPP activity was confirmed by cleavage of the Su9 targeting sequence in Su9-DHFR (Figure S2-2A). Thus, during mitochondrial protein import the N-terminus of Aim32 enters the matrix for processing by MPP.

Because previous studies localized Aim32 to the matrix[24,36], which contrasts with our IMS-based interactions with Erv1 and Osm1, we utilized the TEV protease cleavage assay to

determine the mitochondrial localization of Aim32 *in vivo*[37,38]. The TEV protease, under control of an inducible promoter, was targeted to the IMS (CYB2-TEV) or the matrix (Su9-TEV). A construct that contains Aim32 with a 3X-FLAG tag, TEV cleavage site and HA tag (Aim32 FLAG-TEV-HA) was co-transformed and processing of Aim32 was examined (Figure 2-2E). When the TEV protease was induced in both the IMS and matrix locations, the HA tag from Aim32 was cleaved and an antibody against Aim32 confirmed the presence of this Aim32 form, which corresponds to removal of the ~5 kDa HA tag. Although the processing of Aim32 FLAG-TEV-HA was not complete, additional control experiments indicated that this cleavage was specific to CYB2-TEV and Su9-TEV. In particular, a similarly-tagged construct expressing Nuc1 that localizes exclusively to the IMS[39] was processed only when the IMS-localized TEV protease (CYB2-TEV) was induced (Figure S2-2B). Such incomplete processing by the TEV proteases has been reported by Okamoto et al. for Mmm1p[37].

Aim32 association with the membrane was tested using carbonate extraction over the pH range 10.5 to 12.5 (Figure 2-2F)[40]. In control reactions, integral membrane protein Tim23 remained in the pellet until pH 12, whereas soluble cyt *c* was present in the supernatant over the entire pH range. Mia40, which is anchored by a single transmembrane domain, showed an intermediate pattern switching from the pellet to the supernatant at pH 12. Aim32 remained in the supernatant over the entire pH range, indicating that Aim32 is a soluble protein. In sum, Aim32 is a soluble protein that localizes to the mitochondrial IMS and matrix.

Additional characterization of the Aim32 import pathway revealed that Aim32 import required a membrane potential for translocation, and this import was reduced by 80% in the

tim23-2 mutant mitochondria (Figure 2-2G)[41]. Aim32 import in the presence of the Erv1-specific inhibitor MitoBloCK-6 (MB-6)[42] was also reduced by 55% (Figure 2-2H). Thus, Aim32 translocation requires the TIM23 translocon for import into the mitochondrial matrix, and the MIA pathway may be required for partitioning Aim32 to the IMS or for modification of redox properties.

2.5 Aim32 is structurally similar to thioredoxin-like ferredoxin proteins

To Multiple protein sequence alignment using PROMALS[43] show that the C-terminal portion of Aim32 sequence aligns well with the Sucrase/ferredoxin-like family proteins from *Arabidopsis thaliana* (UniProt identifier, Q9FG75) and *Aspergillus fumigatus* (UniProt identifier, Q4WDI8). Secondary structure predictions revealed that the C-terminal region of Aim32 (~100 amino acids) has an overall α-helix/β-strand architecture, which is a variation of the classical thioredoxin fold (Figure S2-3A). Furthermore, the C-terminal TLF domain contains a CX8C and HX3H motifs and a key tryptophan residue that is conserved among other known ferredoxin proteins (Figure S2-3B). Our analyses are in agreement with studies published by Stegmaier et al. that experimentally show that Aim32 coordinates a [2Fe-2S] cluster[24]. Thus, Aim32 is a bonafide [2Fe-2S] protein, and the CX8CXnHX3H motif within Aim32 most likely constitutes its active site.

2.6 Conserved residues within CX8CXnHX3H motif of Aim32 are important for function

The requirement for Aim32 under different growth conditions was tested with a strain deleted for AIM32 (*Δaim32*). AIM32 is not an essential gene but is required for growth on rich or

minimal glucose medium under anaerobic conditions and on respiratory media at 37°C (Figure 2-3A, B). When rich glucose media was supplemented with ethidium bromide, which causes loss of mitochondrial DNA (referred to as ρ^0)[44], the *Δaim32* strain and control *Δtim54* strain were not viable (Figure 2-3A). Growth in the presence of hydroxyurea (HU) and reductant N-acetylcysteine (NAC) was also tested because deletion of the *AIM32* homolog, APD1, results in hydroxyurea sensitivity[24,45]. The *Δaim32* strain was sensitive to hydroxyurea and the addition of reductant did not restore growth (Figure 2-3C). Furthermore, the *Δaim32* strain displayed increased growth sensitivity in the presence of an uncoupler (Figure S4A). However, growth defects observed under anaerobic conditions and in the presence of hydroxyurea were rescued by subsequent expression of plasmid-borne *AIM32* (Figure 2-3B, C & Figure S2-4D). No change in mitochondrial network morphology was observed between the *Δaim32* and parental WT strain (Figure 2-4C). Thus, the *Δaim32* strain has a petite-negative phenotype and Aim32 is required for respiration at elevated temperatures, and against HU-induced stress. To address the importance of the conserved residues in the CX8CXnHX3H motif as well as the conserved tryptophan (Figure S2-3B), strains that contained mutations in these residues were constructed (termed pC213, 222S; pH249, 253A; and pWStop that terminates at lysine 279 and eliminates the conserved tryptophan and additional 33 C-terminal amino acids). Plasmids expressing WT and *aim32* mutants were transformed into *Δaim32* cells; Aim32 expression was verified by immunoblotting (Figure S2-4E). The strains were tested for growth in the presence of HU and on respiratory media (Figure 2-4D); all mutants showed reduced growth on HU and respiratory media at 37°C. As in Figure S2-4A, the Aim32 mutants also showed decreased growth in the

presence of mitochondrial uncoupler (Figure S2-4B). Thus, the cysteine, and histidine residues that coordinate the [2Fe-2S] cluster[24] and the terminal tryptophan residue are important for Aim32 function.

2.7 Aim32 is required for assembly of the import complexes

Because Aim32 interacts with Erv1, we performed import studies with mitochondria from WT and *Δaim32* cells. The membrane potential (ΔΨ) of isolated mitochondria was measured using the fluorescent dye 3, 3'-dipropylthiadicarbocyanine iodide [DiSC3(5)][46]. Mitochondria from the *Δaim32* strain had a decreased ΔΨ of ~20% (Figure 2-4A). Aim32 seemed to depend on itself for translocation, because import was compromised by 55% in *Δaim32* mitochondria (Figure 2-4B). The import of MIA substrates Tim9 and Tim10 was decreased by ~80%, whereas the import of Cmc1 was reduced by ~50% (Figure 2-4C). However, a modest reduction for a subset of TIM23 substrates (Tim50, Hsp60, and Mia40) and TIM22 substrates (Tim22 and AAC) in import was noted, whereas import of Su9-DHFR was not compromised (Figure 2-4D, E). Finally, import of Osm1 into *Δaim32* mitochondria was strongly decreased. Thus, mitochondria that lack Aim32 are generally compromised in protein import, particularly for proteins that use the MIA pathway. To complement the import studies, the steady-state level of mitochondrial proteins was determined by immunoblot analysis (Figure 2-5A). Mitochondria were purified from the WT and *Δaim32* strains grown in rich glucose media at 30°C to mid-log phase. In agreement with reduced import of the MIA substrates, the abundance of the small Tim proteins was diminished in the *Δaim32* strain. With the exception of Tim23, the steady state level of additional mitochondrial proteins in the TIM23, TIM22, MIA, and respiratory complexes was

not markedly reduced. We followed with blue-native (BN) gel analysis to assess complex assembly. The TIM22, TIM23, and small Tim complexes were markedly decreased in mitochondria from the □aim32 strain (Figure 2-5B). Tim23 assembly into the $TIM23^{SORT}$ complex was particularly defective. In addition, Oxa1 assembly in a large complex was decreased (Figure 2-5B). Similar defects in complex assembly were observed when Tim22 and Tim23 import and complex assembly was analyzed by BN-gels (Figure 2-5C). With two dimensional (2-D) BN/SDS-PAGE analysis, complexes with Osm1, Erv1, and Mia40 were monitored in WT and *Δaim32* mitochondria. Four Aim32 complexes of ~140 to 500 kDa were highlighted with red arrows (Figure 2-5D). In *Δaim32* mitochondria, assembly of Erv1, Mia40, and Osm1 complexes was markedly altered (indicated by black arrows in Figure 2-5D), even though the steady state levels of these proteins were not decreased. Thus, Aim32 seems to be required for correct assembly/stability of numerous import complexes.

2.8 Aim32 has multiple binding partners

Considering that import of diverse precursors and assembly of various import complexes is impaired in cells that lack Aim32, we used mass spectrometry to identify potential Aim32-interacting proteins. Mitochondrial lysates from *Δaim32* strains expressing a C-terminal FLAG-tagged Aim32 ([pAIM32-FLAG], expression controlled from the GPD promoter) or an empty vector (Vec) were purified with FLAG-beads and, after washing, subjected to mass spectrometry. Several key components of the TIM23 translocon (Tim17, Tim23, Tim50) and Mia40 were identified as potential binding partners (Table 2-1). To validate these interactions, specific co-purifications were performed (Figure 2-6A). A fraction (~10%) of Tim17, Tim23, Tim22, Tim50

and Sod2 co-purified with Aim32-FLAG. Reciprocal pull-downs were also performed with His-tagged Tim17 and Tim23 strains and Aim32 co-purified with Tim17 and Tim23 (Figure S2-5). A small fraction of Mia40 also co-purified with FLAG-tagged Aim32, but Erv1 and Osm1 were not detected (Figure 2-6A). To determine if the tag might impact interactions, we placed the HisPC tag on the C-terminus of Aim32. Upon generation of the Aim32-HisPC strain, we showed that Osm1 co-purified with Aim32, but Erv1 and Mia40 were not detected (Figure 2-6B). In sum, Aim32 seems to bind to several proteins, particularly import components, but the stability of interaction may be impacted by the presence or placement of a tag. Thus, Aim32 interactions may be transient with partner proteins.

Because Aim32 was identified as an Erv1-binding partner, we investigated the redox status of Erv1 in mitochondria from WT and *Δaim32* strains using thiol trapping with methyl-PEG-24-maleimide (mmPEG) (Figure 6C)[47]. When presented with reduced substrates in in vitro reconstituted systems, the two shuttle cysteine residues as well as the active site cysteines are crucial for Erv1 oxidase activity[48]. In control reactions in which Erv1 was treated with reductant DTT at 95^0C (Figure 2-6C, lanes 2 and 7), six mmPEG molecules bound to Mia40, resulting in a mass shift of ~ 7 kDa compared to treatment with DTT alone (lanes 1 and 6). In other control reactions, treatment with either IAA or mmPEG alone (lanes 5 and 9) did not result in any mobility shifts. Pretreatment with IAA, followed by disulfide reduction with DTT and subsequent mmPEG modification (Figure 2-6C, lane 3 and 8), resulted in a Erv1 species that migrated more slowly than reactions in lanes 2 and 7, thereby indicating partial oxidation of Erv1 by mmPEG. In WT mitochondria, Erv1 is present in an oxidized state (Figure 2-6C, lane 9

mmPEG addition), whereas a subset of Erv1 remained reduced (marked with an asterisk, lane 4) in *Δaim32* cells. Thus, thiol trapping analysis suggests that Aim32 influences the redox status of Erv1 under aerobic conditions.

2.9 Aim32 is required for maintaining the global redox status

We postulated that analogous to thioredoxin proteins, Aim32 may function in maintaining the global redox status of the mitochondrial proteome. Two-dimensional diagonal gel electrophoresis (2D-DGE) in which the first dimension was non-reducing followed by a reduction in the second dimension was used (scheme in Figure 2-7A). The redox status of specific proteins, previously found to interact with Aim32, was investigated by immunoblot analysis. Osm1, Mia40, Erv1, Tim13, and Tim50 had altered disulfide linkages (as highlighted by arrows in Figure 2-7B) in the *Δaim32*. A fraction of Aim32 migrated below the diagonal (indicated by dashed box), indicating Aim32 seems to form disulfide linkages with several proteins under normal physiological conditions.

In a second approach, we probed the thiol proteome with iodoacetamide-labeled rhodamine (IAA-rhodamine), based on Hill et al[49]. Free thiols in mitochondrial lysates were reacted by irreversible alkylation with IAA-rhodamine and separated by a 2D-DGE as in Figure 2-7B. Increased IAA-rhodamine labeling of proteins with non-native disulfide bonds was observed in the *Δaim32* mitochondria (Figure 2-7C, marked by dashed green circle). Thus, Aim32 plays a role in maintaining the global redox status.

2.10 Conserved cysteine residues in the TLF domain of Aim32 are critical for function

We examined the importance of conserved cysteine residues 213 and 222 of the TLF domain by constructing individual changes to serine (designated C213S and C222S, Figure S2-3). Aim32 and mutant proteins were overexpressed ~10-fold from a 2-micron plasmid (Figure 2-8B), because expression from a centromeric plasmid was not detected. A C-terminal FLAG tag as in Figure 2-6A was also included. These strains grew at 30ºC but arrested growth at 37ºC on ethanol-glycerol media (YPEG & SEG-URA), similar to the *Δaim32* strain expressing the empty vector (Vec, Figure 2-8A). Also, growth of the cysteine mutants was compromised in media supplemented with hydroxyurea (Figure 2-8A)[24]. Additional cysteine mutants were tested (C38S, C40S and C291S) and results indicated these changes did not alter cell growth (data not shown) [24].

The steady-state level of mitochondrial proteins in mitochondria from the cysteine mutants was examined (Figure 2-8B). The Aim32-FLAG proteins migrated slightly higher than Aim32 and were overexpressed ~10-fold. Tim23, Tim22, Tim13, and Yme1 were present at increased abundance in the cysteine mutant strains (Figure 2-8B). In contrast, the amount of Tim13, Tim22, and Tim23 was decreased in the *Δaim32* strain (Figure 2-5A). The abundance of other proteins in the cysteine mutants, however, was not strongly changed (Figure 2-8B). We also tested assembly of the import complexes (Figure 2-8C) and showed that, in the single cysteine mutants, the TIM22 and TIM23 complexes seem to have several assembly states and the small Tim and Yme1 complexes were not impaired in assembly.

Finally, we examined the mitochondrial redox status of protein thiols as in Figure 2-7 in the strains with the single cysteine mutants C213S and C222S. An increase in proteins with non-

native disulfide was observed for the single cysteine mutants in contrast to WT and the strain that lacks Aim32 (Figure 2-9A, green dashed circles). With 2D-DGE followed by immunoblotting against Aim32, an overabundance of disulfide-linked Aim32 heterodimers in the single cysteine mutants (Figure 2-9B) was observed. The overexpression strain (*Δaim32* [pAIM32-FLAG]) was included as a control strain because the expression of Aim32 is comparable across strains (Figure 2-8B). Because we have previously shown that Aim32 interacts with multiple proteins via disulfide-linked heterodimers (Figure 2-7B), the single cysteine mutants may be trapped via intermolecular thiol bonds with many proteins. In sum, cysteine residues, C213 and C222, of the TLF domain are important in redox modulation.

2.11 Discussion

Aim32 is dually localized to the mitochondrial IMS and matrix.

In this study, we report the physiologic characterization of Aim32, a mitochondrial Fe-S protein that has a highly conserved C-terminal TLF domain (Figure S2-3). Stegmaier et al. recently completed a chemical characterization of Aim32 and showed that it is a bis-histidinyl coordinated [2Fe-2S] protein[24]. They also proposed a role for Aim32 in degradation of allelochemicals. Aim32 was also localized to the mitochondrial matrix and/or IM in several studies, including large scale screens[24,36,50]. However, mitochondrial specific functions for Aim32 have not been assigned.

Our analysis reveals that Aim32 is dual-localized to both the IMS and matrix, which is atypical for mitochondrial proteins. As this was unexpected, we used several complementary approaches with endogenous and tagged Aim32 proteins to confirm this localization to both

mitochondrial compartments. Aim32 was identified as an Erv1-interacting protein, suggesting a role for Aim32 in the IMS. Localization of Aim32 to the IMS was corroborated by osmotic gradient experiments with intact mitochondria and with *in vitro* imported Aim32 into mitochondria. Studies with the *in vivo* site-specific (TEV protease) cleavage assay, however, confirmed localization in both the IMS and matrix.

We demonstrate that Aim32 relies mostly on the TIM23 pathway for import into the mitochondria. Aim32 contains an N-terminal mitochondrial-targeting sequence (MTS) that is efficiently cleaved by MPP, in agreement with an MPP cut-site predicted by MitoFates (at the 13th amino acid). Aim32 import also requires a membrane potential to initiate translocation across the TIM23 translocon. Thus, MPP cleaves the MTS of Aim32 as it enters the matrix. An involvement of the MIA pathway for localization to the IMS cannot be excluded based on our localization studies, and reduced import in the presence of MB-6, an Erv1-specific inhibitor (Figure 2-2H). Only one processed form of Aim32 is detected in all our studies. Thus, the Aim32 pool is likely processed by MPP. A pathway for Aim32 import and maturation may be proposed in which a cohort of Aim32 molecules are fully imported into the matrix, processed by MPP, and assembled. Then, some processed Aim32 may halt translocation and fall back into the IMS. This "stop-transfer" of Aim32 into the IMS may be akin to MPP-processed fumarase that accumulates in the cytosol[51], with the exception that the C-terminus of Aim32 completely enters the IMS. The IMS-cohort of Aim32 may be regulated by the activity of molecular chaperones, and/or binding to IMS proteins (e.g., Erv1, Mia40). Aim32 localization in the IMS maybe biased under specific conditions of stress. For example, human CCS1 and SOD1 import into the IMS are linked to

mitochondrial ROS levels[52], and p53 localizes to mitochondria via Mia40 under stress conditions[54]. Future studies to establish the relevance of Aim32 activity in both mitochondrial compartments are warranted.

Aim32 is required for maintaining the global redox status

Although *AIM32* is not essential for viability, the protein is required for respiration at elevated temperature and cells that lack *AIM32* are petite-negative, indicating that the mitochondrial genome cannot be lost when Aim32 is deleted. Moreover, Aim32 is required when cells are challenged with hydroxyurea.

A recent genome-wide screen suggested that Aim32 was a crucial factor for the intracellular sorting of the mitochondrial IM protein Oxa1[55]; however, the mechanism is not clear. In our analyses, cells depleted for *AIM32* showed reduced Oxa1 complex assembly, however, the steady-state levels of Oxa1 remained unaffected (Figure 2-5). The requirement of Aim32 was not restricted to Oxa1 because steady-state levels and import of newly synthesized MIA pathway precursors were severely impacted as well (Figures 4, 5). Furthermore, the assembly profile of several essential protein import complexes (TIM22, TIM23^{SORT}, small TIM, and Erv1) was altered in the absence of functional *AIM32*. Given that Aim32 has numerous binding partners, Aim32 may have a global role in quality control and/or stabilization of mitochondrial protein, including the import complexes.

Our study supports a global role for Aim32 in maintaining the redox status of the mitochondrial proteome. In the absence of *AIM32*, we find that the mitochondrial thiol proteome contains an increase in aberrant thiol linkages (Figure 2-7C). The 2D-DGE/western blot analysis

highlighted several mixed disulfide linkages formed between Aim32 and target proteins (Figure 2-7B) and the redox status of a subset of candidate proteins investigated (i.e., Tim13, Tim50, and Osm1) was altered. Specifically, Aim32 redox-active cysteine mutants displayed an increase of Tim22 dimer and decrease of mature TIM22 complex (Figure 2-8C), suggesting that the Tim22 dimer was not assembling efficiently or the TIM22 complex was destabilized[56]. Similar destabilization of the TIM23^{SORT} complex was observed in the cysteine mutants. Analysis of the mitochondrial thiol proteome in the single cysteine mutants of Aim32 (C213S, C222S) revealed an increase in aberrant thiol interactions (Figure 2-9A), along with several "trapped" mixed disulfide intermediates formed between Aim32 and target proteins (Figure 2-9B).

The trapped intermediates suggest that Aim32 potentially maintains/repairs proteins that maybe oxidized. In the absence of *AIM32* or in the Aim32 cysteine mutants, yeast are susceptible to conditions of stress (Figures 2-4 & 2-8A). We demonstrate that a portion of matrix-localized Aim32 is physically bound to Sod2 (Figure 2-6). Moreover, overexpression of *AIM32* protected yeast cells against PQ-induced oxidative damage in the absence of *SOD2*, the cells primary defense mechanism against mitochondrial ROS[23]. Because Aim32 can repair oxidized cysteine residues, protein activity can be restored after exposure to cellular stress. Because the Aim32 single cysteine mutants form mixed disulfide intermediates, future studies can be designed to identify substrates and determine the molecular basis of the interaction with substrates. In sum, this study begins to dissect the role of Aim32, a thioredoxin-like ferredoxin protein that normally resides within the mitochondrial matrix and functions in quality control.

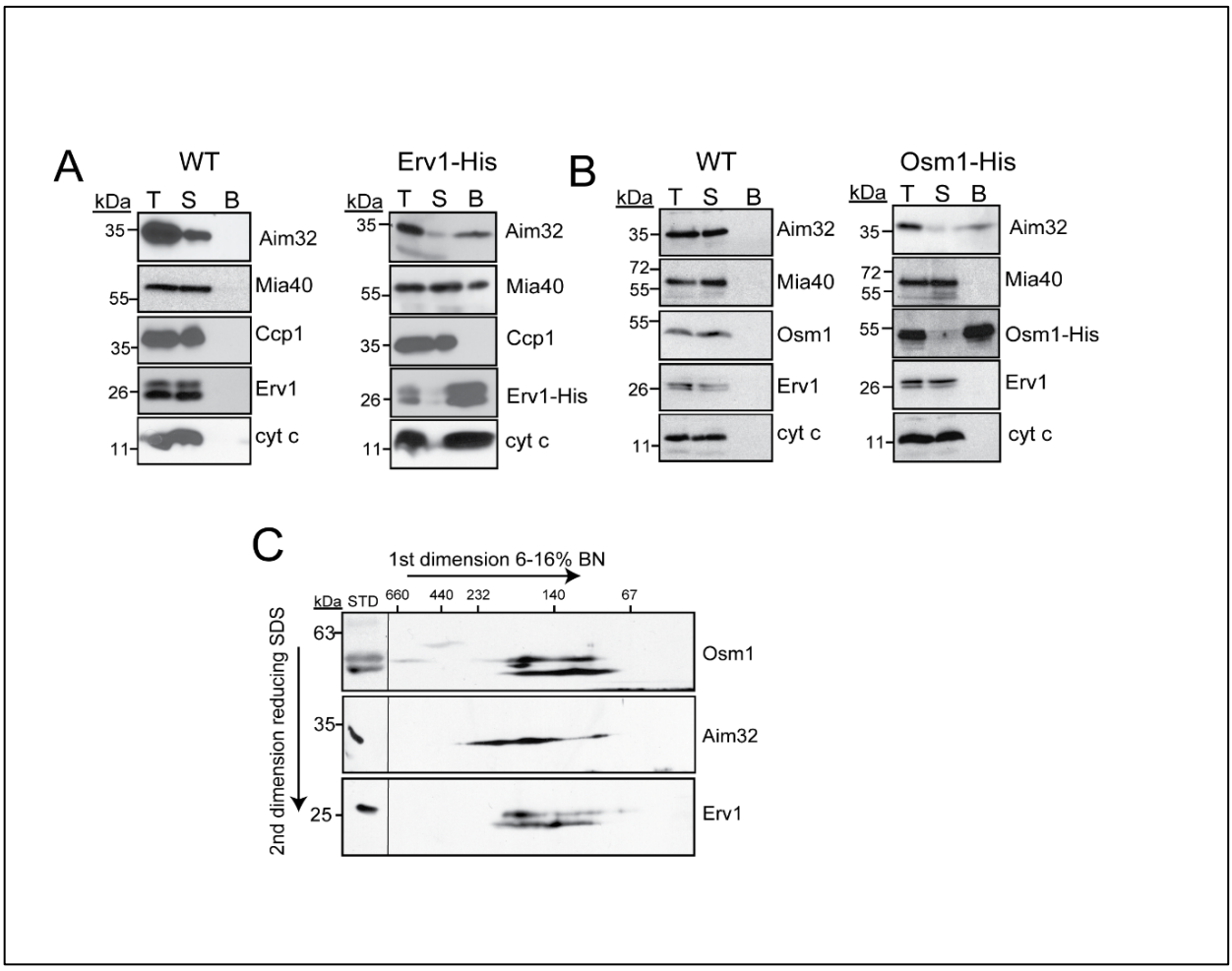

Figure 2-1 Aim32 binds to Osm1 and Erv1. (A) Mitochondria from WT (left panel) or a strain expressing a C-terminal histidine tagged Erv1 (Erv1-His) (right panel) were solubilized in 1% digitonin. As a control, 25 µg of total extract (T) was withdrawn, and 500 µg lysate was incubated with Ni2+-agarose beads. The beads were washed, and bound protein (B) was eluted. 25 µg of the flow-through fraction (S) was also included. Samples were resolved by SDS-PAGE and analyzed by immunoblotting with specific antibodies against Aim32, Mia40, Ccp1, Erv1, and cyt c. (B) As in 'A', except that mitochondria from a strain expressing a C-terminal histidine tagged Osm1 (Osm1-His) was used. (C) WT mitochondria were solubilized as in 'A' and then separated in the first dimension on a 6-16% BN gel, followed by reducing SDS-PAGE in the

second dimension. Aim32, Osm1, and Erv1 were detected by immunoblotting.

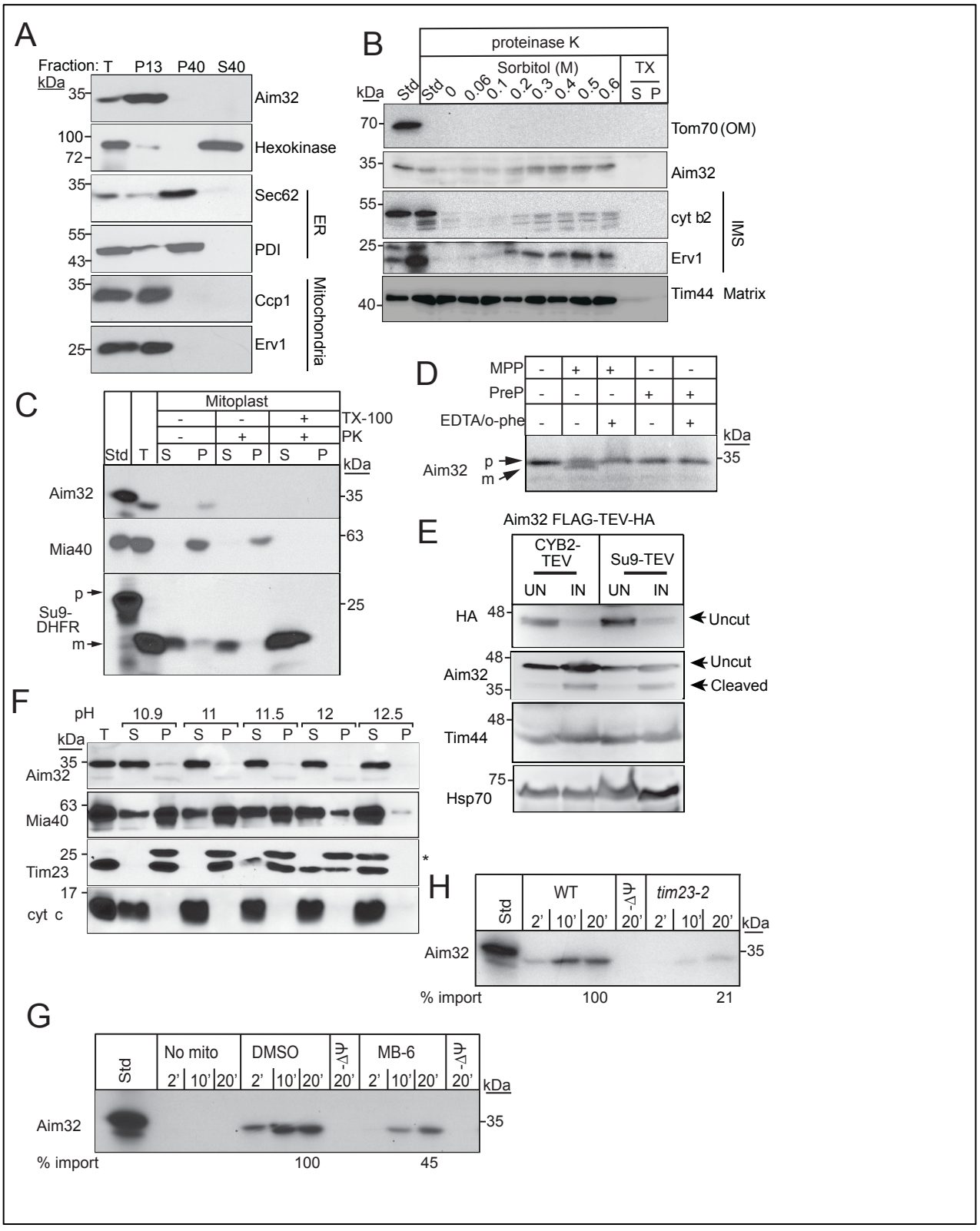
A
Fraction: T P13 P40 S40
kDa
35
Aim32
100
72
Hexokinase
35
Sec62
ER
55
PDI
43
35
Ccp1
Mitochondria
25
Erv1
B
proteinase K
Sorbitol (M)
TX
kDa
Std
Std 0 0.06 0.1 0.2 0.3 0.4 0.5 0.6
S P
70
Tom70 (OM)
35
Aim32
55
cyt b2
IMS
25
Erv1
40
Tim44
Matrix
C
Mitoplast
TX-100
PK
Std T S P S P S P
kDa
Aim32
35
Mia40
63
p
Su9-
DHFR
m
25
D
MPP
PreP
EDTA/o-phe
kDa
Aim32
p
m
35
E
Aim32 FLAG-TEV-HA
CYB2-
TEV
Su9-TEV
UN IN UN IN
HA
48
Uncut
48
Aim32
35
Uncut
Cleaved
48
Tim44
75
Hsp70
F
pH
10.9
11
11.5
12
12.5
kDa
T S P S P S P S P S P
35
Aim32
63
Mia40
25
Tim23
*
17
cyt c
H
Std
WT
-ΔΨ
tim23-2
2’ 10’ 20’ 20’ 2’ 10’ 20’
kDa
Aim32
35
% import
100
21
G
Std
No mito
DMSO
-ΔΨ
MB-6
-ΔΨ
2’ 10’ 20’ 2’ 10’ 20’ 20’ 2’ 10’ 20’ 20’
kDa
Aim32
35
% import
100
45

Figure 2-2 Aim32 is a soluble protein of the mitochondrial IMS and matrix, and import is facilitated by the TIM23 translocon. (A) The WT strain was grown in YPEG at 30^0C and converted to spheroplasts. The total homogenate (T) was fractionated into mitochondria (P13), microsomes (P40), and cytoplasm (S40). An equal amount of each fraction was separated by SDS-PAGE and analyzed by immunoblot using the indicated antibodies. Markers include hexokinase (cytosol), Sec62 and PDI (ER), and Ccp1 and Erv1 (Mitochondria). (B) Mitochondria were incubated in 20 mM HEPES-KOH, pH 7.4, 100 µg/ml proteinase K, and the indicated sorbitol concentrations at 4^0C for 30 min, followed by addition of 1 mM PMSF. After centrifugation, the pellet was analyzed by SDS-PAGE and immunoblotted with antibodies against the indicated proteins. OM, outer membrane; IMS, intermembrane space (C) Import of radiolabeled Aim32 into WT mitochondria was followed by osmotic shock [final concentration 20 mM HEPES-KOH, pH 7.4, 100 µg/ml proteinase K (PK) and 0.06 M sorbitol, termed Mitoplast] as described in (B). Su9-DHFR (matrix-targeted) and Mia40 (IMS-targeted) were used as controls. p, precursor; m, mature (D) Mitochondrial processing peptidase (MPP) cleavage assay was performed with the addition of 10 µg recombinant MPP to radiolabeled Aim32, and the samples were resolved on a 12% Tris-Tricine gel. As a negative control, 10 µg recombinant presequence protease (Cym1) was added to radiolabeled Aim32. 5 mM EDTA and 2 mM o-phenanthroline were added to inhibit activity of MPP. Samples were separated by SDS-PAGE and visualized using autoradiography. (E) *Δaim32* cells expressing Aim32-FLAG-TEV-HA were transformed with plasmids expressing matrix-localized Su9-TEV protease or IMS-localized CYB2 [1-220]-TEV protease. Cells were grown in minimal media supplemented with

2% galactose (IN; induced) or 2% sucrose (UN; uninduced) and harvested in mid-log phase. Whole cell extracts were analyzed by immunoblotting against proteins Aim32, Tim44, Hsp70, and HA. Arrows indicate uncut and cleaved Aim32 FLAG-TEV-HA proteins. (F) WT mitochondria were analyzed by alkali extraction using 0.1 M carbonate at the indicated pH. Equal amounts of the pellet (P) and TCA-precipitated supernatant (S) fractions from 50 μg mitochondria were resolved by SDS-PAGE and immunoblotted for the indicated mitochondrial markers. * indicates non-specific band. (G) Radiolabeled Aim32 was imported into WT and *tim23-2* mutant mitochondria in the indicated time course. Non-imported precursor was removed by protease treatment, and the imported Aim32 was analyzed by SDS-PAGE and autoradiography. A 10% standard (Std) from the translation reaction was included. Import reactions were quantitated using Image J software; 100% was set as the amount of precursor that imported into WT mitochondria at the endpoint of the time course. A representative gel is shown. (n = 3). (H) As in (G), Aim32 was imported into WT mitochondria in the presence and absence of a $\Delta\Psi$ and 25 μM of MitoBLoCK-6 or a vehicle control [1% dimethyl sulfoxide (DMSO)].

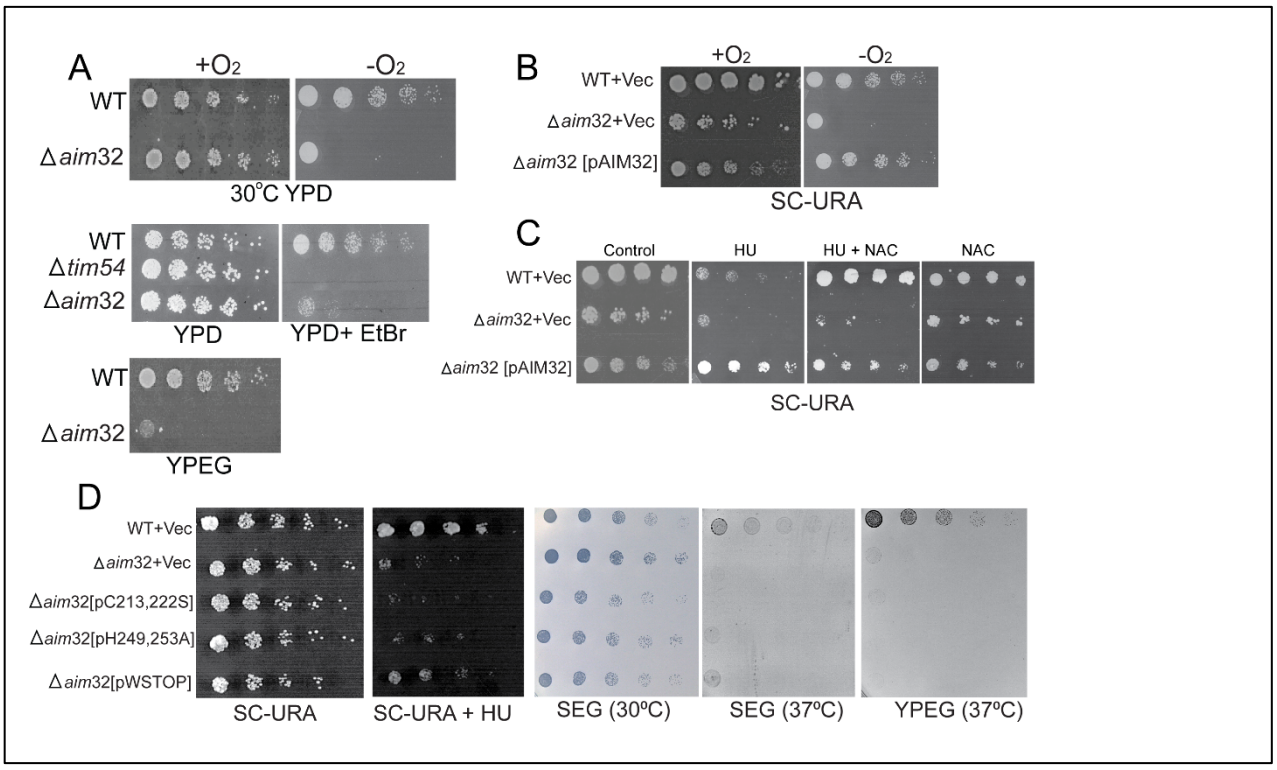

Figure 2-3 Conserved residues within the TLF domain of Aim32 are essential for mitochondrial respiration. (A) Growth analysis of Δ*aim32* and the parental (WT) strains in aerobic ($+O_2$) and anaerobic ($-O_2$) conditions on rich glucose (YPD) and ethanol/glycerol (YPEG) media was analyzed by serial 5-fold dilution of liquid cultures grown to mid-log phase. Ethidium bromide (EtBr) treatment removed the mitochondrial DNA. The *tim54-1* mutant (petite-negative) was included as a control. (B) WT and *Δaim32* strains were transformed with an empty plasmid (+Vec) or plasmid expressing Aim32 protein [pAIM32]. Serial dilutions as in (A) were spotted onto selective minimal glucose media lacking uracil (SC-URA). (C) As in (B) with the addition of 100 mM hydroxyurea (HU) or 150 mM N-acetyl-cysteine (NAC). (D) *aim32* mutants were tested as in 'C' for sensitivity to hydroxyurea or different carbon sources, on minimal ethanol/glycerol (SEG) lacking uracil or rich ethanol/glycerol (YPEG) media at 30ºC

and 37ºC. Photographs were taken after 2-3 days of incubation.

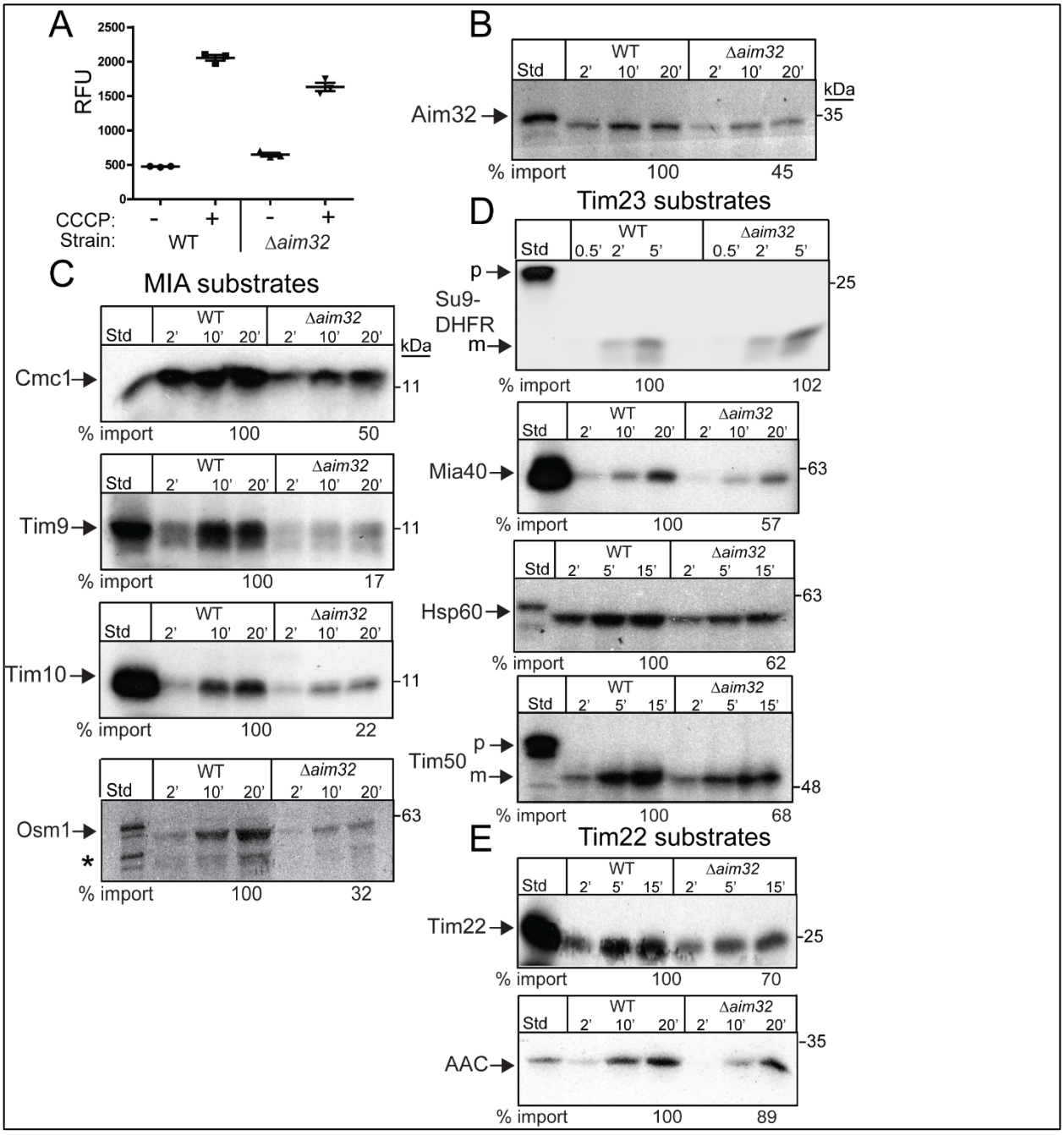

Figure 2-4 Cells lacking functional AIM32 are defective in import of diverse mitochondrial precursors. (A) Membrane potential ($\Delta\Psi$) measurements of purified mitochondria from WT and Δ*aim32* strains were performed with $DiSC_3$ and measured with a FlexStation plate reader (Molecular Devices). Coupled mitochondria sequestered and quenched the dye fluorescence;

collapse of the ΔΨ was achieved with CCCP addition. (B) Radiolabeled Aim32 was imported into WT, and Δ*aim32* mitochondria as in Fig. 2-3G. A representative gel is shown. (n = 3) (C) As in (B), representative MIA precursors (Cmc1, Tim9, Tim10, and Osm1) were imported. (D) As in (B), TIM23 substrates (Su9-DHFR, Mia40, Hsp60, and Tim50) were imported. (E) As in (B), import of TIM22 substrates (Tim22 and ACC) was tested. Samples were subjected to carbonate extraction after protease treatment. p, precursor; m, mature; * denotes nonspecific band.

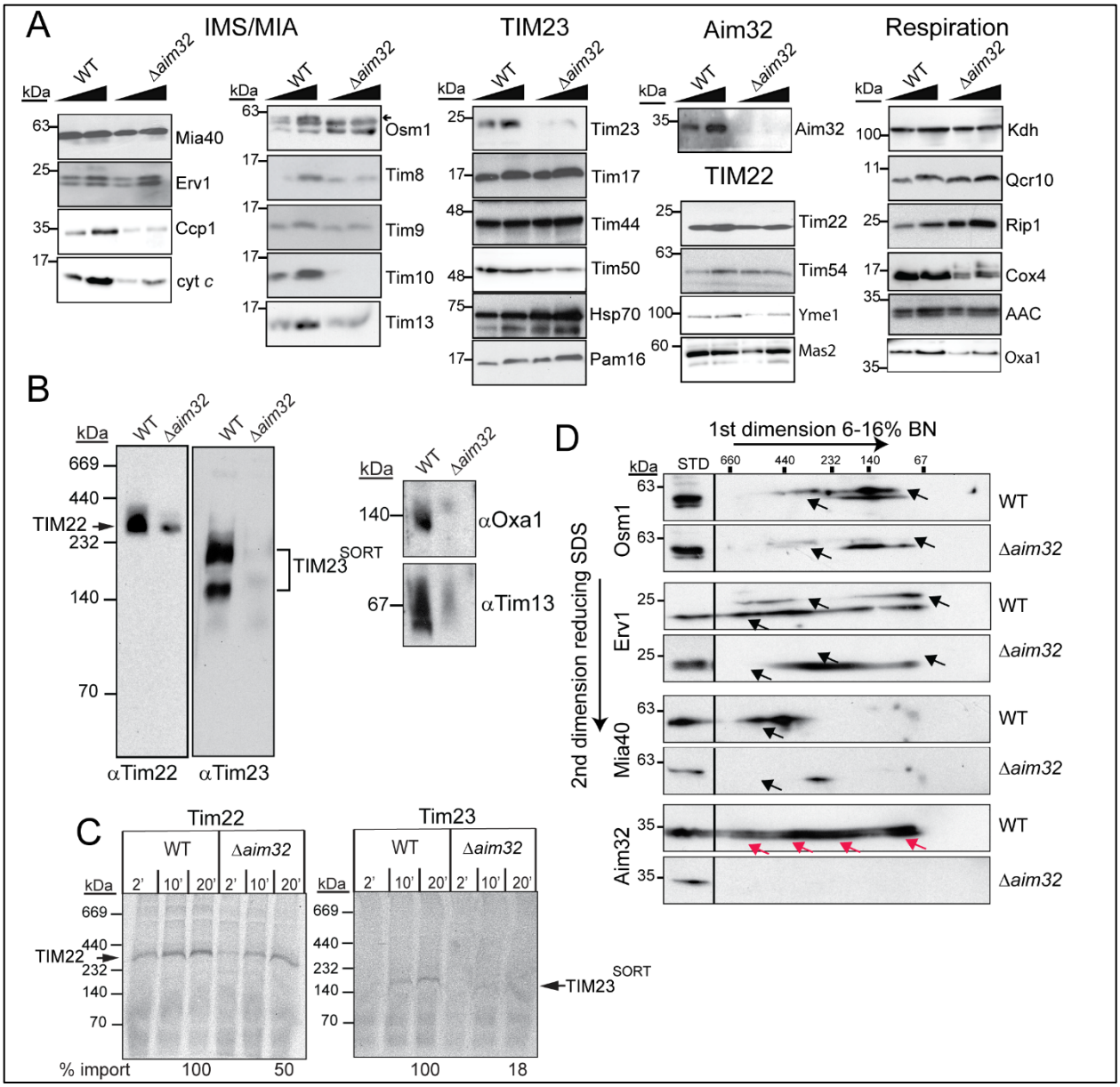

Figure 2-5 Aim32 functions in stabilization of several protein complexes. (A) A systematic analysis of steady-state levels of mitochondrial proteins (50 and 100 µg) from the parent (WT) or Δ*aim32* strain (grown at 30ºC in rich glucose media) was performed by immunoblot with antibodies against the indicated mitochondrial proteins. Proteins were organized by substrates of the MIA, TIM23 and TIM22 pathways and respiratory proteins. (B) 75µg mitochondria from the parent (WT) or Δ*aim32* strain were solubilized in 1% (wt/vol) digitonin and subjected to BN-

PAGE (6-16% acrylamide) to detect TIM22, TIM23, Oxa1, and small TIM complexes. (C) Radiolabeled Tim22 or Tim23 was imported into WT or Δ*aim32* mitochondria in a time course and subjected to BN-PAGE and digital autoradiography. Import reactions were quantitated using Image J software; 100% was set as the amount of precursor that imported into WT mitochondria at the endpoint of the time course. A representative gel is shown. (n = 3). (D) As in (B), except that BN-PAGE was followed by a reducing SDS-PAGE in the second dimension (2D), and the indicated antibodies were used. Red arrows highlight Aim32-containing complexes identified in WT mitochondria. Black arrows indicate protein-containing complexes in the WT mitochondria that are absent in the Δ*aim32* mitochondria. Note that Erv1 and Osm1 typically run as a doublet.

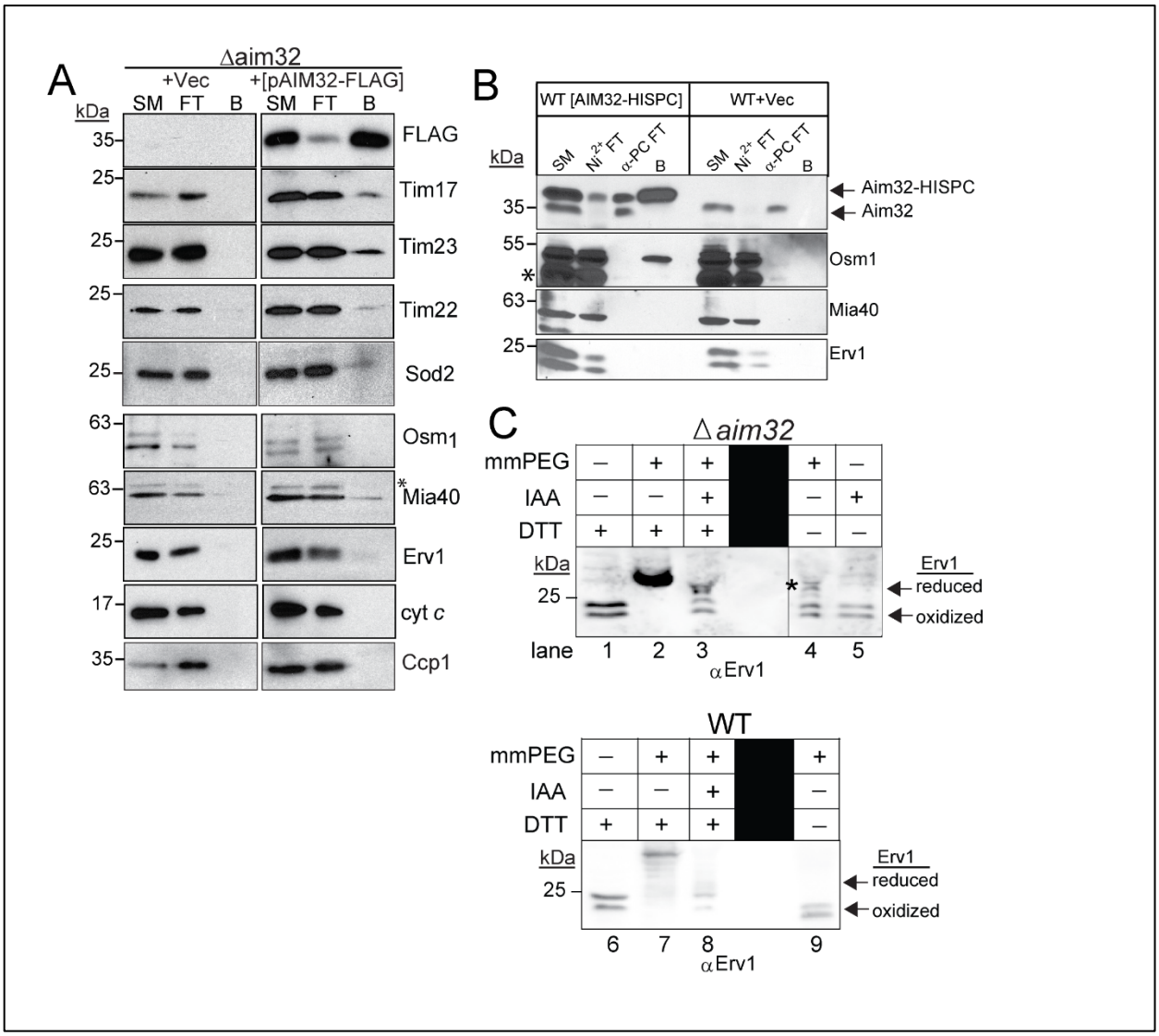

Figure 2-6 Aim32 interacts with key proteins of the MIA, TIM23 and TIM22 pathways. (A) A FLAG tag was appended to the C-terminus of Aim32 (Aim32-FLAG) and transformed into Δ*aim32*. Pull-down assays with FLAG-resin were performed as in Fig. 2-1A with the indicated antibodies. An asterisk indicates non-specific bands detected by the antibody. (B) A consecutive-affinity tag [termed CNAP for purification over Ni^{2+}-resin followed by anti-Protein C affinity (α-PC) resin] was placed on the C-terminus of Aim32. As in Fig. 2-1A, the lysate was incubated with Ni^{2+}-agarose, eluted with 300 mM imidazole and then incubated with the anti-Protein C

resin. After washing, the bound material was eluted and the indicated antibodies were used. Controls include the "flow-through" material from the Ni^{2+}-agarose (Ni^{+2}-FT) and the anti-Protein C resin (α -PCFT). (C) Analysis of the Erv1 oxidation state by thiol trapping assay. Isolated mitochondria from Δ*aim32* (lanes 1-5) and WT (lanes 6-9) were resuspended in sample buffer with dithiothreitol (DTT, lanes 1& 6), iodoacetamide (IAA, lane 5), methyl-PEG_{24}-maleimide (mmPEG, lanes 4& 9), or pretreated with IAA to block free cysteine residues (lanes 3 &8), and disulfide bonds subsequently reduced by DTT, and finally reacted with mmPEG (lanes 2,3,7,8). Samples were analyzed by SDS-PAGE and immunoblotting with anti-Erv1. The asterisk indicates reduced Erv1 species.

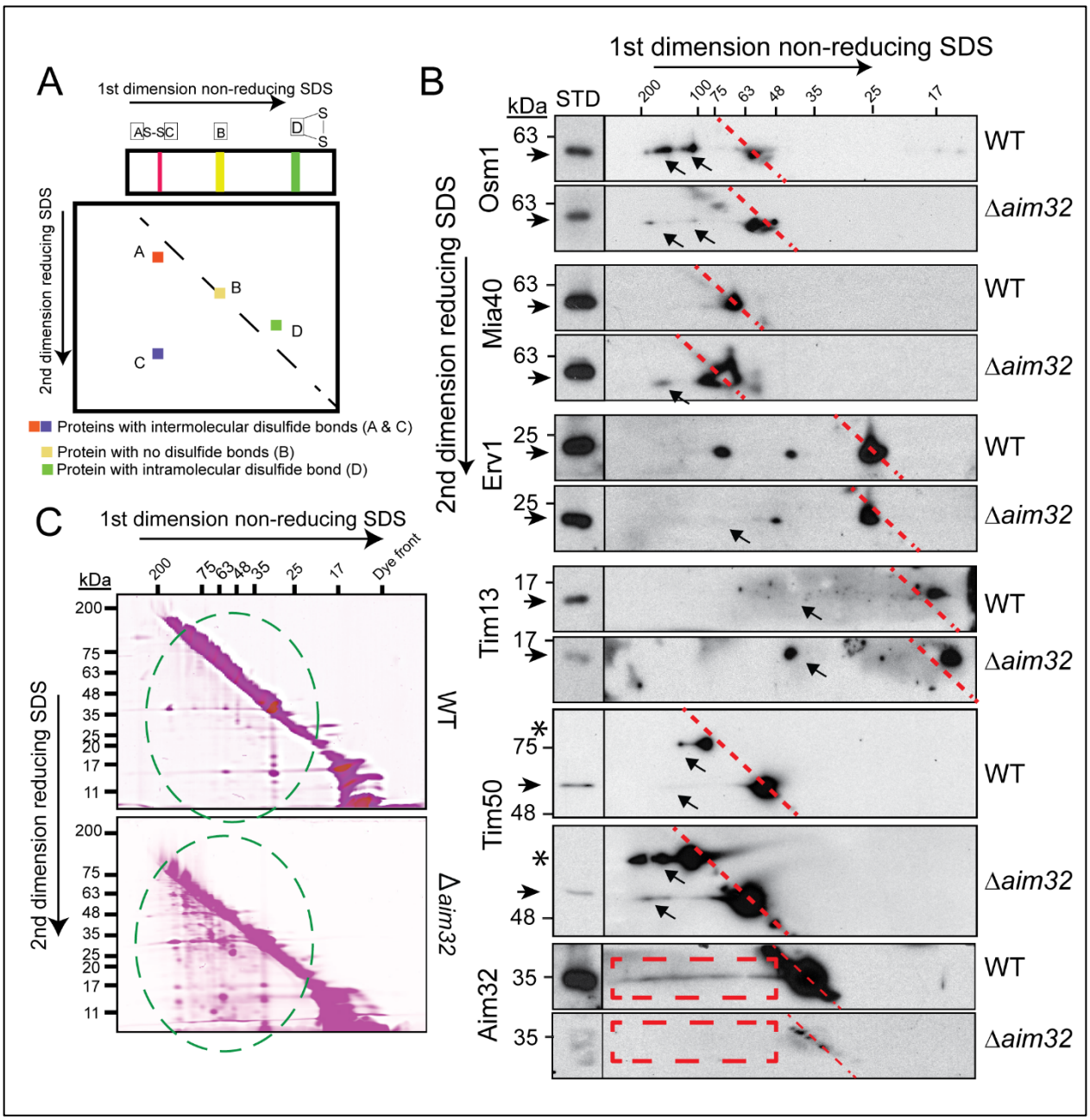

Figure 2-7 Aim32 forms disulfide bonds with diverse mitochondrial proteins and alters the disulfide proteome. (A) A general scheme for the 2-D gel electrophoresis (2DGE) wherein samples were first separated under non-reducing conditions followed by reductant treatment in the second dimension. (B) As in (A), 2DGE was performed on mitochondrial lysates from WT and Δ*aim32* strains and analyzed by immunoblotting. Dashed red line indicates the position of

the diagonal. Red boxes refer to Aim32-specific heterodimers with other mitochondrial proteins in WT mitochondria. Arrows specify places where the disulfide linkages differ in WT vs Δ*aim32* mitochondria. (C) The general redox status of thiols in the mitochondria was assessed. As in "B", except 100µg mitochondrial extract was pretreated with iodoacetamide labeled with rhodamine (IAA-rhodamine) to block free thiols followed by reduction in-gel with 1% β-mercaptoethanol. Gels were visualized using the Sapphire Biomolecular Imaging system. Representative gels are shown (n = 3). Green dashed circle indicates increased rhodamine-labelled proteins running under the diagonal in the Δ*aim32* mitochondrial extracts.

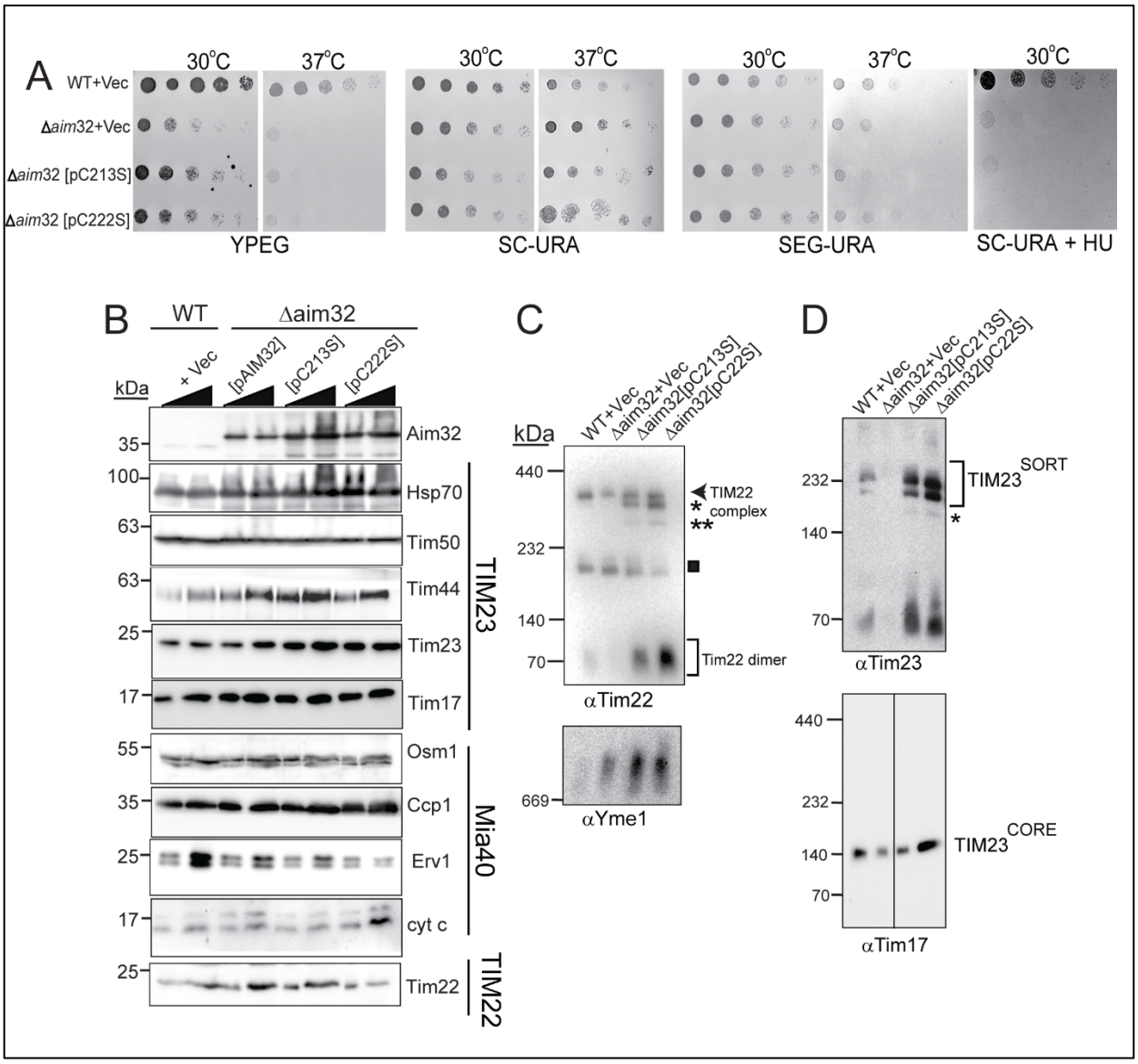

Figure 2-8 Conserved cysteine residues of Aim32 are important for assembly/stabilization of the TIM22 and TIM23 complexes. (A) Growth analysis of the indicated yeast strains at 30ºC and 37ºC on different media as in Fig. 2-4A. Strains include WT and Δ*aim32* transformed with a plasmid that contains *AIM32* with a single cysteine mutation (C213S or C222S) and a C-terminal FLAG tag or the empty vector (Vec). (B) As in Fig. 2-5A, levels of mitochondrial proteins were analyzed by immunoblotting with antibodies against the indicated proteins. Strains are from (A) and also include AIM32 with a C-terminal FLAG tag (pAIM32) (C) As in Fig. 2-5B, 75µg

mitochondria from the indicated strains were solubilized in 1% (wt/vol) digitonin and subjected to blue native (BN)-PAGE (4-16% acrylamide) to detect TIM22, TIM23^{SORT}, and the TIM23^{CORE} complexes. For the Yme1 complex, a 3-12% acrylamide BN-PAGE was used. Asterisks (*, **) indicate sub-complexes of Tim22 and Tim23.

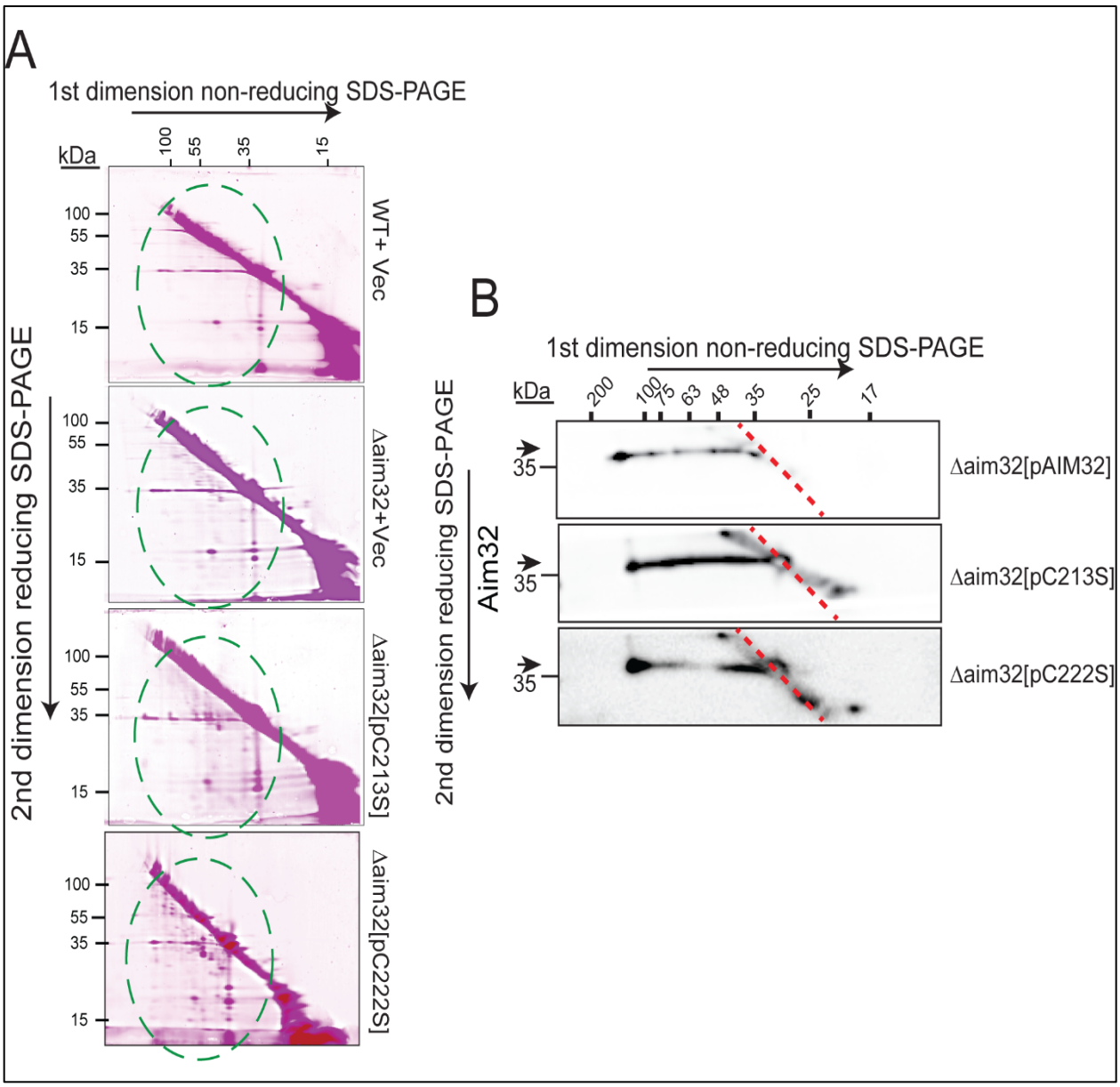

Figure 2-9 Cysteine residues 213 and 222 of Aim32 are critical for native disulfide formation in target proteins. (A) Mitochondrial lysates were analyzed as in Fig. 2-8B. The Δ*aim32* strain was transformed with WT *AIM32* (pAIM32) or *aim32* mutants with single cysteine to serine changes (pC213S or pC222S). Green dashed circles indicate regions of increased rhodamine labeling in the Aim32 cysteine mutants. (B) As in (A), except that 2DGE was performed on the indicated mitochondrial extracts and analyzed by western blotting against

Aim32. Dashed red line indicates the position of the diagonal. Horizontal arrows at the left of the panel align with the location of the signal expected for each of the individual proteins tested.

Protein	**Accession No.**	**Sequence Count-Aim-Flag-IP**	**Spectral Count Δ*aim32* [pAIM32-FLAG]-IP**	**Sequence Count-Aim-VO**	**Spectral Count Δ*aim32*+Vec-IP**	**Sequence coverage % Δ*aim32* [pAIM32-FLAG]-IP**	**Sequence coverage % Δ*aim32*+Vec IP seq coverage percentage Aim-Flag-IP**
Tim23	YNR017W	6	8	0	0	50.5%	0
Tim17	YJL143W	2	2	0	0	21.5%	0
Sod2	YHR008C	8	15	5	6	53.2%	36.6%
Mia40	YKL195W	14	19	5	5	44.2%	16.10%

Table 2-1 Mass spectrometry data containing a list of identified proteins, spectral counts, and sequence coverage from the Δ*aim32* [pAIM32-FLAG] and Δ*aim32* + Vec runs at a false-positive rate of less than 1%.

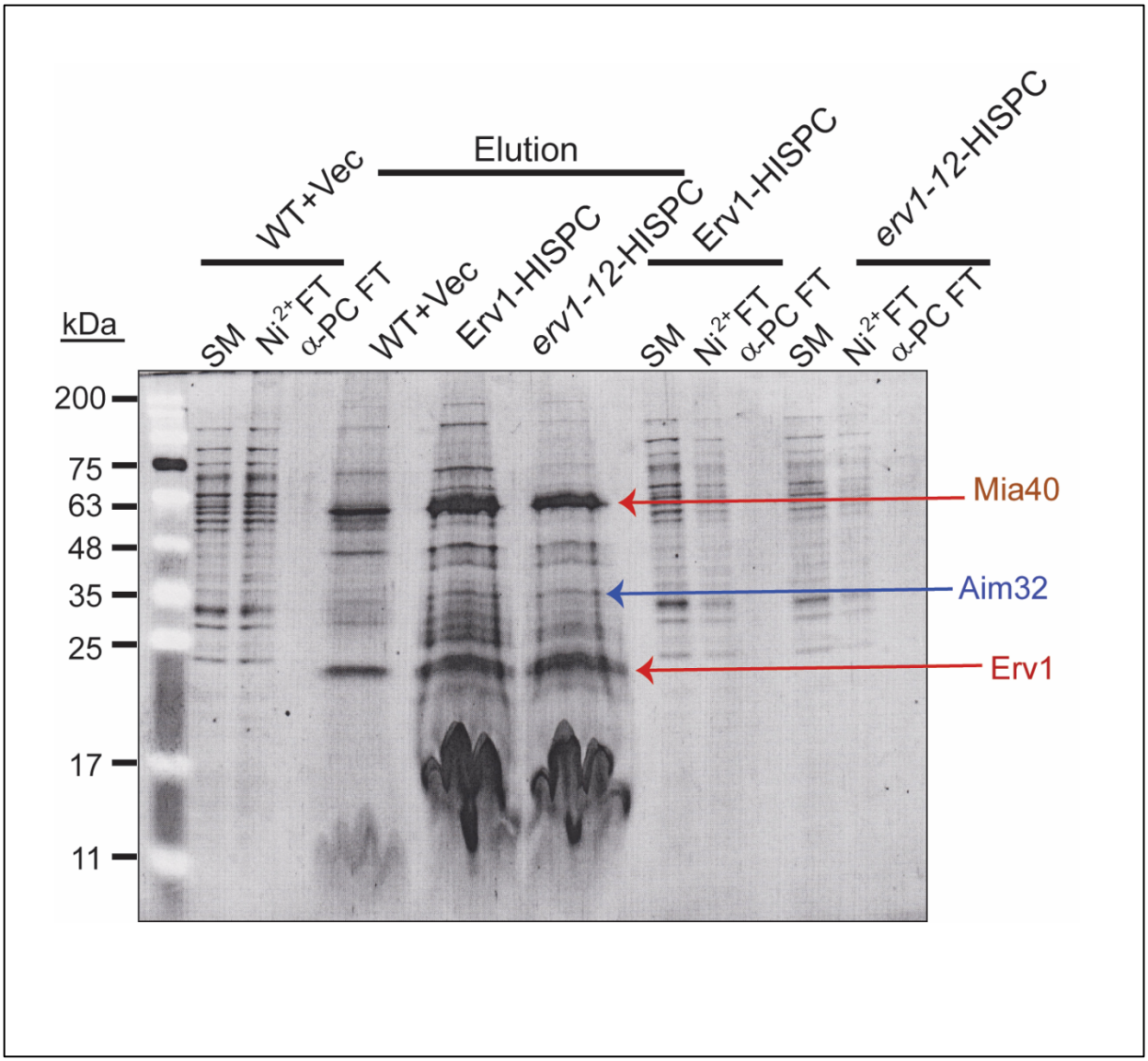

Figure S2-1 Aim32 was identified by mass spectrometry as an Erv1 partner protein. A consecutive-affinity tag [termed CNAP for purification over Ni^{2+}-resin followed by anti-Protein C affinity resin] was placed on the C-terminus of Erv1, designated Erv1-HISPC and *erv1-12*-HISPC. The lysate was incubated with Ni^{2+}-agarose, eluted with 300 mM imidazole and then incubated with the anti-Protein C resin. After washing, the bound material was eluted, resolved by a 10-15% SDS-PAGE, and stained with SYPRO Ruby solution. The indicated bands (highlighted by a red and blue arrows) from WT, Erv1-HISPC, and *erv1-12*-HISPC eluates were

excised, digested with trypsin, and identified by LC-MS/MS. (n = 3)

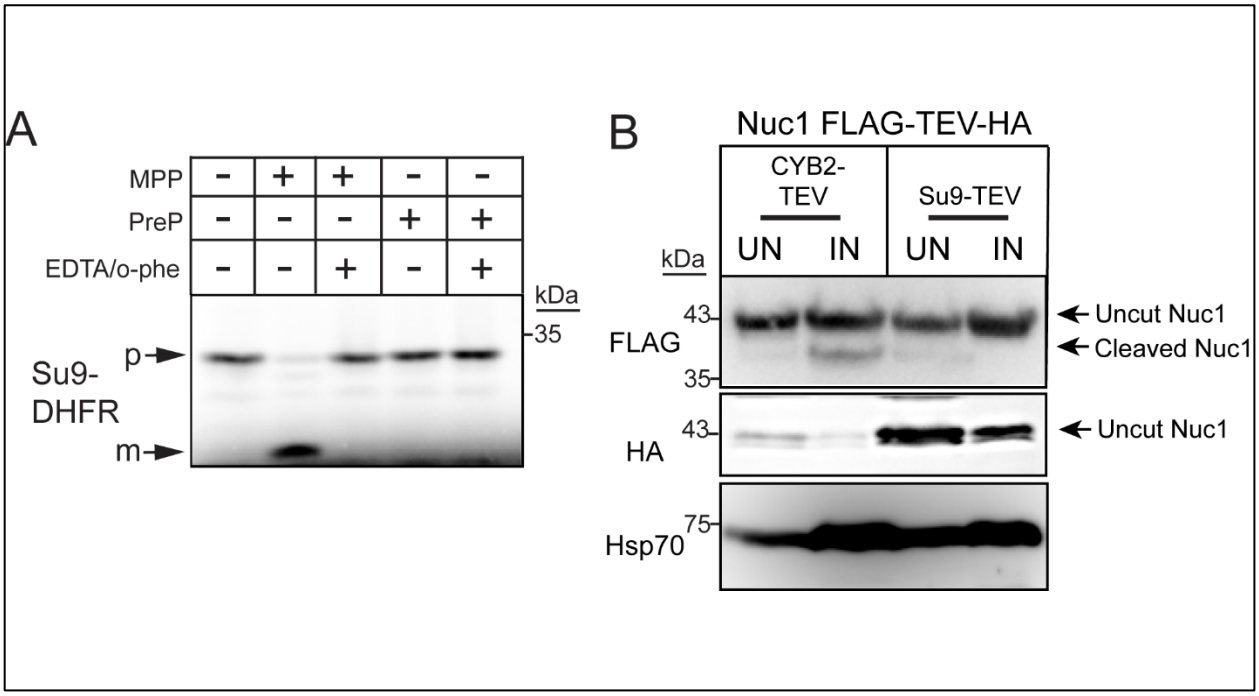

Figure S2-2 Control experiments for protease studies. (A) As in Fig. 2-2D, the MPP cleavage assay was performed with the addition of 10 µg MPP to radiolabeled Su9-DHFR and the samples were resolved on a 12% Tris-Tricine gel. As a negative control, 10 µg of Presequence protease (Cym1) was included. Chelators EDTA and *o*-phenanthroline were included as inhibitors of MPP and Cym1. p, precursor; m, mature. (B) As in Fig. 2-2E, WT cells in which IMS-localized Nuc1 was tagged with FLAG-TEV-HA were transformed with plasmids expressing matrix localized Su9-TEV protease or IMS-localized CYB2[1-220]-TEV protease. Cells were grown in SC-Ura supplemented with 2% galactose (IN; induced), or 2% sucrose (UN; uninduced) and harvested in mid-log phase. Whole cell extracts were analyzed by immunoblotting with antibodies against Hsp70 (loading control) and FLAG and HA for Nuc1. Arrows indicate uncut and TEV cut Nuc1 FLAG-TEV-HA proteins.

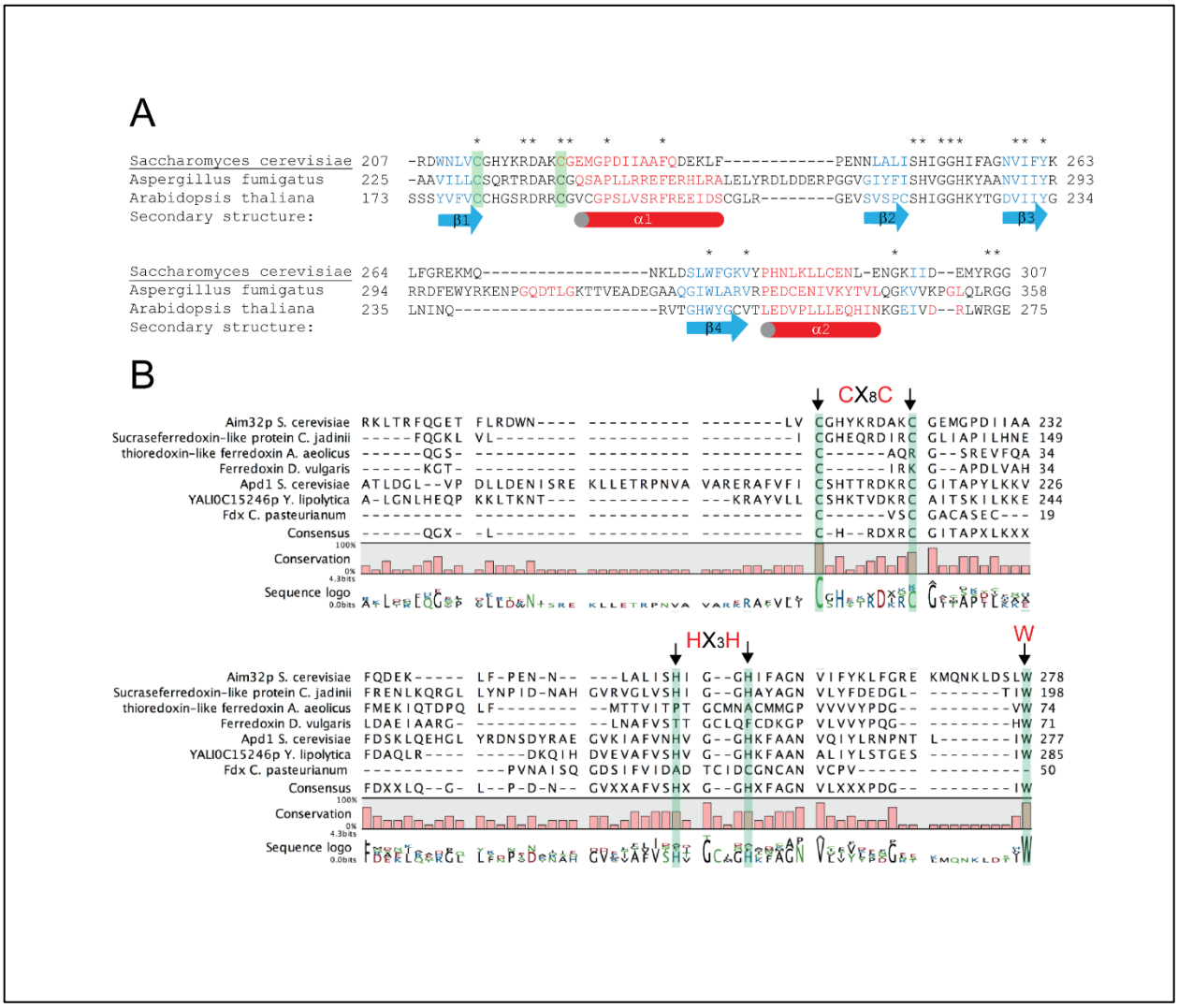

Figure S2-3 Aim32 is a thioredoxin-like ferredoxin protein bearing a CX_8CHX_3H motif. (A) Multiple amino acid sequence alignments of three fungal Aim32 homologs depicting homology of the predicted thioredoxin-like fold (TLF) from amino acids 209-307 (*S. cerevisae*). Sequence alignments were generated using the CLC Workbench software (Qiagen). The helices and strands are labeled in a sequential manner. Starred residues are conserved. (B) Multiple amino acid sequence alignment of Aim32 with other thioredoxin-like ferredoxin proteins was performed as in (A). Sequence logos, consensus, and conservation analysis is provided.

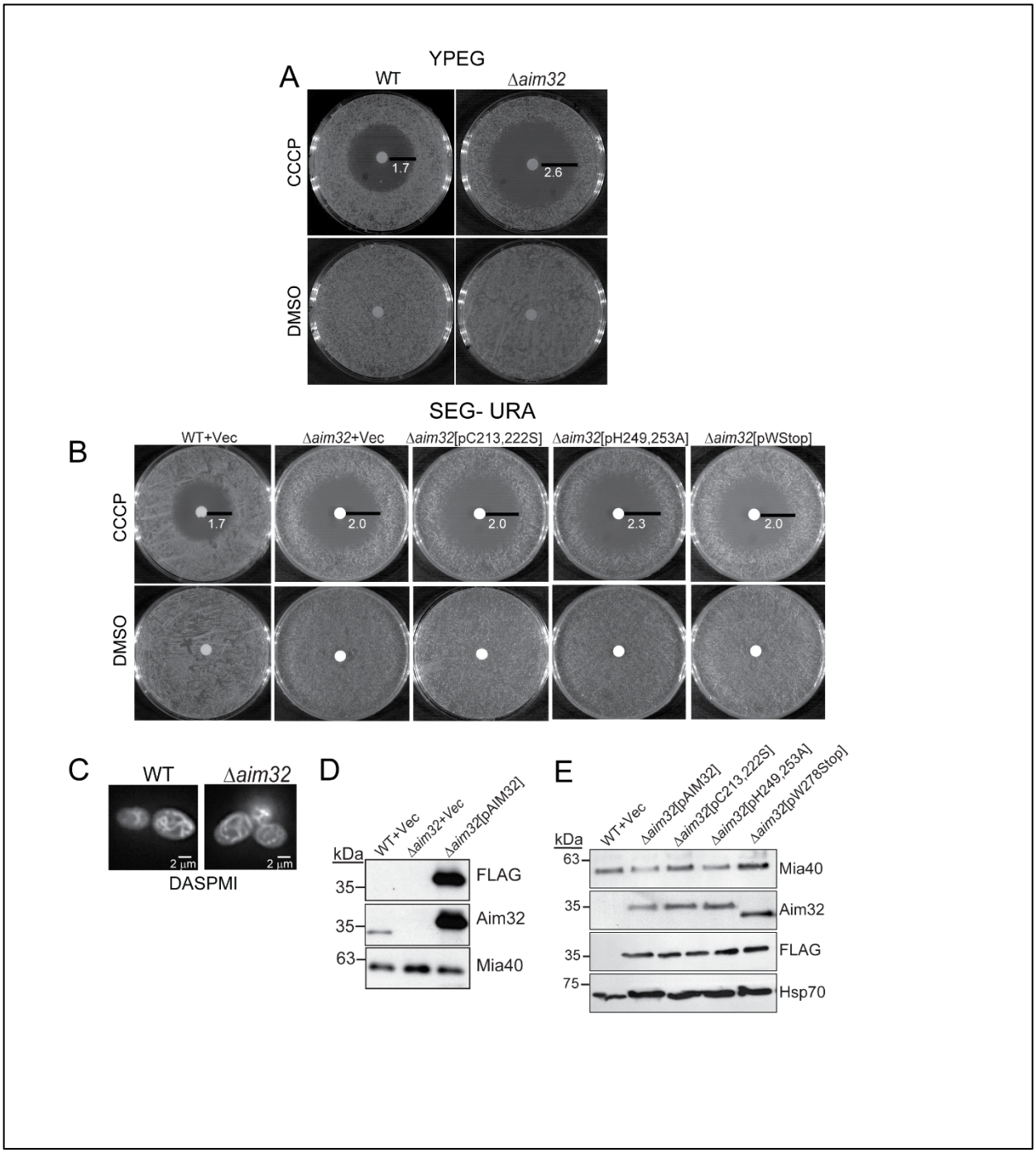

Figure S2-4 The CX_8CHX_3H motif of Aim32 is crucial to its function. (A) WT and *Δaim32* cells were plated on YPEG plates and a disk saturated with 0.1 % CCCP or 0.1 % DMSO was placed in the center. Cells were incubated at 30 ºC for 2 days and then photographed. The line (measured in cm) indicated the ring in which cells failed to grow. (B) As in (A), except that

growth of *Δaim32* cells and CX_8CHX_3H motif variants of Aim32 were analyzed on selective non-fermentable media (SEG-URA). (C) WT and *Δaim32* cells were grown at 30ºC in YPEG media and mitochondria were stained with a potentiometric probe, 2-(4-(dimethylamino)styryl)-1-methylpyridinium iodide (DASPMI). Cells were viewed by fluorescence microscopy. Representative cells are shown. Scale bar, 2μm. (D, E) Expression of Aim32-FLAG fusion proteins was analyzed with antibodies against the FLAG tag and Aim32. Controls are also included.

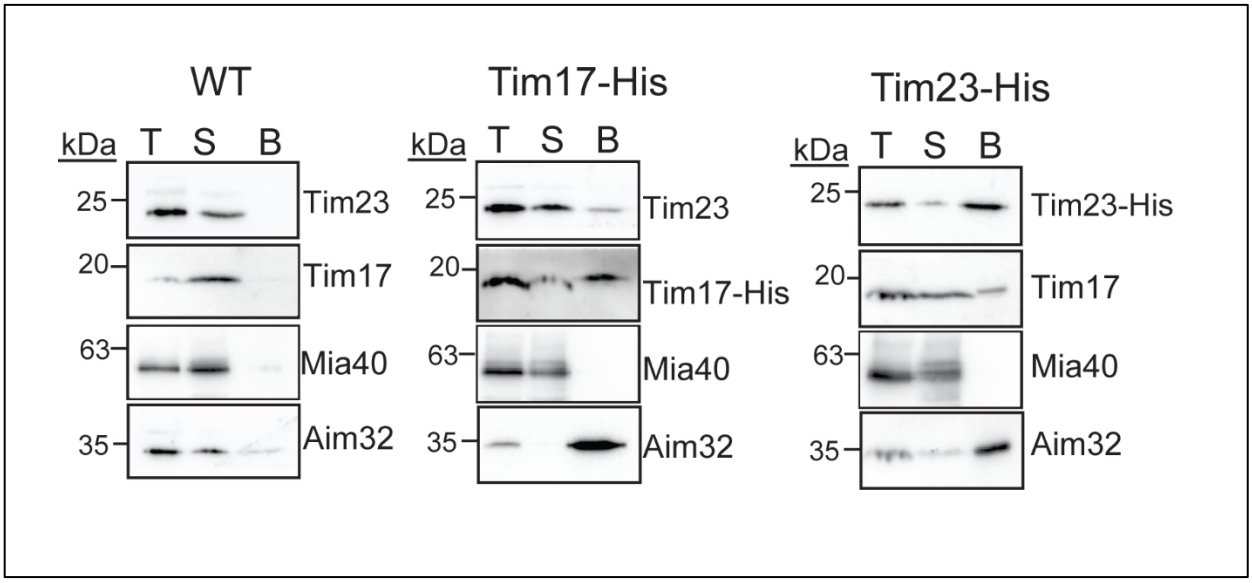

Figure S2-5 Aim32 binds to both Tim17 and Tim23. Mitochondria from WT (left panel) and strains expressing Tim17 (Tim17-His) (middle panel) or Tim23 (Tim23-His) (right panel) were solubilized in 1% digitonin. As a control, (25 μg) of extract was withdrawn (T), and 500 μg lysate was incubated with Ni^{2+}-agarose beads. The beads were washed, and bound protein (B) were eluted. To assess the effectiveness of binding, 25 μg of the unbound protein fraction (S) was also included. Samples were resolved by SDS-PAGE and analyzed by immunoblotting with specific antibodies.

Strain	**Genotype**	**Source**
WT (GA74-1A)	MATα *his3-11,15 leu2 ura3 trp1 ade8 rho+ mit+*	[57]
erv1-12	MATα *his3-11,15 leu2 ura3 trp1 ade8 erv1::HIS3* [p*erv1-12:TRP1* CEN	[10]
Erv1-His	MATα *his3-11,15 leu2 ura3 trp1 ade8 erv1::HIS3* [p*ERV1-10xHis:LEU2* 2μ]	[10]
yEPL1	MATα *his3-11,15 leu2 ura3 trp1 ade8 erv1::HIS3* [pERV1:URA3 2μ]	[10]
Erv1-HISPC	MATα *his3-11,15 leu2 ura3 trp1 ade8 erv1::HIS3* [p*Erv1- PC10xHis:LEU2* 2μ]	This study
erv1-12-HISPC	MATα *his3-11,15 leu2 ura3 trp1 ade8 erv1::HIS3* [p*erv1- 12 PC10xHis:LEU2* 2μ]	This study
Δtim54	MATα *his3-11,15 leu2 ura3 trp1 ade8 tim54::HIS3*	[58]
tim23-2	MATα *his3-11,15 leu2 ura3 trp1 ade8 tim23-2: TRP1*	[59]
Δosm1	MATα *his3-11,15 leu2 ura3 trp1 ade8 osm1::LEU2*	[12]
Osm1-His	MATα *his3-11,15 leu2 ura3 trp1 ade8 osm1::LEU2* [p*OSM1- 10xHis:TRP1* 2μ]	This study
Δaim32	MATα *his3-11,15 leu2 ura3 trp1 ade8 aim32::HIS3*	This study
Δaim32 [pAIM32]	MATα *his3-11,15 leu2 ura3 trp1 ade8 aim32::HIS3* [*pRS316GPD-AIM32 3XFLAG-PGK*]	This study
Δaim32 [pC213, 222S]	MATα *his3-11,15 leu2 ura3 trp1 ade8 aim32::HIS3* [*pRS316GPD-AIM32 C213, 222S 3XFLAG-PGK*]	This study
Δaim32 [pH249, 253A]	MATα *his3-11,15 leu2 ura3 trp1 ade8 aim32::HIS3* [*pRS316GPD-AIM32 H249, 253A 3XFLAG-PGK*]	This study

Δaim32 [pWSTOP]	MATα *his3-11,15 leu2 ura3 trp1 ade8 aim32::HIS3* [*pRS316GPD-AIM32 WSTOP 3XFLAG-PGK*]	This study
Δaim32 [pC213S]	MATα *his3-11,15 leu2 ura3 trp1 ade8 aim32::HIS3* [*pRS316GPD-AIM32 C213S 3XFLAG-PGK*]	This study
Δaim32 [pC222S]	MATα *his3-11,15 leu2 ura3 trp1 ade8 aim32::HIS3* [*pRS316GPD-AIM32 C222S 3XFLAG-PGK*]	This study
Aim32-HisPC	MATα *his3-11,15 leu2 ura3 trp1 ade8* [p*AIM32-PC10xHis:LEU2* 2μ]	This study
Tim23-His	MATα *his3 leu2 ade8 trp1 ura3 TIM23-HIS10:HISMX6*	This study
Tim17-His	MATα *his3 leu2 ade8 trp1 ura3 TIM17-HIS10:HISMX6*	This study
Nuc1-3XFLAG-TEV-3XHA	MATa *his3-11,15 leu2 ura3 trp1 ade8, Nuc1-3XFLAG-TEV-3XHA::KanMX6*	This study
Nuc1-3XFLAG-TEV-3XHA, pCYB2[1-220]-TEV Protease	MATa *his3-11,15 leu2 ura3 trp1 ade8 Nuc1-3XFLAG-TEV-3XHA::KanMX6* [*pRS416GAL1 CYB2[1-220]-TEV Protease: URA3*]	This study
Nuc1-3XFLAG-TEV-3XHA, pSu9-TEV Protease	MATa *his3-11,15 leu2 ura3 trp1 ade8 Nuc1-3XFLAG-TEV-3XHA::KanMX6* [*pRS416 GAL1 Su9-TEV Protease:URA3*]	This study
Δaim32[pAim32-3XFLAG-TEV-3XHA]	MATα *his3-11,15 leu2 ura3 trp1 ade8 aim32::HIS3* [p*RS315 Aim32-3XFLAG-TEV-3XHA: LEU2*]	This study
Δaim32 [pAim32-3XFLAG-TEV-3XHA], pCYB2[1-220]-TEV Protease	MATα *his3-11,15 leu2 ura3 trp1 ade8 aim32::HIS3* [*pRS315 Aim32-3XFLAG-TEV-3XHA:LEU2*] [p*RS416 GAL1 CYB2[1-220]-TEV Protease: URA3*]	This study

Δaim32 [pAim32-3XFLAG-TEV-3XHA], pSu9-TEV Protease	MATα *his3-11,15 leu2 ura3 trp1 ade8 aim32::HIS3* [p*RS315 Aim32-3XFLAG-TEV-3XHA: LEU2*] [p*RS416 GAL1Su9-TEV Protease: URA3*]	This study

Table S2-1 Strains used in this study

Material and Methods

Strains and site-directed mutagenesis. For pull-down analysis and mass spectrometry studies, the designated yeast strains Erv1-HISPC and erv1-12-HISPC were generated. Either *ERV1* or *erv1-12* alleles with 300 nucleotides of the 5' promoter region were cloned into plasmid pRS425 (2 micron, *LEU2*). The HISPC tag (amino acid sequence MEDQVDPRLIDGK–GGAGG–**HHHHHHHHHH**; PC epitope tag underlined) was integrated at the C-terminus of *AIM32* with PCR overlap extension[60]. The plasmids were transformed into strain yEPL (*his3 leu2 ura3 trp1 ade8 erv1::HIS3* [pERV1:URA3 2μ]) and then the WT *ERV1* plasmid was removed by plasmid shuffling.

AIM32 was PCR-amplified from yeast genomic DNA isolated from the WT (GA74-1A) strain and the 3' primer introduced a 3XFLAG tag to the C-terminus. The fragment was cloned into vector pRS316 that contains the *GPD1* promoter and *PGK1* terminator, designated [pAIM32], and transformed into *Δaim32* yeast strain (Fig. S2-4D). Mutagenesis was carried out according to Agilent's site-directed mutagenesis protocols. Mutagenized constructs [pC213S], [pC222S], [pC213, 222S], [pH249, 253A], and [pW278STOP] were generated in the aforementioned pRS316 vector with FLAG-tagged Aim32 and transformed into the *Δaim32* yeast strain.

The parental *S. cerevisiae* yeast strain used in the study was GA74-1A (Table S2-1). The Δ*aim32::HIS* strain was generated by deletion of *AIM32* with *HIS3MX* in GA74-1A using standard procedures[61]. Standard yeast genetics were used to generate the strains and for synthetic lethal analysis[62].

Subcellular fractionation and mitochondrial assays. Subcellular fractionation from spheroplasts was performed as previously described[63]. The fractions were separated by differential centrifugation and an equal amount of each fraction was separated by SDS-PAGE followed by immunoblot analysis.

Mitochondria were purified from yeast cells grown in media with glucose or ethanol/glycerol[64]. Proteins for import studies were synthesized by the TNT Quick Coupled Transcription/Translation kits (Promega) in the presence of [^{35}S] methionine. The radiolabeled precursor was incubated with isolated mitochondria and an import time course was performed. Where indicated, the $\Delta\Psi$ was dissipated with 5 mM CCCP. Non-imported radiolabeled protein was removed by treatment with 100 μg/ml trypsin for 15 minutes on ice and trypsin was inhibited with 200 μg/ml of soybean trypsin inhibitor for 30 min on ice. Samples were separated by SDS-PAGE and visualized using autoradiography. Mitochondria were purified from the Erv1-His_6 strain, and pulldown experiments were performed as previously described10.

Mitochondrial fractionation was performed as previously described[63]. For intact mitochondria, 300 μg of isolated mitochondria were incubated in 0.6 M sorbitol and 20 mM Hepes-KOH, pH 7.4. To generate mitoplasts, 300 μg of isolated mitochondria were incubated in 0.03 M sorbitol and 20 mM Hepes-KOH, pH 7.4. As indicated, 100 μg/ml of Proteinase K and 0.1% Triton-X-100 were added. Samples were centrifuged at 14,000 x*g* for 10 minutes to separate pellet (P) and supernatant (S). The supernatants were precipitated with 20% trichloroacetic acid and resuspended in SDS-sample buffer.

Carbonate extraction was performed as described previously[63]. Briefly, 200 µg of mitochondria were incubated in 200 µl of 0.1 M Na_2CO_3 at the indicated pH for 15 min on ice. Samples were centrifuged at 14,000 x *g* for 10 min to separate the pellet (P) and supernatant (S). The supernatants were precipitated with 20% (wt/vol) TCA and the pellet and supernatant fractions were resuspended in equal volumes of SDS-sample buffer.

1D BN-PAGE was performed as described previously[12]. For 2D blue native/SDS-PAGE60 before resolution by second dimension by SDS-PAGE, the BN-PAGE gel was soaked in 1% (wt/vol) SDS, 1% (vol/vol) β-mercaptoethanol for 30 min at 50^0C, and individual lanes isolated with a razor blade, embedded in a 4% stacking gel.

For indirect thiol trapping assay, isolated mitochondria from the respective strains were treated with 150 mM mmPEG (22713 ThermoFisher, Waltham, MA) for 1 hour at room temperature in the dark. In control reactions, mitochondria were treated with either 20 mM DTT for 15 minutes at 65°C or with 50 mM IAA for 10 minutes at 30°C. Samples were analyzed by non-reducing SDS-PAGE.

TEV protease cleavage assay. Plasmids on the pRS416 backbone containing a matrix localized Su9-TEV protease and IMS localized CYB2[1-220]-TEV protease under the control of the GAL1 promoter were obtained for protease expression[37]. The centromeric pRS315 vector was used for plasmid expression of Nuc1 or Aim32 proteins. The *Δaim32* strain expressing Aim32-3XFLAG-TEV-3HA and WT strain endogenously tagged with Nuc1-3XFLAG-TEV-3HA were transformed with plasmids expressing matrix localized Su9-TEV, or IMS localized CYB2[1-220]-TEV. Strains were grown in SC-Ura galactose and harvested in mid-log phase. Whole cell extracts were

analyzed by immunoblotting with FLAG, HA, Tim44, Hsp70 and Aim32 antibodies.

2D- Diagonal gel electrophoresis. 2D-DGE was performed as described before[65]. Briefly mitochondria (5 mg/ml) were solubilized with 20 mM Hepes-KOH, pH 7.4, 10% glycerol, 50mM NaCl, 1mM EDTA, and 2.5 mM MgCl2 supplemented with 1% (w/v) digitonin and protease inhibitors. Lysates were treated with 500 nM IAA-rhodamine at room temperature followed by resolution in the first dimension on a non-reducing SDS gel. Individual lanes isolated with a razor blade, were soaked in 1% (wt/vol) SDS, 1% (vol/vol) β-mercaptoethanol for 30 min at 50^0C, embedded in a 4% stacking gel, and resolved in the second dimension by SDS-PAGE. Gels were visualized using the Sapphire Biolmolecular Imager (Azure Biosystems).

Protein-protein binding assays and mass spectrometry. Pull-down experiments designed to detect possible complex formation between Erv1 and Aim32 or Osm1 utilizing His-tags were described previously[12]. Briefly, mitochondria were purified, solubilized in 1% digitonin, and subjected to pull-down experiments with Ni^{2+} agarose. FLAG immunoprecipitations were performed using the ANTI-FLAG M2 affinity gel (Sigma Aldrich) using the manufacturers guidelines.

CNAP pulldowns were performed as described in Claypool *et al*.[32]. Briefly, detergent solubilization of mitochondria (5 mg/ml) was performed with 20 mM Hepes-KOH, pH 7.4, 20 mM imidazole, 10% glycerol, 100 mM NaCl, and 1 mM CaCl2, supplemented with 1.5% (wt/vol) digitonin (Biosynth International, Inc.) and protease inhibitors (1 mM PMSF, 10 μM leupeptin, 2 μM pepstatin A, and 10 μM chymostatin). Insoluble material was removed at 20,000 *g* for 30 min at 4°C and extracts transferred to tubes containing 8ml lysis buffer base with added

protease inhibitors and 0.8 ml NiNTA resin (QIAGEN). After rotating at 4°C for 1h, the contents were poured into a column, and the flow-thru collected. After two washes with 8 ml lysis buffer base containing 0.1% (wt/vol) digitonin, bound material was directly eluted into separate columns containing 1 ml equilibrated anti-PC resin (Roche; equilibration buffer 20 mM Hepes-KOH, pH 7.4, 100 mM NaCl, and 1 mM CaCl2) with 8 ml Ni2+ elution buffer (20 mM Hepes-KOH, pH 7.4, 300 mM imidazole, 10% glycerol, 100 mM NaCl, 1 mM CaCl2, and 0.1% digitonin). After 1 h rotating at 4°C, the flow-thru was collected and the columns washed twice with 10 ml anti-PC wash buffer (anti-PC equilibration buffer with 0.1% digitonin). To elute bound material, the columns were capped and 1 ml of EDTA elution solution (20 mM Hepes-KOH, pH 7.4, 100 mM NaCl, 5 mM EDTA, and 0.1% digitonin) was added to the anti-PC resin. Four elutions were performed. The first elution consisted of 15 min at 4°C and then 15 min at room temperature; the remaining three elutions were at room temperature. Eluates were directly pooled in Amicon filtration devices, 10,000 MWCO kept on ice and the pooled eluates concentrated following the provided guidelines (Millipore). Concentrated CNAPed product derived from 4 and 10 mg starting material was analyzed in the preparative 1D-PAGE analyses, and proteins revealed with the SYPRO Ruby stain and protocol (Invitrogen). Gels were imaged and analyzed with PDQuest (Bio-Rad Laboratories) software. Protein bands of interest were excited by a spot-excision robot (Proteome Works; Bio-Rad Laboratories) and deposited into 96-well plates. Gel bands were digested with sequencing-grade trypsin (Promega), and the resulting tryptic peptides were extracted using standard protocol[66]. LC–MS/MS of peptide mixtures was performed on a QSTAR Pulsar XL (QqTOF) mass spectrometer (Applied Biosystems) equipped

with nanoelectrospray interface (Protana) and LC Packings nano-LC system. All searches were performed against the Swiss-Prot protein sequence database.

Liquid chromatography- mass spectrometry analysis. The protein mixtures were reduced, alkylated, and digested by the sequential addition of trypsin and lys-C proteases. Afterwards, samples were desalted using Pierce C18 tips, eluted in 40% ACN, and dried and resuspended in 5% formic acid. Desalted samples were separated on C18 reversed phase (1.9 uM, 100A pores, Dr. Maisch GmbH) columns, packed with 25cm of resin in a 75uM inner diameter fused silica capillary. Digested peptides were fractionated online using a 140-minute water-acetonitrile gradient with 3% DMSO ionized using electrospray ionization by application of a distal 2.2kV. Ionized peptides were interrogated via tandem mass spectrometry (MS/MS) in a Thermo Orbitrap Fusion Lumos. For discovery acquisitions, Data-Dependent Acquisition (DDA) was utilized with an MS1 scan resolution of 120,000 and MS2 resolution of 15,000 and a cycle time of 3 seconds. Data analysis was performed using the Integrated Proteomics pipeline 2 (Integrated Proteomics Applications, San Diego, CA). MS/MS spectra were searched using the ProLuCID algorithm and peptide-to-spectrum matches (PSMs) were organized and filtered based on decoy database-estimated false discovery rate of <1% using the DTASelect algorithm. Database searching was performed using a *Saccharomyces cerevisiae* yeast database downloaded from *Saccharomyces* Genome Database (SGD) on 2-19-2016.

Sequence alignments. Sequence alignments were generated using the CLC Workbench software (Qiagen). Calculation of the information content in sequence logos is provided in the original paper[67]. Multiple protein sequence alignments were generated using PROMALS, a method that

improves alignment quality by using additional homologs from PSI-BLAST searches and secondary structure predictions from PSIPRED[68].

Assessment of mitochondrial membrane potential. The membrane potential ΔΨ of isolated yeast mitochondria was assessed by measuring the fluorescence quenching of the potential-sensitive dye 3,3′-dipropylthiadicarbocyanine iodide [$DiSC_3(5)$; Molecular Probes, Eugene, OR] as described previously[69]. The measurements were performed using a FlexStation plate reader (Molecular Devices) controlled with the SoftMax Pro software package (Molecular Devices) with excitation at 622 nm and emission at 670 nm at 25°C. Mitochondria (21 μg/ml) in buffer (0.6 M sorbitol, 1% BSA, 10 mM $MgCl_2$, 0.5 mM EDTA, 20 mM KPO_4 pH 7.4, and 2 mM NADH) was added to the cuvette, followed by $DiSC_3(5)$ (final concentration of 167 nM in ethanol) addition and the fluorescence was measured. Mitochondria were subsequently uncoupled with CCCP (final concentration of 20 μM in ethanol). The difference in the fluorescence before and after the addition of CCCP represents a relative measurement of ΔΨ.

Antibodies. Most of the antibodies used in this work were generated by vendor Pacific Immunology from recombinant proteins in the Koehler laboratory and have been described previously. Other antibodies used were: anti-Cox-4, anti-Rip1-FeS, anti-Qcr10 and anti-Oxa1 (a gift of Dr. Rosemary Stuart, Marquette University, Milwaukee, WI), and horseradish peroxidase–conjugated secondary antibodies (Thermo Fisher Scientific).

Statistical analyses. Data was plotted using GraphPad Prism version 5.02. Statistical significance of observations was determined using unpaired t tests (two tailed), unless otherwise noted.

Data availability: All data are contained within the article. The mass spectrometry proteomics data are available via ProteomeXchange with identifier PXD021662

References

1. Chacinska, A. *et al.* Essential role of Mia40 in import and assembly of mitochondrial intermembrane space proteins. *EMBO J.* **23**, 3735–3746 (2004).
2. Allen, S., Balabanidou, V., Sideris, D. P., Lisowsky, T. & Tokatlidis, K. Erv1 mediates the Mia40-dependent protein import pathway and provides a functional link to the respiratory chain by shuttling electrons to cytochrome c. *J. Mol. Biol.* **353**, 937–944 (2005).
3. Mesecke, N. *et al.* A disulfide relay system in the intermembrane space of mitochondria that mediates protein import. *Cell* **121**, 1059–1069 (2005).
4. Tienson, H. L. *et al.* Reconstitution of the Mia40-Erv1 oxidative folding pathway for the small tim proteins. *Mol. Biol. Cell* **20**, 3481–3490 (2009).
5. Koehler, C. M. & Tienson, H. L. Redox regulation of protein folding in the mitochondrial intermembrane space. *Biochimica et Biophysica Acta - Molecular Cell Research* vol. 1793 139–145 (2009).
6. Chacinska, A., Koehler, C. M., Milenkovic, D., Lithgow, T. & Pfanner, N. Importing Mitochondrial Proteins: Machineries and Mechanisms. *Cell* vol. 138 628–644 (2009).
7. Sideris, D. P. & Tokatlidis, K. Oxidative protein folding in the mitochondrial intermembrane space. *Antioxidants and Redox Signaling* vol. 13 1189–1204 (2010).
8. Weckbecker, D., Longen, S., Riemer, J. & Herrmann, J. M. Atp23 biogenesis reveals a chaperone-like folding activity of Mia40 in the IMS of mitochondria. *EMBO J.* **31**, 4348–4358 (2012).
9. Bien, M. *et al.* Mitochondrial Disulfide Bond Formation Is Driven by Intersubunit Electron Transfer in Erv1 and Proofread by Glutathione. *Mol. Cell* **37**, 516–528 (2010).
10. Dabir, D. V. *et al.* A role for cytochrome c and cytochrome c peroxidase in electron shuttling from Erv1. *EMBO J.* **26**, 4801–4811 (2007).
11. Bihlmaier, K. *et al.* The disulfide relay system of mitochondria is connected to the respiratory chain. *J. Cell Biol.* **179**, 389–395 (2007).
12. Neal, S. E., Dabir, D. V., Wijaya, J., Boon, C. & Koehler, C. M. Osm1 facilitates the transfer of electrons from Erv1 to fumarate in the redox-regulated import pathway in the mitochondrial intermembrane space. *Mol. Biol. Cell* **28**, 2773–2785 (2017).

13. Fraga, H. *et al.* The mitochondrial intermembrane space oxireductase mia40 funnels the oxidative folding pathway of the cytochrome c oxidase assembly protein cox19. *J. Biol. Chem.* **289**, 9852–9864 (2014).

14. Hudson, D. A. & Thorpe, C. Mia40 is a facile oxidant of unfolded reduced proteins but shows minimal isomerase activity. *Arch. Biochem. Biophys.* **579**, 1–7 (2015).

15. Fischer, M. *et al.* Protein import and oxidative folding in the mitochondrial intermembrane space of intact mammalian cells. *Mol. Biol. Cell* **24**, 2160–2170 (2013).

16. Neal, S. E. *et al.* Mia40 protein serves as an electron sink in the Mia40-Erv1 import pathway. *J. Biol. Chem.* **290**, 20804–20814 (2015).

17. Hu, J., Dong, L. & Outten, C. E. The redox environment in the mitochondrial intermembrane space is maintained separately from the cytosol and matrix. *J. Biol. Chem.* **283**, 29126–29134 (2008).

18. Ayer, A. *et al.* The critical role of glutathione in maintenance of the mitochondrial genome. *Free Radic. Biol. Med.* **49**, 1956–1968 (2010).

19. Kojer, K. *et al.* Glutathione redox potential in the mitochondrial intermembrane space is linked to the cytosol and impacts the Mia40 redox state. *EMBO J.* **31**, 3169–3182 (2012).

20. Ayer, A. *et al.* A Genome-Wide Screen in Yeast Identifies Specific Oxidative Stress Genes Required for the Maintenance of Sub-Cellular Redox Homeostasis. *PLoS One* **7**, e44278 (2012).

21. Palma, F. R. *et al.* Mitochondrial Superoxide Dismutase: What the Established, the Intriguing, and the Novel Reveal about a Key Cellular Redox Switch. *Antioxidants and Redox Signaling* vol. 32 701–714 (2020).

22. Tu, B. P. & Weissman, J. S. Oxidative protein folding in eukaryotes: Mechanisms and consequences. *Journal of Cell Biology* vol. 164 341–346 (2004).

23. Lalève, A. *et al.* The antimalarial drug primaquine targets Fe-S cluster proteins and yeast respiratory growth. *Redox Biol.* **7**, 21–29 (2016).

24. Stegmaier, K. *et al.* Apd1 and Aim32 Are Prototypes of Bishistidinyl-Coordinated Non-Rieske [2Fe-2S] Proteins. *J. Am. Chem. Soc.* **141**, 5753–5765 (2019).

25. Lu, J. & Holmgren, A. The thioredoxin superfamily in oxidative protein folding. *Antioxidants and Redox Signaling* vol. 21 457–470 (2014).

26. Hanschmann, E. M., Godoy, J. R., Berndt, C., Hudemann, C. & Lillig, C. H. Thioredoxins, glutaredoxins, and peroxiredoxins-molecular mechanisms and health significance: From cofactors to antioxidants to redox signaling. *Antioxidants and Redox Signaling* vol. 19 1539–1605 (2013).

27. Groitl, B. & Jakob, U. Thiol-based redox switches. *Biochimica et Biophysica Acta - Proteins and Proteomics* vol. 1844 1335–1343 (2014).

28. Couturier, J., Przybyla-Toscano, J., Roret, T., Didierjean, C. & Rouhier, N. The roles of glutaredoxins ligating Fe-S clusters: Sensing, transfer or repair functions? *Biochimica et Biophysica Acta - Molecular Cell Research* vol. 1853 1513–1527 (2015).

29. Mössner, E., Huber-Wunderlich, M. & Glockshuber, R. Characterization of Escherichia coli thioredoxin variants mimicking the active-sites of other thiol/disulfide oxidoreductases. *Protein Sci.* **7**, 1233–1244 (1998).

30. Maskos, K., Huber-Wunderlich, M. & Glockshuber, R. DsbA and DsbC-catalyzed oxidative folding of proteins with complex disulfide bridge patterns in vitro and in vivo. *J. Mol. Biol.* **325**, 495–513 (2003).

31. Huber-Wunderlich, M. & Glockshuber, R. A single dipeptide sequence modulates the redox properties of a whole enzyme family. *Fold. Des.* **3**, 161–171 (1998).

32. Claypool, S. M., Oktay, Y., Boontheung, P., Loo, J. A. & Koehler, C. M. Cardiolipin defines the interactome of the major ADP/ATP carrier protein of the mitochondrial inner membrane. *J. Cell Biol.* **182**, 937–950 (2008).

33. Rainey, R. N. *et al.* A New Function in Translocation for the Mitochondrial i-AAA Protease Yme1: Import of Polynucleotide Phosphorylase into the Intermembrane Space. *Mol. Cell. Biol.* **26**, 8488–8497 (2006).

34. Fukasawa, Y. *et al.* MitoFates: Improved prediction of mitochondrial targeting sequences and their cleavage sites. *Mol. Cell. Proteomics* **14**, 1113–1126 (2015).

35. Deng, K. *et al.* Activation of a matrix processing peptidase from the crystalline cytochrome complex of bovine heart mitochondria. *J. Biol. Chem.* **273**, 20752–20757 (1998).

36. Vögtle, F. N. *et al.* Landscape of submitochondrial protein distribution. *Nat. Commun.* **8**, 1–10 (2017).

37. Kondo-Okamoto, N., Shaw, J. M. & Okamoto, K. Mmm1p spans both the outer and inner mitochondrial membranes and contains distinct domains for targeting and foci formation. *J. Biol. Chem.* **278**, 48997–49005 (2003).

38. Faber, K. N., Kram, A. M., Ehrmann, M. & Veenhuis, M. A Novel Method to Determine the Topology of Peroxisomal Membrane Proteins in Vivo Using the Tobacco Etch Virus Protease. *J. Biol. Chem.* **276**, 36501–36507 (2001).

39. Büttner, S. *et al.* Endonuclease G Regulates Budding Yeast Life and Death. *Mol. Cell* **25**, 233–246 (2007).

40. Fujiki, Y., Hubbard, L., Fowler, S. & Lazarow, P. B. Isolation of intracellular membranes

by means of sodium carbonate treatment: Application to Endoplasmic Reticulum. *J. Cell Biol.* **93**, 97–102 (1982).

41. Gevorkyan-Airapetov, L. *et al.* Interaction of Tim23 with Tim50 is essential for protein translocation by the mitochondrial TIM23 complex. *J. Biol. Chem.* **284**, 4865–4872 (2009).

42. Dabir, D. V. *et al.* A small molecule inhibitor of redox-regulated protein translocation into mitochondria. *Dev. Cell* **25**, 81–92 (2013).

43. Pei, J., Kim, B. H., Tang, M. & Grishin, N. V. PROMALS web server for accurate multiple protein sequence alignments. *Nucleic Acids Res.* **35**, (2007).

44. Slonimski, P. P., Perrodin, G. & Croft, J. H. Ethidium bromide induced mutation of yeast mitochondria: Complete transformation of cells into respiratory deficient non-chromosomal 'petites'. *Biochem. Biophys. Res. Commun.* **30**, 232–239 (1968).

45. Tang, H. M. V. *et al.* Loss of APD1 in Yeast Confers Hydroxyurea Sensitivity Suppressed by Yap1p Transcription Factor. *Sci. Rep.* **5**, (2015).

46. [Interaction of diS-C3-(5) and ethylrhodamine with lymphocyte mitochondria] - PubMed. https://pubmed.ncbi.nlm.nih.gov/6626607/.

47. Habich, M. *et al.* Vectorial Import via a Metastable Disulfide-Linked Complex Allows for a Quality Control Step and Import by the Mitochondrial Disulfide Relay. *Cell Rep.* **26**, 759-774.e5 (2019).

48. Ang, S. K., Zhang, M., Lodi, T. & Lu, H. Mitochondrial thiol oxidase Erv1: Both shuttle cysteine residues are required for its function with distinct roles. *Biochem. J.* **460**, 199–210 (2014).

49. Hill, B. G., Reily, C., Oh, J. Y., Johnson, M. S. & Landar, A. Methods for the determination and quantification of the reactive thiol proteome. *Free Radical Biology and Medicine* vol. 47 675–683 (2009).

50. Morgenstern, M. *et al.* Definition of a High-Confidence Mitochondrial Proteome at Quantitative Scale. *Cell Rep.* **19**, 2836–2852 (2017).

51. Stein, I., Peleg, Y., Even-Ram, S. & Pines, O. The single translation product of the FUM1 gene (fumarase) is processed in mitochondria before being distributed between the cytosol and mitochondria in Saccharomyces cerevisiae. *Mol. Cell. Biol.* **14**, 4770–4778 (1994).

52. Lundström, J. & Holmgren, A. Determination of the Reduction—Oxidation Potential of the Thioredoxin-like Domains of Protein Disulfide-Isomerase from the Equilibrium with Glutathione and Thioredoxin. *Biochemistry* **32**, 6649–6655 (1993).

53. Sturtz, L. A., Diekert, K., Jensen, L. T., Lill, R. & Culotta, V. C. A fraction of yeast Cu,Zn-superoxide dismutase and its metallochaperone, CCS, localize to the intermembrane space

of mitochondria. A physiological role for SOD1 in guarding against mitochondrial oxidative damage. *J. Biol. Chem.* **276**, 38084–38089 (2001).

54. Zhuang, J. *et al.* Mitochondrial disulfide relay mediates translocation of p53 and partitions its subcellular activity. *Proc. Natl. Acad. Sci. U. S. A.* **110**, 17356–17361 (2013).

55. Hansen, K. G. *et al.* An ER surface retrieval pathway safeguards the import of mitochondrial membrane proteins in yeast. *Science (80-.).* **361**, 1118–1122 (2018).

56. Okamoto, H., Miyagawa, A., Shiota, T., Tamura, Y. & Endo, T. Intramolecular disulfide bond of TIM22 protein maintains integrity of the TIM22 complex in the mitochondrial inner membrane. *J. Biol. Chem.* **289**, 4827–4838 (2014).

57. Koehler, C. M. *et al.* Tim9p, an essential partner subunit of Tim10p for the import of mitochondrial carrier proteins. *EMBO J.* **17**, 6477–6486 (1998).

58. Hwang, D. K., Claypool, S. M., Leuenberger, D., Tienson, H. L. & Koehler, C. M. Tim54p connects inner membrane assembly and proteolytic pathways in the mitochondrion. *J. Cell Biol.* **178**, 1161–1175 (2007).

59. Dekker, P. J. T. *et al.* The Tim core complex defines the number of mitochondrial translocation contact sites and can hold arrested preproteins in the absence of matrix Hsp70-Tim44. *EMBO J.* **16**, 5408–5419 (1997).

60. Ho, S. N., Hunt, H. D., Horton, R. M., Pullen, J. K. & Pease, L. R. Site-directed mutagenesis by overlap extension using the polymerase chain reaction. *Gene* **77**, 51–59 (1989).

61. Gueldener, U., Heinisch, J., Koehler, G. J., Voss, D. & Hegemann, J. H. A second set of loxP marker cassettes for Cre-mediated multiple gene knockouts in budding yeast. *Nucleic Acids Res.* **30**, 23 (2002).

62. Guide to Yeast Genetics and Molecular Biology, Volume 194 - 1st Edition. https://www.elsevier.com/books/guide-to-yeast-genetics-and-molecular-biology/abelson/978-0-12-182095-4.

63. Claypool, S. M., McCaffery, J. M. & Koehler, C. M. Mitochondrial mislocalization and altered assembly of a cluster of Barth syndrome mutant tafazzins. *J. Cell Biol.* **174**, 379–390 (2006).

64. Glick, B. S. & Pon, L. A. Isolation of highly purified mitochondria from Saccharomyces cerevisiae. *Methods Enzymol.* **260**, 213–223 (1995).

65. Sommer, A. & Traut, R. R. Diagonal polyacrylamide dodecyl sulfate gel electrophoresis for the identification of ribosomal proteins crosslinked with methyl 4 mercaptobutyrimidate. *Proc. Natl. Acad. Sci. U. S. A.* **71**, 3946–3950 (1974).

66. Shevchenko, A. *et al.* A strategy for identifying gel-separated proteins in sequence

databases by MS alone. in *Biochemical Society Transactions* vol. 24 893–896 (Portland Press Ltd, 1996).

67. Schneider, T. D. & Stephens, R. M. Sequence logos: A new way to display consensus sequences. *Nucleic Acids Res.* **18**, 6097–6100 (1990).

68. Pei, J. & Grishin, N. V. PROMALS: Towards accurate multiple sequence alignments of distantly related proteins. *Bioinformatics* **23**, 802–808 (2007).

69. Geissler, A. *et al.* Membrane potential-driven protein import into mitochondria: The sorting sequence of cytochrome b2 modulates the Δψ-dependence of translocation of the matrix-targeting sequence. *Mol. Biol. Cell* **11**, 3977–3991 (2000).

Chapter 3: Aim32 forms disulfide interactions and functions in two mitochondrial compartments

3.1 Introduction

Iron-sulfur clusters are present in nearly all organisms and required for a variety of important protein biological functions, such as enzyme activity, protein regulation, and translation[1]. Fe/S proteins are unique in that they have potential roles in redox sensing and electron transfer. The simplest form found in nature is [2Fe-2S] ferredoxins; two irons that are bridged by two inorganic sulfides and usually coordinated by four cysteine thiolates. These inorganic molecules are excellent examples of co-factors that are highly reactive and suitable for many catalytic reactions. The thioredoxin fold is a characteristic motif shared by many proteins involved in thiol-redox state modification such as Dsb proteins, PDI, glutaredoxins and thioredoxins[2]. Thioredoxins are known to modulate target protein activity via reversible oxidative changes mediated by a pair of redox-active cysteines and function as a redox-powered chaperone interacting with unfolded and denatured proteins[3]. Despite this, the functions of these thioredoxins-like ferredoxin proteins are not well elaborated.

Previous chapter has demonstrated that Aim32 is a novel Fe-S protein that are found in bacteria, plants, and fungi. It is uniquely localized to two sub-compartments of the mitochondria: the intermembrane space (IMS) and matrix with a potential role in redox homeostasis. Aim32 has the highly conserved C-terminal thioredoxin-like fold (TLF) domain with a [2Fe-2S] cluster. The conserved cysteine residues C213 and C222 that occur in a CX_8C motif most likely

constitute the redox active site of Aim32. Previous analysis showed that in the absence of *AIM32*, the mitochondrial thiol proteome displayed aberrant thiol linkages. The redox status of a subset of candidate proteins was altered. Based on our previous data, we hypothesized that Aim32 acts to maintain or repair the redox status of proteins and provides a protein disulfide isomerase (PDI) function[4]. Aim32 may use the redox active cysteines to form mixed disulfide bonds with substrates and repair oxidized cysteine, allowing translocated proteins the opportunity to fold properly akin to the role of PDIs in the ER. In this chapter, we identified potential substrates of Aim32 disulfide linkages and gave further insight on the functions in both mitochondrial compartments.

3.2 The redox active cysteines of Aim32 are important for MIA pathway

Aim32 has multiple binding partners including components of MIA pathway, particularly import proteins Mia40 and Erv1. Also considering that import of diverse precursors of MIA pathway is dramatically impaired in cells that lack Aim32, we investigated the redox status of Erv1 and Mia40 in mitochondria from WT, Δ*aim32*, and single cysteine mutant strains Δ*aim32*[pC213S] and Δ*aim32*[pC222S] using thiol trapping with methyl-PEG-24-maleimide ($mmPEG_{24}$) (Figure 3-1). Erv1 contains a redox active disulfide (Cys^{130}-Cys^{133}) and a shuttle disulfide (Cys^{30}-Cys^{33}) that are both important for oxidative function, and a structural disulfide (Cys^{159}-Cys^{176})[5]. In control reactions where Erv1 was treated with reductant DTT at 95^0C (Figure 2-1A, lane 2), six mmPEG molecules bound to Erv1 resulting in a mass shift of ~ 7 kDa compared to treatment with DTT alone (lane 1). In other control reactions, treatment with either IAA or mmPEG alone (lanes 4 and 5) did not result in any shift. Pretreatment with IAA,

followed by disulfide reduction with DTT and subsequent mmPEG modification (Figure 2-1A, lane 3), resulted in a Erv1 species that migrated more slowly than reactions in lane 2, thereby indicating partial oxidation of Erv1 by mmPEG. In WT mitochondria, Erv1 is in an oxidized state, whereas a subset of Erv1 remained reduced in Δ*aim32* , Δ*aim32*[pC213S] and Δ*aim32*[pC222S]. The redox status of Mia40 was also investigated (Figure 2-1B). Mia40 can serve as an electron sink and acquire six electrons at once, when presented with reduced substrates[6]. In control reactions in which Mia40 was treated with reductant DTT at 95^0C (Figure 2-1B, lanes 2), six mmPEG molecules bound to Mia40 resulting in a mass shift of ~ 7kDa (full reduction of Mia40 compared to reduced Mia40, lane1). Pretreatment with IAA, followed by disulfide reduction with DTT and mmPEG24 modification, resulted in a slower migrating, reflective of addition of four mmPEG molecules (Figure 2-1B, lane 3). In WT mitochondria, Mia40 was oxidized. In contrast, Mia40 from Δ*aim32* and Δ*aim32*[pC213S] was in an oxidized state. This thiol trapping analysis suggests that Aim32 influences the redox status of Erv1 and Mia40, and the redox active cysteines of Aim32 play roles.

Next, we performed import studies with mitochondria from WT and single cysteine mutants Δ*aim32*[pC213S] and Δ*aim32*[pC222S] (Figure 2-2). The import of MIA substrates Tim9 and Tim10, and TIM22 substrate Tim22 was increased into Δ*aim32*[pC213S], whereas the import of Cmc1 and Su9-DHFR was not compromised. The import of Cmc1 and Tim10 was decreased by ~30% into Δ*aim32*[pC222S], while the import of Tim9 didn't change in Δ*aim32*[pC222S]. The import of Su9-DHFR and Tim22 has modest reduction in Δ*aim32*[pC222S]. Steady-state level of mitochondrial proteins in Δ*aim32*[pC213S] and Δ*aim32*[pC222S] mutants has been examined in

the previous chapter that there was not strongly changed. Thus, Aim32 cysteine mutants have mild effects on protein import and levels in mitochondria.

3.3 Identifying Aim32 disulfide substrates

In the previous chapter, we found that single cysteine mutants stabilize the mixed disulfide intermediates, we used mass spectrometry to identify potential disulfide substrates. Mitochondria from Δ*aim32*[pAim32], Δ*aim32*[pC213S] and Δ*aim32*[pC222S] strains expressing a C-terminal FLAG tag or WT were lysed in 0.1% SDS lysis buffer that only disulfide linkages remain intact. The lysates were purified with FLAG-beads and, after washing, were eluted. Note that the SDS concentration has been diluted to 0.01% during binding that it does not disrupt the beads. Immunoblotting with Aim32 antibody has performed to validate efficiency of the FLAG tag immunoprecipitation (Figure 3-3A). The eluates were also examined in both nonreducing and reducing SDS-PAGE and visualized with SYPRO Ruby stain that more high molecular weight bands were observed in nonreducing condition (Figure 3-3B). The eluates were subjected to mass spectrometry analysis. Potential binding partners are listed in Table 3-1. To validate these interactions, specific co-purifications were performed (Figure 3-4A). Mia40, Cox2, and Sod2 did not co-purified with Aim32 (Figure 3-4B, data not shown). A fraction of Mas2 co-purified with both Aim32 cysteine mutants. A fraction of Mdj1 co-purified with Aim32-FLAG and both cysteine mutants. To further validate the disulfide interaction, bound proteins from co-purification of Δ*aim32*[pC213S] and Δ*aim32*[pC222S] strains were eluted in either nonreducing, or reducing as control, elution buffer and subjected to 2D- Diagonal gel electrophoresis (2DGE) (Figure 3-4B,C). High molecular species of Aim32 below the diagonal are found in both single

cysteine mutants (Figure 3-4B), indicating Aim32 forms disulfide linkages with several proteins when one of the conserved cysteines is mutated. As control, no high molecular species were found in the reducing elution, also indicating no protein aggregations. The disulfide linkages between Aim32 and potential substrates Mas2 and Mdj1, previously found to interact with Aim32, were also investigated by 2DGE and immunoblotting, and were highlighted as red arrow (Figure 3-4B). Thus, the redox active cysteines of Aim32 forms disulfide bonds with substrates including Mas2 and Mdj1 and potentially repair oxidized substrates.

3.4 Aim32 functions in two mitochondrial compartments

Aim32 is unique that it has been localized to both mitochondria IMS and matrix. Aim32 interacts with MIA pathway and influences the redox status of Erv1 and Mia40 suggesting a role for Aim32 in the IMS. To further investigate the function in two compartments, we first generated strains of IMS or matrix targeted Aim32 strains (Figure 3-5A, 3-6A). For IMS targeting, targeting sequences from Cytochrome b2 or Mia40 were added onto N-terminus of Aim32 with first 15 residues removed. Aim32 C-terminally tagged with a triple HA tag was transformed into Δ*aim32* strain. The expression of IMS targeting constructs has been confirmed by total extraction and immunoblotting (Figure 3-5B). To confirm the localization, lysates from spheroplasts of Δ*aim32*[pCYB2-Aim32] were subjected to differential centrifugation and fractions from the 13K pellet (mitochondria) and the 40K supernatant (cytosol) and 40K pellet (microsomes) were separated by SDS-PAGE. Immunoblotting with appropriate markers, Erv1 and Tim44 for mitochondria and Sec62 for ER, verified integrity of the fractionation (Figure 3-5C). IMS-targeted Aim32 purified with the mitochondrial fraction. The sub-mitochondrial

localization of IMS-targeted Δ*aim32*[pb2-Aim32] was determined using osmotic shock in the presence of proteinase K (Figure 3-5D). OM marker Tom70 was degraded immediately, whereas matrix marker Tim44 was inaccessible to protease, even in low sorbitol concentration. IMS markers Cyt b2 and Erv1 were degraded as the sorbitol concentration decreased. Aim32 showed a similar degradation pattern to the IMS markers. As a control, the addition of detergent resulted in degradation of all proteins. For matrix targeting, targeting sequences from Sod2 or Su9 were added onto N-terminus of Aim32 with first 15 residues removed. Aim32 C-terminally tagged with a triple Flag tag was transformed into Δ*aim32* strain (Figure 3-6A). The expression of Δ*aim32*[pSOD22-Aim32] and Δ*aim32*[pSU9-Aim32] has been confirmed by total extraction and immunoblotting (Figure 3-6B). Subcellular and sub-mitochondrial localization of Δ*aim32*[pSOD2-Aim32] have confirmed with mitochondrial matrix localization(Figure 3-6C,D). The steady-state level of mitochondrial proteins was determined by immunoblotting analysis (Figure 3-7). Mitochondria were purified from the WT, Δ*aim32* strain, Δ*aim32*[pCYB2-AIM32], and Δ*aim32*[pSOD2-AIM32] strains grown in rich glucose media at 30°C to mid-log phase. The Cyb2-Aim32 and Sod2-Aim32 proteins migrated slightly higher than endogenous Aim32 and were overexpressed. It is consistent from previous results that the abundance of Tim23, Tim22, and Tim10 was diminished in Δ*aim32* strain, but the level was recovered in both Δ*aim32*[pCYB2-AIM32], and Δ*aim32*[pSOD2-AIM32] strains. For further analysis, complex assembly could be analyzed.

To examine the importance of Aim32 in each compartment of IMS or matrix, the requirement for Aim32 under different growth conditions was tested with IMS-targeted

Δ*aim32*[pCYB2-AIM32] and matrix-targeted Δ*aim32*[pSOD2-AIM32] strains (Figure 3-8). These strains, same as Δ*aim32* strain expressing an empty vector, grew at 30°C but arrested at 37°C on rich glucose media. Also, neither IMS-targeted or matrix-targeted strains rescued the growth defects on respiratory media or in the presence of hydroxyurea(HU). Thus, cells require both IMS and matrix Aim32 for respiration and against HU-induced stress.

3.5 Discussion

In previous study, we reported that Aim32 is dually localized to the mitochondrial IMS and matrix and is required for maintaining the global redox status. Aim32 contains the thioredoxin-like ferredoxin domain[7]. Thioredoxin-like ferredoxin proteins are Fe-S proteins with unknown functions, but potential roles in redox sensing and electron transfer[8]. Our study has supported a global role for Aim32 in maintaining the redox status of the mitochondrial proteome. Specifically, aberrant thiol interactions were observed in the Aim32 deletion mutant or in the single redox-active cysteine mutants. Single cysteine mutants stabilized mixed disulfide intermediates between Aim32 and target proteins. Thus, Aim32 may function as thiol-based molecular switches by modulating disulfide bond formation in their target proteins. Therefore, we designed immunoprecipitation and mass spectrometry to identify disulfide substrates. Mitochondria were lysed in 0.1% SDS that proteins were denatured but only retained in disulfides. Table 3-1 shows candidate substrates identified by mass spectrometry. It is unexpected that proteins of MIA and TIM23 translocon that were identified interact with Aim32 were not candidates of disulfide substrates in this study. We further analyzed candidates that were both identified interact with Aim32 and candidates of disulfide substrates in Table 3-2.

Candidate proteins with more than one cysteine residues were interested in further analysis. Among the candidates, Mas2 and Mdj1 have been validated with specific co-immunoprecipitation and 2DGE. Mas2 is the alpha subunit of matrix processing peptidase (MPP). MPP assembles as a heterodimer of α-MPP (Mas2/PMPCA) and β-MPP (Mas1/PMPCB)[9,10]. MPP is the major presequence peptidase responsible for the initial cleavage of N-terminal targeted precursors in mitochondrial matrix. Both subunits of MPP are essential for cell survival that MPP is crucial in cell viability and mitochondrial homeostasis[11,12]. Defects in MPP processing would lead to effects in protein import and complex assembly and overall mitochondrial function. Another verified Aim32 disulfide substrate Mdj1 belongs to Hsp40(DnaJ) family and is a co-chaperone that stimulate the ATPase activity of mtHsp70[13,14]. It is involved in protein folding in mitochondrial matrix and mtDNA maintenance[15–17]. Mdj1 and mtHsp70 prevent protein aggregation especially under stress conditions[18]. Future studies can be designed to investigate the redox status of MPP and Mdj1 in different conditions. Additional studies are required to elucidate how Aim32 would affect the function of substrates of MPP and Mdj1. Besides those substrates have been verified, additional disulfide candidates from mass spectrometry including Isu2, Nfu1, Yfh1, Oct1, Mxr2, Cox12, and Isa1 would be interesting to investigate.

Aim32 is unique that it dually localizes to both IMS and matrix where it interacts with numerous proteins in both compartments. Indeed, neither IMS-targeted or matrix-targeted Aim32 strains rescued the growth defects on respiratory media or in stress condition of hydroxyurea (HU), which not only prove the dual-localized characterization but functional roles in both

compartments. We have suggested Aim32 a quality control function to maintain global redox status, and it is interesting that substrates of Aim32 disulfide linkages identified were mostly located in the mitochondrial matrix. Previous chapter showed that Aim32 interacts with proteins within MIA pathway and influences the redox status of Mia40 and Erv1 and IMS protein import, suggesting an important role in the IMS. However, Aim32 localization maybe regulated under different conditions. Aim32 uses TIM23 pathway for import and gets processed by MPP, and the reverse translocation to IMS may be regulated by interaction with MIA pathway or IMS chaperons. Both previous studies and our data suggest Aim32 is required for cell growth under stress conditions. Thus, we speculated that Aim32 functions in redox quality control, potentially protecting cells under stress conditions and functions in different compartments. Therefore, additional studies are required to further elucidate the role of Aim32 under stress conditions such as in the presence of hydroxyurea and to investigate the redox profile and disulfide interactions.

In conclusion, Aim32 is a prototype of the class of Fe-S proteins bearing a C-terminal TLF (thioredoxin-like ferredoxin) domain coordinating a [2Fe-2S] cluster. Work presented in Chapter 2 and 3 demonstrate that Aim32 is uniquely localized in two different sub-compartments of the mitochondria. Aim32 functions in redox, more specifically in a mechanism for “quality control” during disulfide bond formation with substrates such as MPP and Mdj1. Aim32 also plays a potential role in electron transport within the MIA pathway. Our study provides insight into the multifunctional nature of a mitochondrial Fe-S protein and provides insight into potential mechanisms of redox sensing within the mitochondria.

3.6 Future perspectives

Aim32 and its cytosolic homolog Apd1 share similar C-terminal thioredoxin-like ferredoxins (TLF) domain[7]. Our analyses showed the C-terminal TLF domain of Aim32 contains a CX8CXnHX3H motif which constitutes the active site and a key tryptophan residue which is conserved among other known ferredoxin proteins (Figure S2-3). These analyses agreed with the amino acid sequence analysis of Apd1 and Aim32 done by Stegmaier et al that also provided evidence for the cluster type and coordination of Apd1[7]. EPR spectroscopy analysis showed that in vivo Apd1 binds a bis-histidinyl coordinated [2Fe-2S] cluster, and UV-Vis, EPR and Mössbauer spectroscopy demonstrated ligands of two cysteine and two histidine[7]. From structure homolog modeling, it is predicted that residues C213, C222 and H249, H253 in Aim32 are the ligands coordinate the [2Fe-2S] cluster. However, direct evidence has not been reported. It is important to analyze Aim32 structure to fully understand the function and support a role in redox. Fe/S cluster binding domain, including TLF, has been found in redox enzymes in many biological systems. Examples include the HndA subunit of NADP-reducing hydrogenase complex and subunit Nqo15 of respiratory complex I that modulate electron transfer and coordinate the [2Fe-2S] cluster[19,20]. Moreover, Aim32 has unique dual localization that it uses TIM23 complex for translocation, cleaved by MPP in matrix, and partially gets reverse translocated to IMS. It is unclear how Fe/S coordination is involved in the biogenesis of Aim32 in different localization that if both IMS and matrix Aim32 have Fe/S binding. Furthermore, it is speculated that Fe/S motif is critical for stress resistance that Aim32 has been found to be essential for cell viability under stress conditions. Mutants of cysteine and histidine residues of

TLF domain compromise the ability of Aim32 to rescue HU sensitivity (Figure 2-3, 2-8). Disruption of the binding motif interferes the Fe/S binding, therefore affecting the function of Aim32. It is exciting to place Aim32 in novel category of bis-histidinyl-coordinated [2Fe-2S] proteins that the putative TLF domain is highly suggestive of a role in redox sensing and electron transfer, potentially protecting cell under conditions of stress, which would also fit well within the scope of the function within MIA pathway.

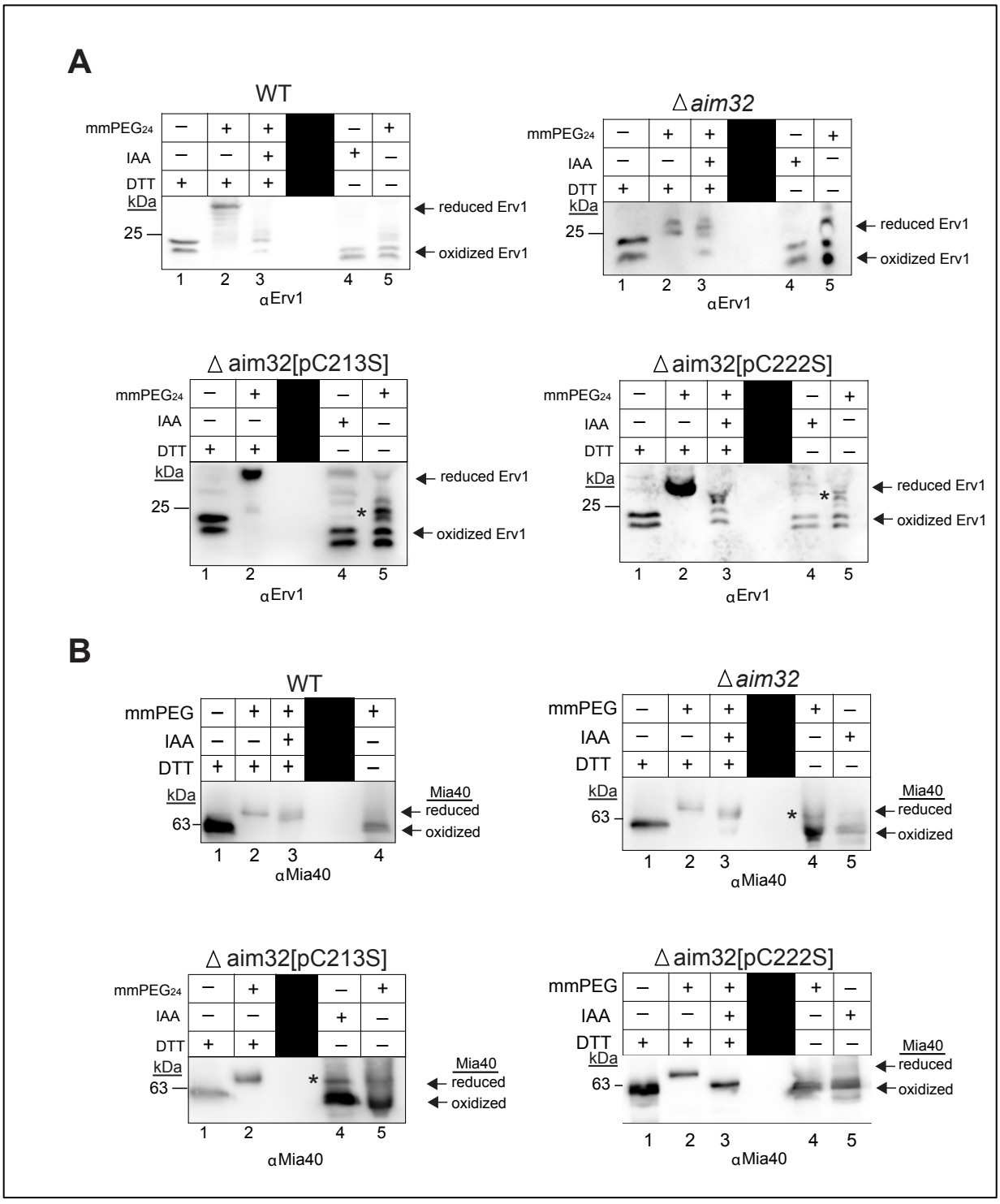

Figure 3-1 Analysis of the Mia40 and Erv1 oxidation state by thiol trapping assay. (A) Isolated mitochondria from WT, Δ*aim32*, Δ*aim32*[pC213S] and Δ*aim32*[pC222S] were resuspended in sample buffer with dithiothreitol (DTT, lanes 1), iodoacetamide (IAA, lane 4),

methyl-PEG_{24}-maleimide ($mPEG_{24}$, lane 5), or pretreated with IAA to block free cysteine residues (lane 3), and disulfide bonds subsequently reduced by DTT, and finally reacted with $mPEG_{24}$ (lane 2). Samples were analyzed by SDS-PAGE and immunoblotting with Erv1 specific antibody. (B) As in (A), immunoblotting with Mia40 specific antibody. * indicates reduced species.

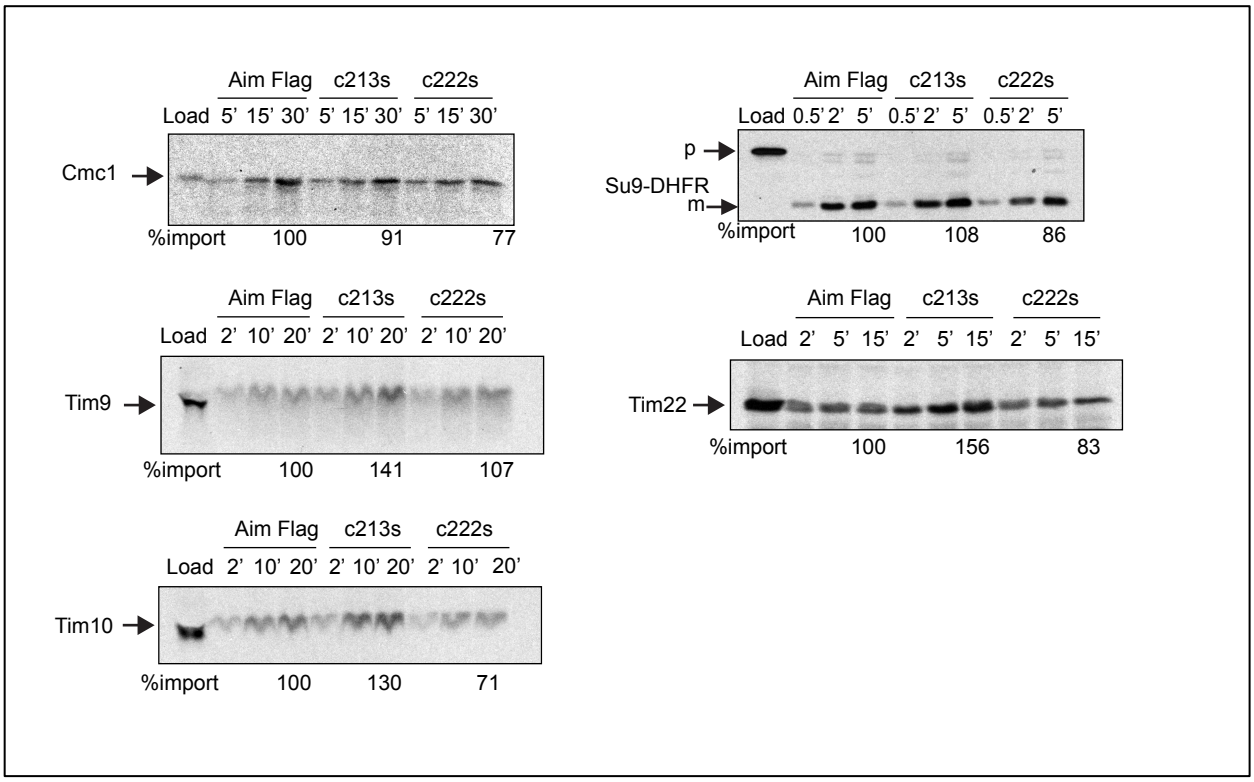

Figure 3-2 Import of diverse mitochondrial precursors into Aim32 single cysteine mutants. Radiolabeled precursors (Cmc1, Tim9, Tim10, Su9-DHFR, and Tim22) were imported into Δ*aim32*[pAim32], Δ*aim32*[pC213S], and Δ*aim32*[pC222S] mutant mitochondria in the indicated time course. Non-imported precursor was removed by protease treatment, and the imported protein was analyzed by SDS-PAGE and autoradiography. A 10% loading control (Load) from the translation reaction was included. Import reactions were quantitated using Image J software; 100% was set as the amount of precursor that imported into Δ*aim32*[pAim32] mitochondria at the endpoint of the time course. A representative gel is shown. (n = 3). p, precursor; m, mature.

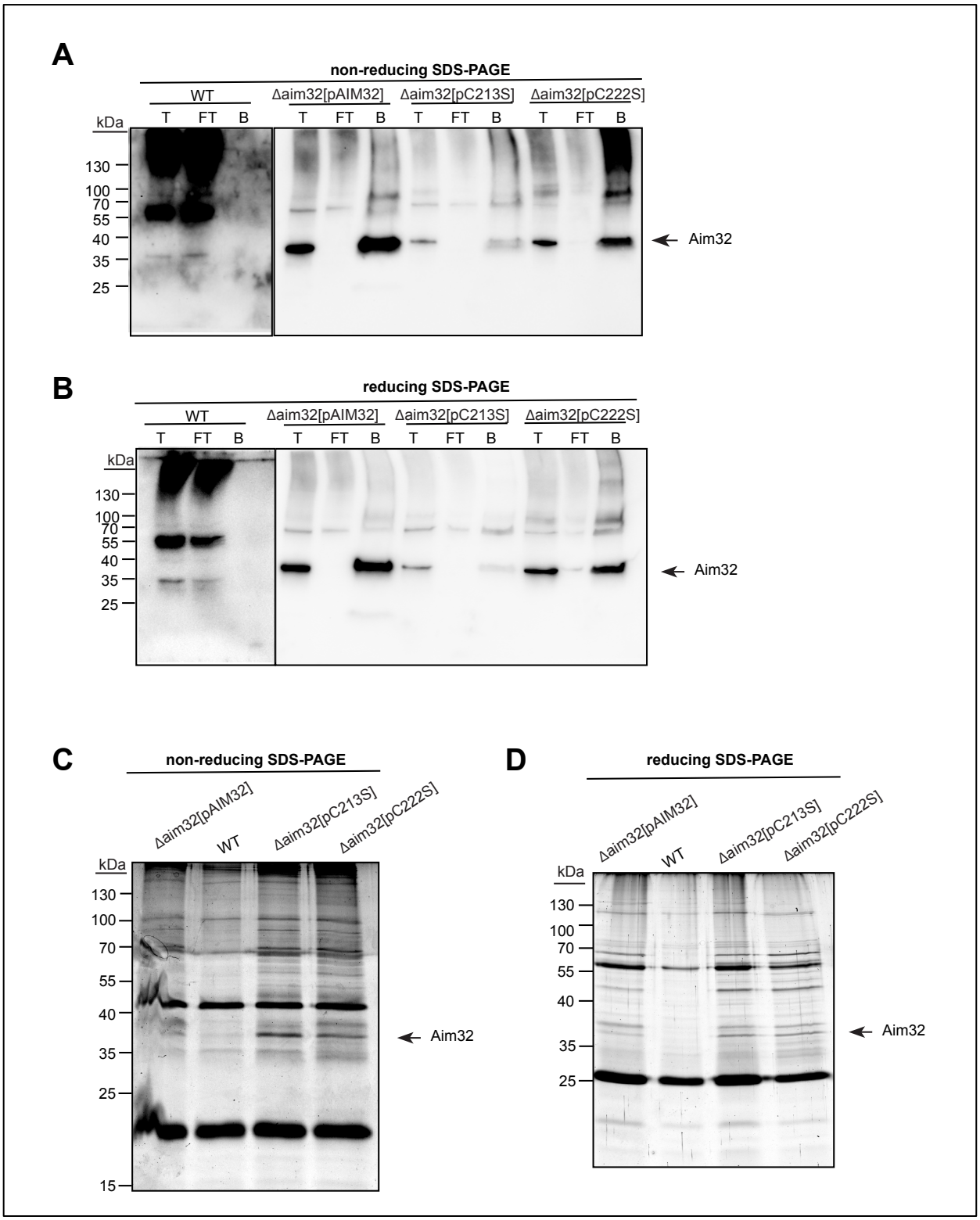

Figure 3-3 Immunoprecipitation of Flag-tagged Aim32 single cysteine mutants. (A)

Mitochondria from WT, or strains expressing a C-terminal Flag tagged Aim32

(Δ*aim32*[pAim32]) and single cysteine mutants (Δ*aim32*[pC213S] and Δ*aim32*[pC222S]) were solubilized in 0.1% SDS. As a control, 10 µg of total extract (T) was withdrawn, and 250µg lysate was incubated with ANTI-FLAG M2 affinity gel. The bindings were washed, and bound protein (B) was eluted. 10 µg of the flow-through fraction (FT) was also included. Samples were resolved by non-reducing SDS-PAGE and analyzed by immunoblotting with specific antibodies against Aim32. (B) As in (A), samples were resolved by reducing SDS-PAGE. (C) As in (A), the bound proteins were resolved by non-reducing SDS-PAGE, stained with SYPRO Ruby gel stain, and visualized using the Bio-Rad ChemiDoc MP imaging system. (D) As in (C), the bound proteins were resolved by reducing SDS-PAGE.

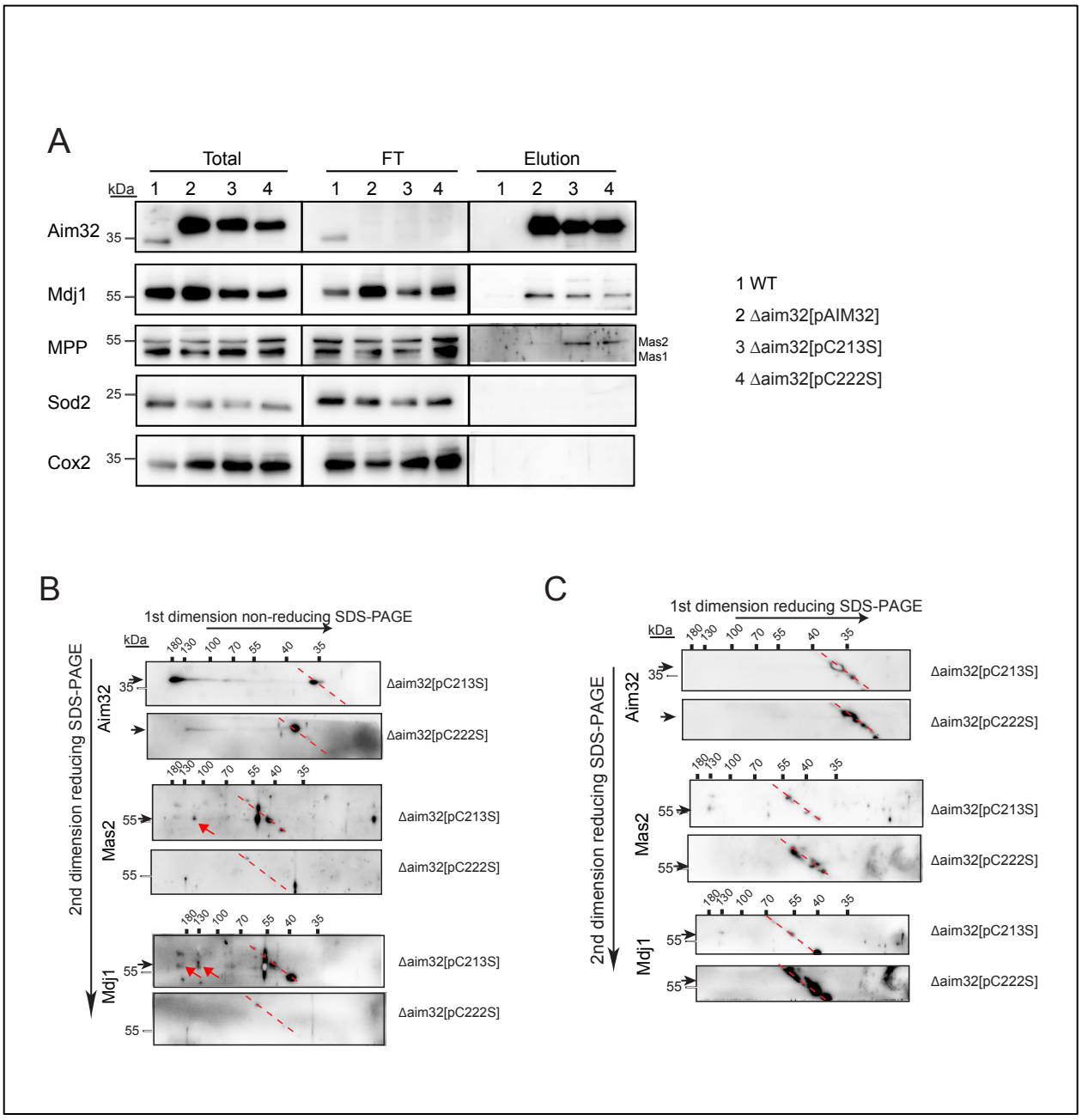

Figure 3-4 Aim32 forms disulfide bonds with substrates. (A) Pull-down assays with FLAG-resin were performed as in Fig. 3-3 with the indicated antibodies. (B) Bound proteins from (A) were eluted in non-reducing condition from Δ*aim32*[pC213S] and Δ*aim32*[pC222S] stains and analyzed by 2DGE immunoblotting. Dashed red line indicates the position of the diagonal. Black arrows at the left of the panel align with the location of the signal expected for each of the

individual proteins tested. Red arrows specify places where the disulfide linkages. (C) As in (B), bound proteins were eluted in reducing condition.

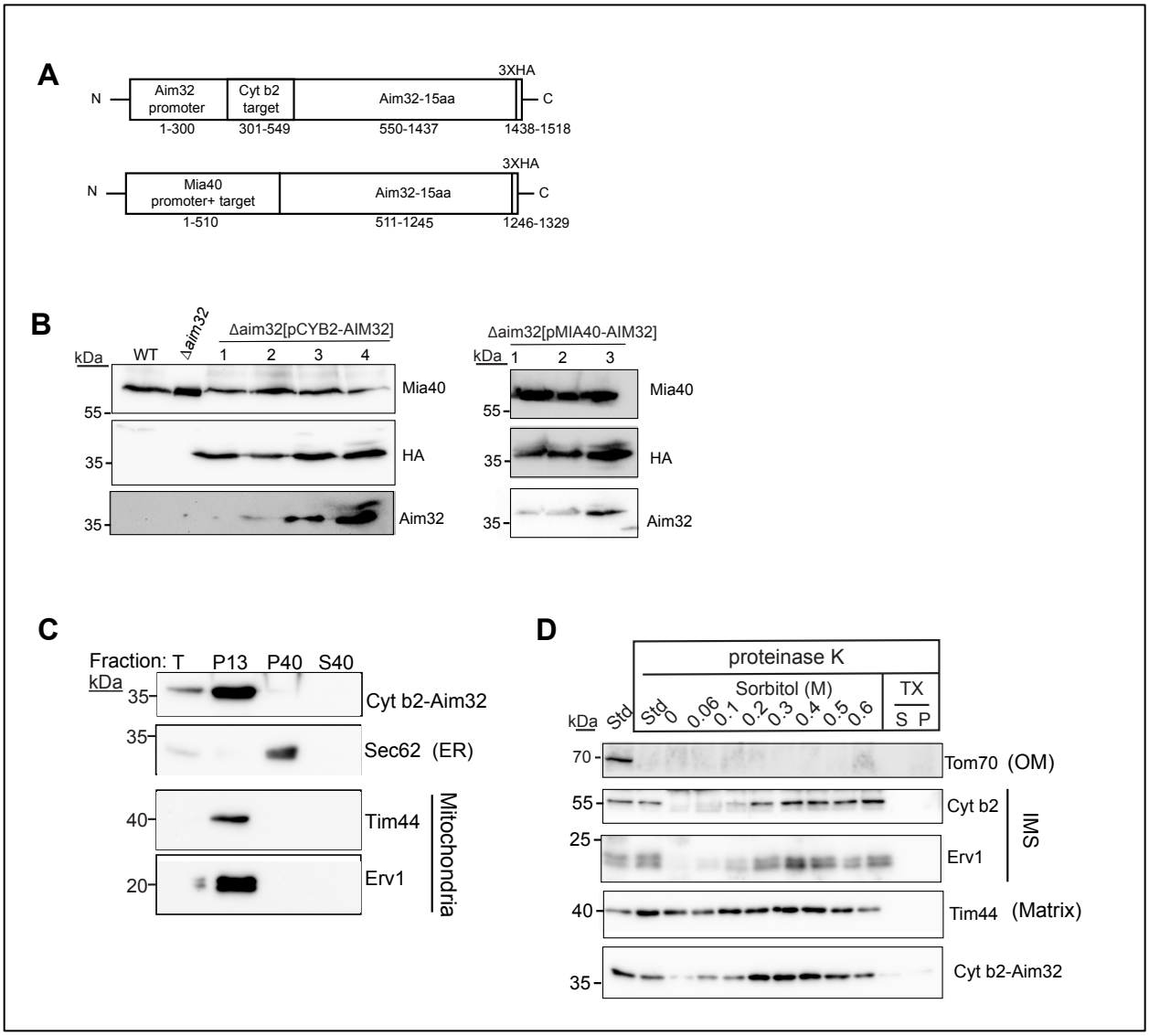

Figure 3-5 Generating IMS-targeted Aim32. (A) IMS-targeted constructs. Targeting sequences from Cytochrome b2 or Mia40 were added onto Aim32 removed first 15 amino acids. C-terminal triple HA tag was added. (B) IMS-targeted construct Δ*aim32*[pCYB2-AIM32] and Δ*aim32*[pMIA40-AIM32] were transformed into Δ*aim32* strain. Total cell lysis was used to check expression of selected colonies by immunoblotting. (C) The Δ*aim32*[pCYB2-AIM32] strain was grown in YPEG at 30^0C and converted to spheroplasts. The total homogenate (T) was fractionated into mitochondria (P13), microsomes (P40), and cytoplasm (S40). An equal amount

of each fraction was separated by SDS-PAGE and analyzed by immunoblot using the indicated antibodies. Markers include Sec62 (ER), and Tim44 and Erv1 (Mitochondria). (D) Mitochondria isolated from Δ*aim32*[pCYB2-AIM32] strain were incubated in 20 mM HEPES-KOH, pH 7.4, 100 μg/ml proteinase K, and the indicated sorbitol concentrations at 4^0C for 30 min, followed by addition of 1 mM PMSF. After centrifugation, the pellet was analyzed by SDS-PAGE and immunoblotted with antibodies against the indicated proteins. OM, outer membrane; IMS, intermembrane space.

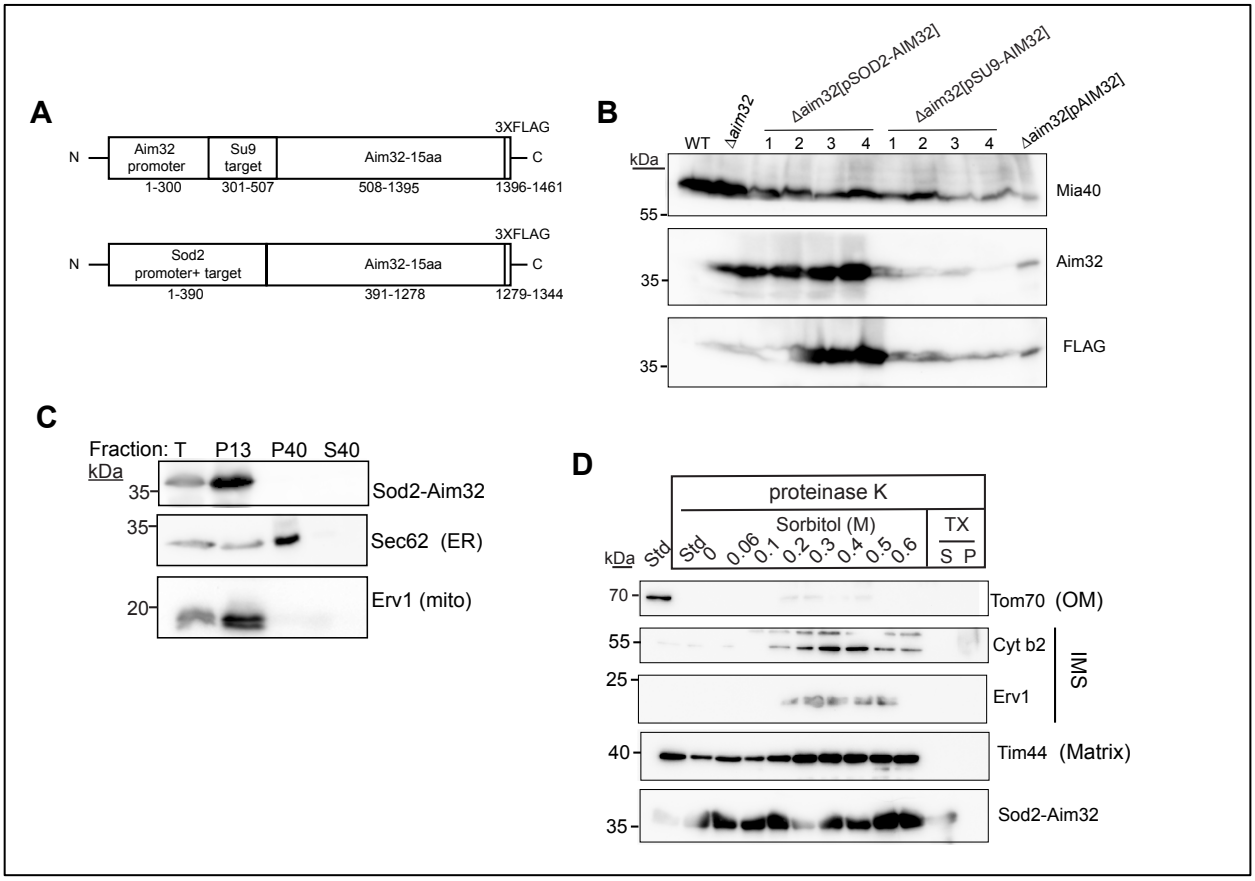

Figure 3-6 Generating matrix targeted Aim32. (A) Matrix-targeted constructs. Targeting sequences from Su9 or Sod2 were added onto Aim32 removed first 15 amino acids. C-terminal triple Flag tag was added. (B) Matrix-targeted construct Δ*aim32*[pSOD2-AIM32] and Δ*aim32*[pSU9-AIM32] were transformed into Δ*aim32* strain. Total cell lysis was used to check expression of selected four colonies by immunoblotting. (C) As in Fig 3-5(C), strain Δ*aim32*[pSOD2-AIM32] was fractioned. (D) As in Fig3-5(D), mitochondria isolated from Δ*aim32*[pSOD2-AIM32] strain was analyzed.

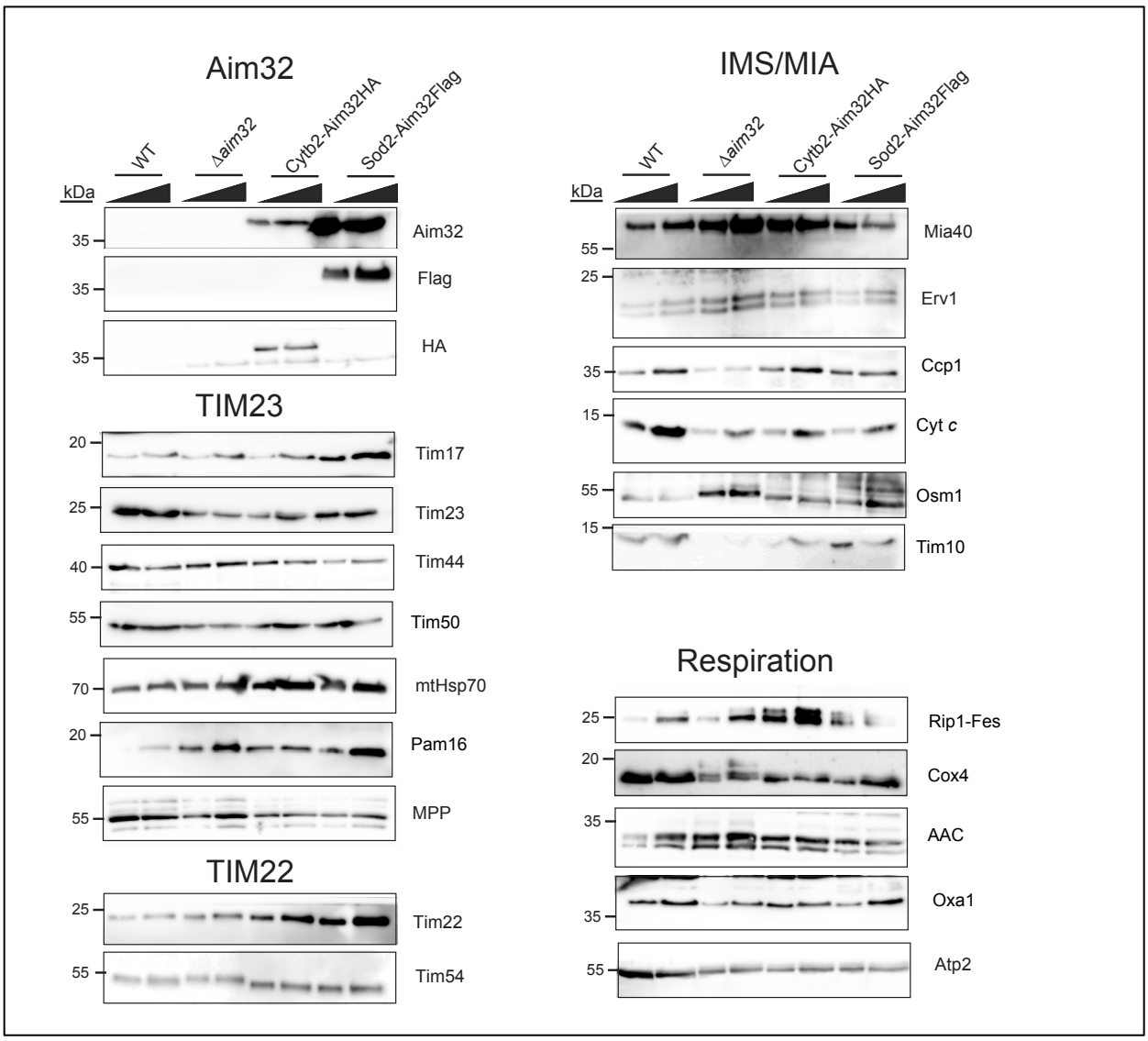

Figure 3-7 Steady-state levels of mitochondrial proteins in IMS and matrix targeted Aim32 strains. A systematic analysis of steady-state levels of mitochondrial proteins (50 and 100 µg) from the parent (WT) or Δ*aim32* strain, Δ*aim32*[pCYB2-AIM32], and Δ*aim32*[pSOD2-AIM32] (grown at 30ºC in rich glucose media) was performed by immunoblot with antibodies against the indicated mitochondrial proteins. Proteins were organized by substrates of the MIA, TIM23 and TIM22 pathways and respiratory proteins.

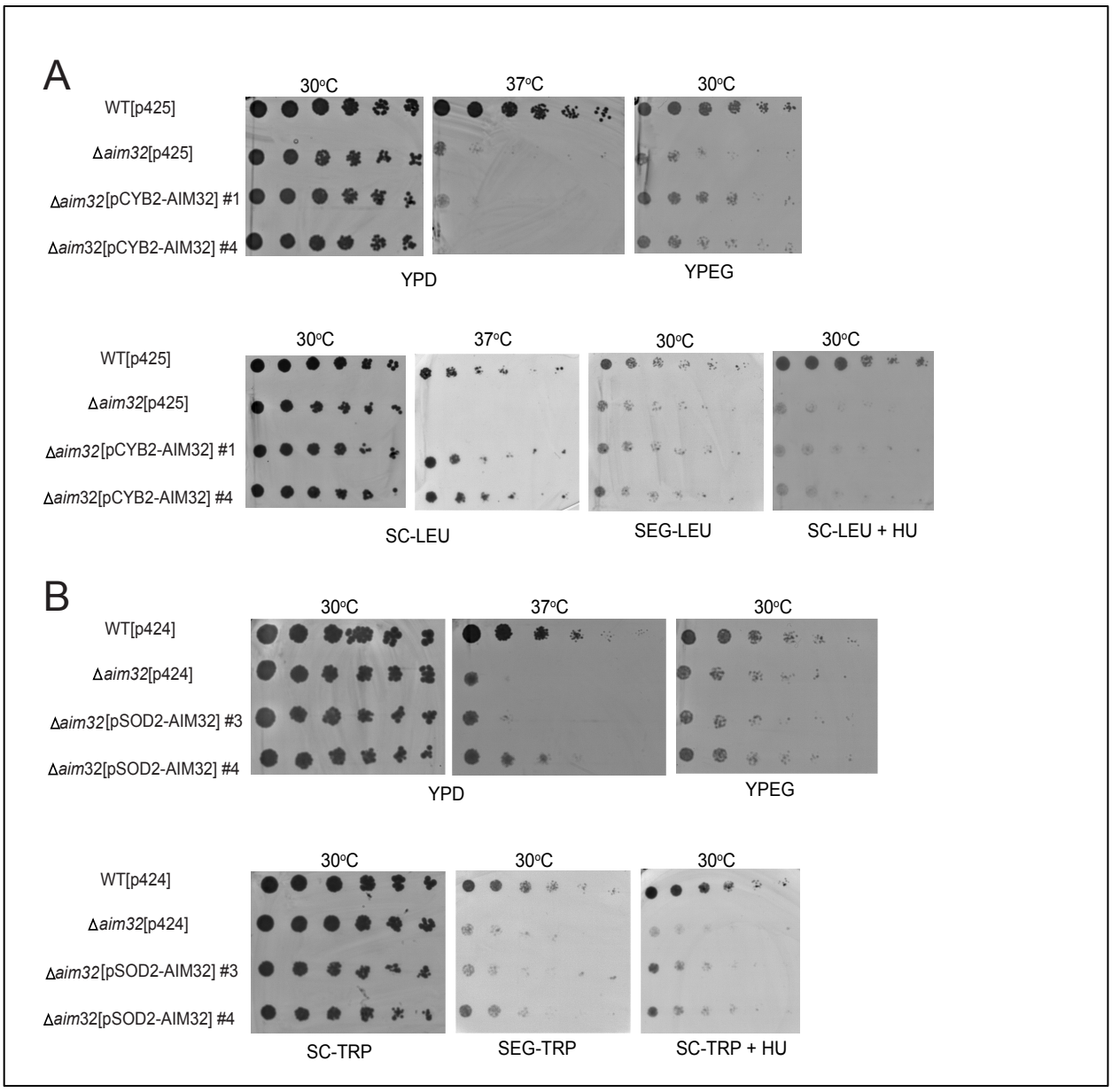

Figure 3-8 Both IMS and matrix Aim32 are essential for mitochondrial respiration. (A) Growth analysis of WT and Δ*aim32* strains transformed with an empty plasmid, and two Δ*aim32*[pCYB2-AIM32] strains on rich glucose (YPD), ethanol/glycerol (YPEG) media, selective minimal glucose media lacking leucine (SC-LEU) with or without the addition of 100 mM hydroxyurea (HU), and minimal ethanol/glycerol lacking leucine (SEG-LEU) was analyzed by serial 5-fold dilution of liquid cultures grown to mid-log phase at 30ºC and 37ºC. (B) As in

(A), WT and Δ*aim32* strains transformed with an empty plasmid, and two Δ*aim32*[pSOD2-AIM32] strains were analyzed.

Protein	DESCRIPTION	Spectral Count-WT	Spectral Count-Δaim32 [pAIM32-FLAG]	Spectral Count-Δaim32 [pC213S]	Spectral Count-Δaim32 [pC222S]
YML050W	AIM32 SGDID:S000004514, Chr XIII from 173139-174074, Genome Release 64-2-1, Verified ORF, Putative protein of unknown function; null mutant is viable and displays elevated frequency of mitochondrial genome loss	**0**	**56**	**40**	**131**
YMR189W	GCV2 SGDID:S000004801, Chr XIII from 637500-640604, Genome Release 64-2-1, Verified ORF, P subunit of the mitochondrial glycine decarboxylase complex; glycine decarboxylase is required for the catabolism of glycine to 5,10-methylene-THF; expression is regulated by levels of 5,10-methylene-THF in the cytoplasm	**0**	**14**	**14**	**108**
YOR226C	ISU2 SGDID:S000005752, Chr XV from 762084-761614, Genome Release 64-2-1, reverse complement, Verified ORF, Protein required for synthesis of iron-sulfur proteins; localized to the mitochondrial matrix; performs a scaffolding function in mitochondria during Fe/S cluster assembly; involved in Fe-S cluster assembly for both mitochondrial and cytosolic proteins; isu1 isu2 double mutant is inviable; protein abundance increases in response to DNA replication stress; evolutionarily conserved; ISU2 has a paralog, ISU1, that arose from the whole genome duplication	**0**	**10**	**5**	**15**
YIL022W	TIM44 SGDID:S000001284, Chr IX from 311165-312460, Genome Release 64-2-1, Verified ORF, Essential component of the TIM23 complex; tethers the import motor and regulatory factors (PAM complex) to the translocation channel (Tim23p-Tim17p core complex); TIM23 complex is short for the translocase of the inner mitochondrial membrane	**0**	**9**	**0**	**4**
YLR163C	MAS1 SGDID:S000004153, Chr XII from 493254-491866, Genome Release 64-2-1, reverse complement, Verified ORF, Beta subunit of the mitochondrial processing protease (MPP); essential processing enzyme that cleaves the N-terminal targeting sequences from mitochondrially imported proteins	**0**	**8**	**2**	**12**
YKL040C	NFU1 SGDID:S000001523, Chr XI from 361828-361058, Genome Release 64-2-1, reverse complement, Verified ORF, Protein involved in iron metabolism in mitochondria; similar to NifU, which is a protein required for the maturation of the Fe/S clusters of nitrogenase in nitrogen-fixing bacteria	**0**	**7**	**4**	**20**
YHR199C	AIM46 SGDID:S000001242, Chr VIII from 498422-497490, Genome Release 64-2-1, reverse complement, Verified ORF, Putative protein of unknown function; the authentic, non-tagged protein is detected in highly purified mitochondria in high-throughput studies; null mutant displays elevated frequency of mitochondrial genome loss	**0**	**6**	**3**	**12**
YLR369W	SSQ1 SGDID:S000004361, Chr XII from 859552-861525, Genome Release 64-2-1, Verified ORF, Mitochondrial hsp70-type molecular chaperone; required for assembly of iron/sulfur clusters into proteins at a step after cluster synthesis, and for maturation of Yfh1p, which is a homolog of human frataxin implicated in Friedreich's ataxia	**0**	**6**	**3**	**19**
YDR529C	QCR7 SGDID:S000002937, Chr IV from 1496548-1496165, Genome Release 64-2-1, reverse complement, Verified ORF, Subunit 7 of ubiquinol cytochrome-c reductase (Complex III); Complex III is a component of the mitochondrial inner membrane electron transport chain; oriented facing the mitochondrial matrix; N-terminus appears to play a role in complex	**0**	**6**	**0**	**5**

Protein	DESCRIPTION	Spectral Count-WT	Spectral Count-Δaim32 [pAIM32-FLAG]	Spectral Count-Δaim32 [pC213S]	Spectral Count-Δaim32 [pC222S]
YMR194C-B	CMC4 SGDID:S000028514, Chr XIII from 652775-652594,652887-652848, Genome Release 64-2-1, reverse complement, Verified ORF, Protein that localizes to the mitochondrial intermembrane space; localizes via the Mia40p-Erv1p system; contains twin cysteine-x(9)-cysteine motifs	**0**	**5**	**0**	**4**
YDL120W	YFH1 SGDID:S000002278, Chr IV from 245923-246447, Genome Release 64-2-1, Verified ORF, Mitochondrial matrix iron chaperone; oxidizes and stores iron; interacts with Isu1p to promote Fe-S cluster assembly; mutation results in multiple Fe/S-dependent enzyme deficiencies; human frataxin homolog is mutated in Friedrich's ataxia	**0**	**4**	**0**	**5**
YFR033C	QCR6 SGDID:S000001929, Chr VI from 224769-224326, Genome Release 64-2-1, reverse complement, Verified ORF, Subunit 6 of the ubiquinol cytochrome-c reductase complex; the complex, also known as the cytochrome bc(1) complex or Complex III, is a component of the mitochondrial inner membrane electron transport chain; highly acidic protein; required for maturation of cytochrome c1; may be loosely associated with the complex since it is easily released into the intermembrane space	**0**	**4**	**0**	**6**
YPL078C	ATP4 SGDID:S000005999, Chr XVI from 408744-408010, Genome Release 64-2-1, reverse complement, Verified ORF, Subunit b of the stator stalk of mitochondrial F1F0 ATP synthase; ATP synthase is a large, evolutionarily conserved enzyme complex required for ATP synthesis; contributes to the oligomerization of the complex, which in turn determines the shape of inner membrane cristae; phosphorylated	**0**	**4**	**0**	**9**
YJR048W	CYC1 SGDID:S000003809, Chr X from 526335-526664, Genome Release 64-2-1, Verified ORF, Cytochrome c, isoform 1; also known as iso-1-cytochrome c; electron carrier of the mitochondrial intermembrane space that transfers electrons from ubiquinone-cytochrome c oxidoreductase to cytochrome c oxidase during cellular respiration; mutations in human homolog cause insulin-responsive hyperglycemia; CYC1 has a paralog, CYC7, that arose from the whole genome duplication	**0**	**3**	**0**	**3**
YKL134C	OCT1 SGDID:S000001617, Chr XI from 191442-189124, Genome Release 64-2-1, reverse complement, Verified ORF, Mitochondrial intermediate peptidase; cleaves destabilizing N-terminal residues of a subset of proteins upon import, after their cleavage by mitochondrial processing peptidase (Mas1p-Mas2p); may contribute to mitochondrial iron homeostasis	**0**	**3**	**0**	**6**
YKL195W	MIA40 SGDID:S000001678, Chr XI from 75821-77032, Genome Release 64-2-1, Verified ORF, Mitochondrial oxidoreductase; involved in mitochondrial intermembrane space import; component of MIA pathway which mediates import and oxidative folding of substrates including small proteins containing twin cysteine motifs; acts in concert with Erv1p, which oxidizes the cysteine residues of Mia40p to comprise a disulfide relay system that catalyzes import; also mediates folding of Atp23p via a chaperone-like activity; forms a dimer that binds iron-sulfur cluster in vitro	**0**	**3**	**0**	**2**

Protein	DESCRIPTION	Spectral Count-WT	Spectral Count-Δaim32 [pAIM32-FLAG]	Spectral Count-Δaim32 [pC213S]	Spectral Count-Δaim32 [pC222S]
YCL033C	MXR2 SGDID:S000000538, Chr III from 63282-62776, Genome Release 64-2-1, reverse complement, Verified ORF, Methionine-R-sulfoxide reductase; involved in the response to oxidative stress; protects iron-sulfur clusters from oxidative inactivation along with MXR1; involved in the regulation of lifespan	**0**	**2**	**0**	**4**
YCR083W	TRX3 SGDID:S000000679, Chr III from 259578-259961, Genome Release 64-2-1, Verified ORF, Mitochondrial thioredoxin; highly conserved oxidoreductase required to maintain the redox homeostasis of the cell, forms the mitochondrial thioredoxin system with Trr2p, redox state is maintained by both Trr2p and Glr1p	**0**	**2**	**0**	**6**
YDR232W	HEM1 SGDID:S000002640, Chr IV from 927452-929098, Genome Release 64-2-1, Verified ORF, 5-aminolevulinate synthase; catalyzes the first step in the heme biosynthetic pathway; an N-terminal signal sequence is required for localization to the mitochondrial matrix; expression is regulated by Hap2p-Hap3p	**0**	**2**	**0**	**6**
YHR005C-A	TIM10 SGDID:S000003530, Chr VIII from 115901-115620, Genome Release 64-2-1, reverse complement, Verified ORF, Essential protein of the mitochondrial intermembrane space; forms a complex with Tim9p (TIM10 complex) that delivers hydrophobic proteins to the TIM22 complex for insertion into the inner membrane	**0**	**2**	**0**	**3**
YLR038C	COX12 SGDID:S000004028, Chr XII from 225172-224921, Genome Release 64-2-1, reverse complement, Verified ORF, Subunit VIb of cytochrome c oxidase; cytochrome c oxidase is also known as respiratory Complex IV and is the terminal member of the mitochondrial inner membrane electron transport chain; required for assembly of cytochrome c oxidase but not required for activity after assembly; phosphorylated; easily released from the intermembrane space, suggesting a loose association with Complex IV	**0**	**2**	**0**	**2**
YML120C	NDI1 SGDID:S000004589, Chr XIII from 29807-28266, Genome Release 64-2-1, reverse complement, Verified ORF, NADH:ubiquinone oxidoreductase; transfers electrons from NADH to ubiquinone in the respiratory chain but does not pump protons, in contrast to the higher eukaryotic multisubunit respiratory complex I; phosphorylated; involved in Mn and H2O2 induced apoptosis; upon apoptotic stress, Ndip is activated in the mitochondria by N-terminal cleavage, and the truncated protein translocates to the cytoplasm to induce apoptosis; homolog of human AMID	**0**	**2**	**0**	**18**
YPR006C	ICL2 SGDID:S000006210, Chr XVI from 568996-567269, Genome Release 64-2-1, reverse complement, Verified ORF, 2-methylisocitrate lyase of the mitochondrial matrix; functions in the methylcitrate cycle to catalyze the conversion of 2-methylisocitrate to succinate and pyruvate; ICL2 transcription is repressed by glucose and induced by ethanol	**0**	**2**	**0**	**14**
Q0250	COX2 SGDID:S000007281, Chr Mito from 73758-74513, Genome Release 64-2-1, Verified ORF, Subunit II of cytochrome c oxidase (Complex IV); Complex IV is the terminal member of the mitochondrial inner membrane electron transport chain; one of three mitochondrially-encoded subunits	**0**	**0**	**0**	**6**

Protein	DESCRIPTION	Spectral Count-WT	Spectral Count-Δaim32 [pAIM32-FLAG]	Spectral Count-Δaim32 [pC213S]	Spectral Count-Δaim32 [pC222S]
YER053C	PIC2 SGDID:S000000855, Chr V from 259639-258737, Genome Release 64-2-1, reverse complement, Verified ORF, Mitochondrial copper and phosphate carrier; imports copper and inorganic phosphate into mitochondria; functionally redundant with Mir1p but less abundant than Mir1p under normal conditions; expression is induced at high temperature	**0**	**0**	**0**	**10**
YER073W	ALD5 SGDID:S000000875, Chr V from 304030-305592, Genome Release 64-2-1, Verified ORF, Mitochondrial aldehyde dehydrogenase; involved in regulation or biosynthesis of electron transport chain components and acetate formation; activated by K+; utilizes NADP+ as the preferred coenzyme; constitutively expressed	**0**	**0**	**0**	**13**
YER141W	COX15 SGDID:S000000943, Chr V from 453459-454919, Genome Release 64-2-1, Verified ORF, Protein required for the hydroxylation of heme O to form heme A; heme A is an essential prosthetic group for cytochrome c oxidase	**0**	**0**	**0**	**18**
YER154W	OXA1 SGDID:S000000956, Chr V from 475020-476228, Genome Release 64-2-1, Verified ORF, Mitochondrial inner membrane insertase; mediates the insertion of both mitochondrial- and nuclear-encoded proteins from the matrix into the inner membrane; also has a role in insertion of carrier proteins into the inner membrane; acts as a voltage-gated ion channel, activated by substrate peptides; interacts with mitochondrial ribosomes; conserved from bacteria to animals	**0**	**0**	**0**	**4**
YGR033C	TIM21 SGDID:S000003265, Chr VII from 554967-554248, Genome Release 64-2-1, reverse complement, Verified ORF, Nonessential component of the TIM23 complex; interacts with the Translocase of the Outer Mitochondrial membrane (TOM complex) and with respiratory enzymes; may regulate the Translocase of the Inner Mitochondrial membrane (TIM23 complex) activity	**0**	**0**	**0**	**7**
YGR062C	COX18 SGDID:S000003294, Chr VII from 617278-616328, Genome Release 64-2-1, reverse complement, Verified ORF, Protein required for membrane insertion of C-terminus of Cox2p; mitochondrial integral inner membrane protein; interacts genetically and physically with Mss2p and Pnt1p; similar to S. cerevisiae Oxa1, N. crassa Oxa2p, and E. coli YidC	**0**	**0**	**0**	**5**
YJL166W	QCR8 SGDID:S000003702, Chr X from 106434-106718, Genome Release 64-2-1, Verified ORF, Subunit 8 of ubiquinol cytochrome-c reductase (Complex III); Complex III is a component of the mitochondrial inner membrane electron transport chain; oriented facing the intermembrane space; expression is regulated by Abf1p and Cpf1p	**0**	**0**	**0**	**6**
YJL208C	NUC1 SGDID:S000003744, Chr X from 41183-40194, Genome Release 64-2-1, reverse complement, Verified ORF, Major mitochondrial nuclease; has RNAse and DNA endo- and exonucleolytic activities; roles in mitochondrial recombination, apoptosis and maintenance of polyploidy; involved in fragmentation of genomic DNA during PND (programmed nuclear destruction); encodes ortholog of mammalian endoG	**0**	**0**	**0**	**23**

Protein	DESCRIPTION	Spectral Count-WT	Spectral Count-Δaim32 [pAIM32-FLAG]	Spectral Count-Δaim32 [pC213S]	Spectral Count-Δaim32 [pC222S]
YOR037W	CYC2 SGDID:S000005563, Chr XV from 401555-402655, Genome Release 64-2-1, Verified ORF, Mitochondrial peripheral inner membrane protein; contains a FAD cofactor in a domain exposed in the intermembrane space; exhibits redox activity in vitro; likely participates in ligation of heme to acytochromes c and c1 (Cyc1p and Cyt1p)	**0**	**0**	**0**	**15**
YPL172C	COX10 SGDID:S000006093, Chr XVI from 225741-224353, Genome Release 64-2-1, reverse complement, Verified ORF, Heme A:farnesyltransferase; catalyzes the first step in the conversion of protoheme to the heme A prosthetic group required for cytochrome c oxidase activity; human ortholog is associated with mitochondrial disorders	**0**	**0**	**0**	**10**
YPR002W	PDH1 SGDID:S000006206, Chr XVI from 558385-559935, Genome Release 64-2-1, Verified ORF, Putative 2-methylcitrate dehydratase; mitochondrial protein that participates in respiration; induced by diauxic shift; homologous to E. coli PrpD, may take part in the conversion of 2-methylcitrate to 2-methylisocitrate	**3**	**24**	**10**	**33**
YAL038W	CDC19 SGDID:S000000036, Chr I from 71786-73288, Genome Release 64-2-1, Verified ORF, Pyruvate kinase; functions as a homotetramer in glycolysis to convert phosphoenolpyruvate to pyruvate, the input for aerobic (TCA cycle) or anaerobic (glucose fermentation) respiration; regulated via allosteric activation by fructose bisphosphate; CDC19 has a paralog, PYK2, that arose from the whole genome duplication	**3**	**18**	**10**	**33**
YFL016C	MDJ1 SGDID:S000001878, Chr VI from 106236-104701, Genome Release 64-2-1, reverse complement, Verified ORF, Co-chaperone that stimulates HSP70 protein Ssc1p ATPase activity; involved in protein folding/refolding in the mitochodrial matrix; required for proteolysis of misfolded proteins; member of the HSP40 (DnaJ) family of chaperones	**3**	**17**	**6**	**43**
YDR298C	ATP5 SGDID:S000002706, Chr IV from 1058814-1058176, Genome Release 64-2-1, reverse complement, Verified ORF, Subunit 5 of the stator stalk of mitochondrial F1F0 ATP synthase; F1F0 ATP synthase is a large, evolutionarily conserved enzyme complex required for ATP synthesis; homologous to bovine subunit OSCP (oligomycin sensitivity-conferring protein); phosphorylated	**3**	**13**	**4**	**21**
YPL135W	ISU1 SGDID:S000006056, Chr XVI from 297553-298050, Genome Release 64-2-1, Verified ORF, Conserved protein of the mitochondrial matrix; performs a scaffolding function during assembly of iron-sulfur clusters, interacts physically and functionally with yeast frataxin (Yfh1p); isu1 isu2 double mutant is inviable; ISU1 has a paralog, ISU2, that arose from the whole genome duplication	**3**	**12**	**6**	**21**
YHR051W	COX6 SGDID:S000001093, Chr VIII from 209705-210151, Genome Release 64-2-1, Verified ORF, Subunit VI of cytochrome c oxidase (Complex IV); Complex IV is the terminal member of the mitochondrial inner membrane electron transport chain; expression is regulated by oxygen levels	**3**	**8**	**0**	**10**

Protein	DESCRIPTION	Spectral Count-WT	Spectral Count-Δaim32 [pAIM32-FLAG]	Spectral Count-Δaim32 [pC213S]	Spectral Count-Δaim32 [pC222S]
YKL016C	ATP7 SGDID:S000001499, Chr XI from 407989-407465, Genome Release 64-2-1, reverse complement, Verified ORF, Subunit d of the stator stalk of mitochondrial F1F0 ATP synthase; F1F0 ATP synthase is a large, evolutionarily conserved enzyme complex required for ATP synthesis	3	2	0	11
YEL020W-A	TIM9 SGDID:S000007256, Chr V from 117211-117474, Genome Release 64-2-1, Verified ORF, Essential protein of the mitochondrial intermembrane space; forms a complex with Tim10p (TIM10 complex) that delivers hydrophobic proteins to the TIM22 complex for insertion into the inner membrane	4	7	4	4
YEL024W	RIP1 SGDID:S000000750, Chr V from 107260-107907, Genome Release 64-2-1, Verified ORF, Ubiquinol-cytochrome-c reductase; a Rieske iron-sulfur protein of the mitochondrial cytochrome bc1 complex; transfers electrons from ubiquinol to cytochrome c1 during respiration; during import, Rip1p is first imported into the mitochondrial matrix where it is processed, acquires its Fe-S cluster, and is folded, then is translocated into the inner membrane by the action of a homo-oligomer of Bcs1p, and finally is delivered by Bcs1p to Complex III for assembly	4	7	2	9
YOR020C	HSP10 SGDID:S000005546, Chr XV from 370844-370524, Genome Release 64-2-1, reverse complement, Verified ORF, Mitochondrial matrix co-chaperonin; inhibits the ATPase activity of Hsp60p, a mitochondrial chaperonin; involved in protein folding and sorting in the mitochondria; 10 kD heat shock protein with similarity to E. coli groES	5	12	8	9
YHR008C	SOD2 SGDID:S000001050, Chr VIII from 123590-122889, Genome Release 64-2-1, reverse complement, Verified ORF, Mitochondrial manganese superoxide dismutase; protects cells against oxygen toxicity; phosphorylated	6	8	0	9
YGL187C	COX4 SGDID:S000003155, Chr VII from 150171-149704, Genome Release 64-2-1, reverse complement, Verified ORF, Subunit IV of cytochrome c oxidase; the terminal member of the mitochondrial inner membrane electron transport chain; precursor N-terminal 25 residues are cleaved during mitochondrial import; phosphorylated; spermidine enhances translation	7	15	6	18
YIL125W	KGD1 SGDID:S000001387, Chr IX from 122689-125733, Genome Release 64-2-1, Verified ORF, Subunit of the mitochondrial alpha-ketoglutarate dehydrogenase complex; catalyzes a key step in the tricarboxylic acid (TCA) cycle, the oxidative decarboxylation of alpha-ketoglutarate to form succinyl-CoA	8	53	18	114
YIL155C	GUT2 SGDID:S000001417, Chr IX from 53708-51759, Genome Release 64-2-1, reverse complement, Verified ORF, Mitochondrial glycerol-3-phosphate dehydrogenase; expression is repressed by both glucose and cAMP and derepressed by non-fermentable carbon sources in a Snf1p, Rsf1p, Hap2/3/4/5 complex dependent manner	8	17	2	34

Protein	DESCRIPTION	Spectral Count-WT	Spectral Count-Δaim32 [pAIM32-FLAG]	Spectral Count-Δaim32 [pC213S]	Spectral Count-Δaim32 [pC222S]
YBL045C	COR1 SGDID:S000000141, Chr II from 135516-134143, Genome Release 64-2-1, reverse complement, Verified ORF, Core subunit of the ubiquinol-cytochrome c reductase complex; the ubiquinol-cytochrome c reductase complex (bc1 complex) is a component of the mitochondrial inner membrane electron transport chain	**21**	**50**	**43**	**62**
YPR191W	QCR2 SGDID:S000006395, Chr XVI from 919381-920487, Genome Release 64-2-1, Verified ORF, Subunit 2 of ubiquinol cytochrome-c reductase (Complex III); Complex III is a component of the mitochondrial inner membrane electron transport chain; phosphorylated; transcription is regulated by Hap1p, Hap2p/Hap3p, and heme	**24**	**44**	**47**	**66**
YBL064C	PRX1 SGDID:S000000160, Chr II from 101156-100371, Genome Release 64-2-1, reverse complement, Verified ORF, Mitochondrial peroxiredoxin with thioredoxin peroxidase activity; has a role in reduction of hydroperoxides; reactivation requires Trr2p and glutathione; induced during respiratory growth and oxidative stress; phosphorylated; protein abundance increases in response to DNA replication stress	**30**	**31**	**20**	**31**
YLR259C	HSP60 SGDID:S000004249, Chr XII from 665002-663284, Genome Release 64-2-1, reverse complement, Verified ORF, Tetradecameric mitochondrial chaperonin; required for ATP-dependent folding of precursor polypeptides and complex assembly; prevents aggregation and mediates protein refolding after heat shock; role in mtDNA transmission; phosphorylated	**50**	**126**	**76**	**154**
YJR045C	SSC1 SGDID:S000003806, Chr X from 521602-519638, Genome Release 64-2-1, reverse complement, Verified ORF, Hsp70 family ATPase; constituent of the import motor component of the Translocase of the Inner Mitochondrial membrane (TIM23 complex); involved in protein translocation and folding; subunit of SceI endonuclease; SSC1 has a paralog, ECM10, that arose from the whole genome duplication	**52**	**130**	**94**	**170**

Table 3-1 Aim32 single cysteine mutants co-immunoprecipitation hits identified by mass spectrometry. Purified mitochondria from WT, or strains expressing a C-terminal Flag tagged Aim32 (Δ*aim32*[pAim32]) and single cysteine mutants (Δ*aim32*[pC213S] and Δ*aim32*[pC222S]) were solubilized in 0.1% SDS. Lysate was incubated with ANTI-FLAG M2 affinity gel. After wash, bound proteins were eluted in 10mM DTT and subjected to mass spectrometry analysis.

Protein	DESCRIPTION	Molecular Weight	#cysteine
YMR189W	GCV2 SGDID:S000004801, Chr XIII from 637500-640604, Genome Release 64-2-1, Verified ORF, P subunit of the mitochondrial glycine decarboxylase complex; glycine decarboxylase is required for the catabolism of glycine to 5,10-methylene-THF; expression is regulated by levels of 5,10-methylene-THF in the cytoplasm	114	17
YOR226C	ISU2 SGDID:S000005752, Chr XV from 762084-761614, Genome Release 64-2-1, reverse complement, Verified ORF, Protein required for synthesis of iron-sulfur proteins; localized to the mitochondrial matrix; performs a scaffolding function in mitochondria during Fe/S cluster assembly; involved in Fe-S cluster assembly for both mitochondrial and cytosolic proteins; isu1 isu2 double mutant is inviable; protein abundance increases in response to DNA replication stress; evolutionarily conserved; ISU2 has a paralog, ISU1, that arose from the whole genome duplication	17	3
YIL022W	TIM44 SGDID:S000001284, Chr IX from 311165-312460, Genome Release 64-2-1, Verified ORF, Essential component of the TIM23 complex; tethers the import motor and regulatory factors (PAM complex) to the translocation channel (Tim23p-Tim17p core complex); TIM23 complex is short for the translocase of the inner mitochondrial membrane	49	1
YLR163C	MAS1 SGDID:S000004153, Chr XII from 493254-491866, Genome Release 64-2-1, reverse complement, Verified ORF, Beta subunit of the mitochondrial processing protease (MPP); essential processing enzyme that cleaves the N-terminal targeting sequences from mitochondrially imported proteins	51	0
YKL040C	NFU1 SGDID:S000001523, Chr XI from 361828-361058, Genome Release 64-2-1, reverse complement, Verified ORF, Protein involved in iron metabolism in mitochondria; similar to NifU, which is a protein required for the maturation of the Fe/S clusters of nitrogenase in nitrogen-fixing bacteria	29	3
YHR199C	AIM46 SGDID:S000001242, Chr VIII from 498422-497490, Genome Release 64-2-1, reverse complement, Verified ORF, Putative protein of unknown function; the authentic, non-tagged protein is detected in highly purified mitochondria in high-throughput studies; null mutant displays elevated frequency of mitochondrial genome loss	34	4
YDR529C	QCR7 SGDID:S000002937, Chr IV from 1496548-1496165, Genome Release 64-2-1, reverse complement, Verified ORF, Subunit 7 of ubiquinol cytochrome-c reductase (Complex III); Complex III is a component of the mitochondrial inner membrane electron transport chain; oriented facing the mitochondrial matrix; N-terminus appears to play a role in complex assembly	14	0
YHR024C	MAS2 SGDID:S000001066, Chr VIII from 159192-157744, Genome Release 64-2-1, reverse complement, Verified ORF, Alpha subunit of the mitochondrial processing protease (MPP); essential processing enzyme that cleaves the N-terminal targeting sequences from mitochondrially imported proteins	53	6
YDL120W	YFH1 SGDID:S000002278, Chr IV from 245923-246447, Genome Release 64-2-1, Verified ORF, Mitochondrial matrix iron chaperone; oxidizes and stores iron; interacts with Isu1p to promote Fe-S cluster assembly; mutation results in multiple Fe/S-dependent enzyme deficiencies; human frataxin homolog is mutated in Friedrich's ataxia	19	2

Protein	DESCRIPTION	Molecular Weight	#cysteine
YPL078C	ATP4 SGDID:S000005999, Chr XVI from 408744-408010, Genome Release 64-2-1, reverse complement, Verified ORF, Subunit b of the stator stalk of mitochondrial F1F0 ATP synthase; ATP synthase is a large, evolutionarily conserved enzyme complex required for ATP synthesis; contributes to the oligomerization of the complex, which in turn determines the shape of inner membrane cristae; phosphorylated	27	1
YJR048W	CYC1 SGDID:S000003809, Chr X from 526335-526664, Genome Release 64-2-1, Verified ORF, Cytochrome c, isoform 1; also known as iso-1-cytochrome c; electron carrier of the mitochondrial intermembrane space that transfers electrons from ubiquinone-cytochrome c oxidoreductase to cytochrome c oxidase during cellular respiration; mutations in human homolog cause insulin-responsive hyperglycemia; CYC1 has a paralog, CYC7, that arose from the whole genome duplication	12	3
YKL134C	OCT1 SGDID:S000001617, Chr XI from 191442-189124, Genome Release 64-2-1, reverse complement, Verified ORF, Mitochondrial intermediate peptidase; cleaves destabilizing N-terminal residues of a subset of proteins upon import, after their cleavage by mitochondrial processing peptidase (Mas1p-Mas2p); may contribute to mitochondrial iron homeostasis	88	17
YKL195W	MIA40 SGDID:S000001678, Chr XI from 75821-77032, Genome Release 64-2-1, Verified ORF, Mitochondrial oxidoreductase; involved in mitochondrial intermembrane space import; component of MIA pathway which mediates import and oxidative folding of substrates including small proteins containing twin cysteine motifs; acts in concert with Erv1p, which oxidizes the cysteine residues of Mia40p to comprise a disulfide relay system that catalyzes import; also mediates folding of Atp23p via a chaperone-like activity; forms a dimer that binds iron-sulfur cluster in vitro	44	8
YOR065W	CYT1 SGDID:S000005591, Chr XV from 447439-448368, Genome Release 64-2-1, Verified ORF, Cytochrome c1; component of the mitochondrial respiratory chain; expression is regulated by the heme-activated, glucose-repressed Hap2p/3p/4p/5p CCAAT-binding complex	34	0
YCL033C	MXR2 SGDID:S000000538, Chr III from 63282-62776, Genome Release 64-2-1, reverse complement, Verified ORF, Methionine-R-sulfoxide reductase; involved in the response to oxidative stress; protects iron-sulfur clusters from oxidative inactivation along with MXR1; involved in the regulation of lifespan	19	7
YJR121W	ATP2 SGDID:S000003882, Chr X from 647607-649142, Genome Release 64-2-1, Verified ORF, Beta subunit of the F1 sector of mitochondrial F1F0 ATP synthase; which is a large, evolutionarily conserved enzyme complex required for ATP synthesis; F1 translationally regulates ATP6 and ATP8 expression to achieve a balanced output of ATP synthase genes encoded in nucleus and mitochondria; phosphorylated	55	1
YLR038C	COX12 SGDID:S000004028, Chr XII from 225172-224921, Genome Release 64-2-1, reverse complement, Verified ORF, Subunit VIb of cytochrome c oxidase; cytochrome c oxidase is also known as respiratory Complex IV and is the terminal member of the mitochondrial inner membrane electron transport chain; required for assembly of cytochrome c oxidase but not required for activity after assembly; phosphorylated; easily released from the intermembrane space, suggesting a loose association with Complex IV	10	4

Protein	DESCRIPTION	Molecular Weight	#cysteine
YML120C	NDI1 SGDID:S000004589, Chr XIII from 29807-28266, Genome Release 64-2-1, reverse complement, Verified ORF, NADH:ubiquinone oxidoreductase; transfers electrons from NADH to ubiquinone in the respiratory chain but does not pump protons, in contrast to the higher eukaryotic multisubunit respiratory complex I; phosphorylated; involved in Mn and H2O2 induced apoptosis; upon apoptotic stress, Ndip is activated in the mitochondria by N-terminal cleavage, and the truncated protein translocates to the cytoplasm to induce apoptosis; homolog of human AMID	57	0
YPR006C	ICL2 SGDID:S000006210, Chr XVI from 568996-567269, Genome Release 64-2-1, reverse complement, Verified ORF, 2-methylisocitrate lyase of the mitochondrial matrix; functions in the methylcitrate cycle to catalyze the conversion of 2-methylisocitrate to succinate and pyruvate; ICL2 transcription is repressed by glucose and induced by ethanol	65	0
Q0250	COX2 SGDID:S000007281, Chr Mito from 73758-74513, Genome Release 64-2-1, Verified ORF, Subunit II of cytochrome c oxidase (Complex IV); Complex IV is the terminal member of the mitochondrial inner membrane electron transport chain; one of three mitochondrially-encoded subunits	29	4
YDL198C	GGC1 SGDID:S000002357, Chr IV from 104551-103649, Genome Release 64-2-1, reverse complement, Verified ORF, Mitochondrial GTP/GDP transporter; essential for mitochondrial genome maintenance; has a role in mitochondrial iron transport; member of the mitochondrial carrier family	33	1
YER053C	PIC2 SGDID:S000000855, Chr V from 259639-258737, Genome Release 64-2-1, reverse complement, Verified ORF, Mitochondrial copper and phosphate carrier; imports copper and inorganic phosphate into mitochondria; functionally redundant with Mir1p but less abundant than Mir1p under normal conditions; expression is induced at high temperature	34	0
YER073W	ALD5 SGDID:S000000875, Chr V from 304030-305592, Genome Release 64-2-1, Verified ORF, Mitochondrial aldehyde dehydrogenase; involved in regulation or biosynthesis of electron transport chain components and acetate formation; activated by K+; utilizes NADP+ as the preferred coenzyme; constitutively expressed	57	6
YER141W	COX15 SGDID:S000000943, Chr V from 453459-454919, Genome Release 64-2-1, Verified ORF, Protein required for the hydroxylation of heme O to form heme A; heme A is an essential prosthetic group for cytochrome c oxidase	55	0
YER154W	OXA1 SGDID:S000000956, Chr V from 475020-476228, Genome Release 64-2-1, Verified ORF, Mitochondrial inner membrane insertase; mediates the insertion of both mitochondrial- and nuclear-encoded proteins from the matrix into the inner membrane; also has a role in insertion of carrier proteins into the inner membrane; acts as a voltage-gated ion channel, activated by substrate peptides; interacts with mitochondrial ribosomes; conserved from bacteria to animals	45	1
YGR033C	TIM21 SGDID:S000003265, Chr VII from 554967-554248, Genome Release 64-2-1, reverse complement, Verified ORF, Nonessential component of the TIM23 complex; interacts with the Translocase of the Outer Mitochondrial membrane (TOM complex) and with respiratory enzymes; may regulate the Translocase of the Inner Mitochondrial membrane (TIM23 complex) activity	27	1

Protein	DESCRIPTION	Molecular Weight	#cysteine
YJL166W	QCR8 SGDID:S000003702, Chr X from 106434-106718, Genome Release 64-2-1, Verified ORF, Subunit 8 of ubiquinol cytochrome-c reductase (Complex III); Complex III is a component of the mitochondrial inner membrane electron transport chain; oriented facing the intermembrane space; expression is regulated by Abf1p and Cpf1p	11	0
YOR037W	CYC2 SGDID:S000005563, Chr XV from 401555-402655, Genome Release 64-2-1, Verified ORF, Mitochondrial peripheral inner membrane protein; contains a FAD cofactor in a domain exposed in the intermembrane space; exhibits redox activity in vitro; likely participates in ligation of heme to acytochromes c and c1 (Cyc1p and Cyt1p)	42	3
YPL172C	COX10 SGDID:S000006093, Chr XVI from 225741-224353, Genome Release 64-2-1, reverse complement, Verified ORF, Heme A:farnesyltransferase; catalyzes the first step in the conversion of protoheme to the heme A prosthetic group required for cytochrome c oxidase activity; human ortholog is associated with mitochondrial disorders	52	0
YPR002W	PDH1 SGDID:S000006206, Chr XVI from 558385-559935, Genome Release 64-2-1, Verified ORF, Putative 2-methylcitrate dehydratase; mitochondrial protein that participates in respiration; induced by diauxic shift; homologous to E. coli PrpD, may take part in the conversion of 2-methylcitrate to 2-methylisocitrate	58	6
YLL027W	ISA1 SGDID:S000003950, Chr XII from 87403-88155, Genome Release 64-2-1, Verified ORF, Protein required for maturation of mitochondrial [4Fe-4S] proteins; functions in a complex with Isa2p and possibly Iba57p; isa1 deletion causes loss of mitochondrial DNA and respiratory deficiency; depletion reduces growth on nonfermentable carbon sources; functional ortholog of bacterial A-type ISC proteins	28	5
YFL016C	MDJ1 SGDID:S000001878, Chr VI from 106236-104701, Genome Release 64-2-1, reverse complement, Verified ORF, Co-chaperone that stimulates HSP70 protein Ssc1p ATPase activity; involved in protein folding/refolding in the mitochodrial matrix; required for proteolysis of misfolded proteins; member of the HSP40 (DnaJ) family of chaperones	56	10
YDR298C	ATP5 SGDID:S000002706, Chr IV from 1058814-1058176, Genome Release 64-2-1, reverse complement, Verified ORF, Subunit 5 of the stator stalk of mitochondrial F1F0 ATP synthase; F1F0 ATP synthase is a large, evolutionarily conserved enzyme complex required for ATP synthesis; homologous to bovine subunit OSCP (oligomycin sensitivity-conferring protein); phosphorylated	23	0
YPL135W	ISU1 SGDID:S000006056, Chr XVI from 297553-298050, Genome Release 64-2-1, Verified ORF, Conserved protein of the mitochondrial matrix; performs a scaffolding function during assembly of iron-sulfur clusters, interacts physically and functionally with yeast frataxin (Yfh1p); isu1 isu2 double mutant is inviable; ISU1 has a paralog, ISU2, that arose from the whole genome duplication	18	0
YHR051W	COX6 SGDID:S000001093, Chr VIII from 209705-210151, Genome Release 64-2-1, Verified ORF, Subunit VI of cytochrome c oxidase (Complex IV); Complex IV is the terminal member of the mitochondrial inner membrane electron transport chain; expression is regulated by oxygen levels	17	0

Protein	DESCRIPTION	Molecular Weight	#cysteine
YOR020C	HSP10 SGDID:S000005546, Chr XV from 370844-370524, Genome Release 64-2-1, reverse complement, Verified ORF, Mitochondrial matrix co-chaperonin; inhibits the ATPase activity of Hsp60p, a mitochondrial chaperonin; involved in protein folding and sorting in the mitochondria; 10 kD heat shock protein with similarity to E. coli groES	11	0
YHR008C	SOD2 SGDID:S000001050, Chr VIII from 123590-122889, Genome Release 64-2-1, reverse complement, Verified ORF, Mitochondrial manganese superoxide dismutase; protects cells against oxygen toxicity; phosphorylated	26	1
YEL024W	RIP1 SGDID:S000000750, Chr V from 107260-107907, Genome Release 64-2-1, Verified ORF, Ubiquinol-cytochrome-c reductase; a Rieske iron-sulfur protein of the mitochondrial cytochrome bc1 complex; transfers electrons from ubiquinol to cytochrome c1 during respiration; during import, Rip1p is first imported into the mitochondrial matrix where it is processed, acquires its Fe-S cluster, and is folded, then is translocated into the inner membrane by the action of a homo-oligomer of Bcs1p, and finally is delivered by Bcs1p to Complex III for assembly	23	0
YKL016C	ATP7 SGDID:S000001499, Chr XI from 407989-407465, Genome Release 64-2-1, reverse complement, Verified ORF, Subunit d of the stator stalk of mitochondrial F1F0 ATP synthase; F1F0 ATP synthase is a large, evolutionarily conserved enzyme complex required for ATP synthesis	20	0
YGL187C	COX4 SGDID:S000003155, Chr VII from 150171-149704, Genome Release 64-2-1, reverse complement, Verified ORF, Subunit IV of cytochrome c oxidase; the terminal member of the mitochondrial inner membrane electron transport chain; precursor N-terminal 25 residues are cleaved during mitochondrial import; phosphorylated; spermidine enhances translation	17	0
YPR191W	QCR2 SGDID:S000006395, Chr XVI from 919381-920487, Genome Release 64-2-1, Verified ORF, Subunit 2 of ubiquinol cytochrome-c reductase (Complex III); Complex III is a component of the mitochondrial inner membrane electron transport chain; phosphorylated; transcription is regulated by Hap1p, Hap2p/Hap3p, and heme	40	0
YLR259C	HSP60 SGDID:S000004249, Chr XII from 665002-663284, Genome Release 64-2-1, reverse complement, Verified ORF, Tetradecameric mitochondrial chaperonin; required for ATP-dependent folding of precursor polypeptides and complex assembly; prevents aggregation and mediates protein refolding after heat shock; role in mtDNA transmission; phosphorylated	61	5
YJR045C	SSC1 SGDID:S000003806, Chr X from 521602-519638, Genome Release 64-2-1, reverse complement, Verified ORF, Hsp70 family ATPase; constituent of the import motor component of the Translocase of the Inner Mitochondrial membrane (TIM23 complex); involved in protein translocation and folding; subunit of SceI endonuclease; SSC1 has a paralog, ECM10, that arose from the whole genome duplication	71	0

Table 3-2 Combined Aim32 co-immunoprecipitation hits identified by mass spectrometry.

Proteins identified from both mass spectrometry analysis that potentially interact with Aim32 in Δ*aim32* [pAIM32-FLAG] and form disulfide with Aim32 single cysteine mutants (Δ*aim32*[pC213S] and Δ*aim32*[pC222S]) (Table 3-1).

Material and Methods

Plasmids and strains. Standard set of genetic and molecular techniques was used to generate the strains in this study. For IMS-targeted Aim32 plasmid, endogenous promoter 300bp upstream of the start codon of *AIM32*, first 249bp of targeting sequence from cytochrome b2, and *AIM32* without first 45bp were PCR-amplified from yeast genomic DNA isolated from the WT (GA74-1A) strain. 3' primer introduced a 3XHA tag to the C-terminus. Fragments were cloned into pRS425 with BamHI and SalI restriction sites, designated [pb2-AIM32], and transformed into Δ*aim32* yeast strain.

Primers for PCR amplification for endogenous promoter:

Fwd 5'- CGCTCTAGAACTAGTGGATCCTATAAAAGTAACATGATGGGCTCC-3'

Rev 5'- AAAGGTTTGTATTTTAGCATTTTATTTTTTGTGTCAGTG-3'

Primers for targeting sequence from cytochrome b2:

Fwd 5'- CACTGACAC AAAAAATAAA ATGCTAAAAT ACAAACCTTT -3'

Rev 5'- ATGTTTGAAGCTATGATGTTTCGGCTCGTTGTCTATTTGG-3'

Primers for HA-tagged Aim32:

Fwd 5'- CCAAATAGACAACGAGCCGAAACATCATAGCTTCAAACAT-3'

Rev 5'- GGCATATCGATGAATTACCCATACGATGTTCCAGATTACGCTTACCCATACGAT GTTCCAGATTACGCTTACCCATACGATGTTCCAGATTACGCT-3'

For IMS-targeted Aim32 plasmid using promoter and targeting sequence from Mia40, promoter 300bp upstream of the start codon of *MIA40* with first 210bp of targeting sequence from Mia40, and *AIM32* without first 45bp were PCR-amplified from yeast genomic DNA isolated from the

WT (GA74-1A) strain. 3' primer introduced a 3XHA tag to the C-terminus. Fragments were cloned into pRS425 with BamHI and SalI restriction sites, designated [pmia-AIM32], and transformed into Δ*aim32* yeast strain.

Primers for PCR amplification for endogenous promoter and targeting sequence from *MIA40*:

Fwd 5'- CGCTCTAGAACTAGTGGATCCTAGTAGATTCTCATTGCCAA-3'

Rev 5'- ATG TTT GAA GCT ATG ATG AGG CTT CCT ATT AGG AGC-3'

Primers for HA-tagged Aim32:

Fwd 5'- GCT CCT AAT AGG AAG CCT CATCA TAGCTTCAAA CAT-3'

Rev 5'- ACC GGG CCC CCC CTC GAG GTC GAC TCA AGC GTA ATC TGG AAC ATC GTA TGG GTA AGC GTA ATC TGG AAC ATC GTA TGG GTA AGC GTA ATC TGG AAC ATC GTA TGG GTA ATT CAT CGA TAT GCC-3'

For matrix-targeted Aim32 plasmid, endogenous promoter 300bp upstream of the start codon of *SOD2*, first 90bp of targeting sequence from Sod2, and *AIM32* without first 45bp were PCR-amplified from yeast genomic DNA isolated from the WT (GA74-1A) strain. 3' primer introduced a 3XFlag tag to the C-terminus. Fragments were cloned into pRS424 with BamHI and SalI restriction sites, designated [psod2-AIM32], and transformed into Δ*aim32* yeast strain.

Primers for PCR amplification for endogenous promoter and targeting sequence from *SOD2*:

Fwd 5'- CGCTCTAGAACTAGTGGATCCTGCACGTGTAGTATTC-3'

Rev 5'- ATGTTTGAAGCTATGATG CAAGGTGACTTTGGTTCTCC-3'

Primers for Flag-tagged Aim32:

Fwd 5'- GGAGAACCAA AGTCACCTTGCATCATAGCTTCAAACAT-3'

Rev 5'-ACCGGGCCCCCCCTCGAGGTCGACTCACTTGTCATCGTCATCCTTGTAATCG

ATATCATGATCTTTATAATCACCGTCATGGTCTTTGTAGTCATTCATCGATATGCC- 3'

For matrix-targeted Aim32 plasmid, endogenous promoter 300bp upstream of the start codon of *AIM32*, first 207bp of targeting sequence from Su9, and *AIM32* without first 45bp were PCR-amplified from yeast genomic DNA isolated from the WT (GA74-1A) strain. 3' primer introduced a 3XFlag tag to the C-terminus. Fragments were cloned into pRS424 with BamHI and SalI restriction sites, designated [psu9-AIM32], and transformed into Δ*aim32* yeast strain.

Strain	**Genotype**	**Source**
WT (GA74-1A)	MATα *his3-11,15 leu2 ura3 trp1 ade8 rho+ mit+*	[21]
Δaim32	MATα *his3-11,15 leu2 ura3 trp1 ade8 aim32::HIS3*	This study
Δaim32 [pAIM32]	MATα *his3-11,15 leu2 ura3 trp1 ade8 aim32::HIS3* [*pRS316GPD-AIM32 3XFLAG-PGK*]	This study
Δaim32 [pMIA40-AIM32]	MATα *his3-11,15 leu2 ura3 trp1 ade8 aim32::HIS3* [*pRS425 MIA40-AIM32 3XHA*]	This study
Δaim32 [pCYB2-AIM32]	MATα *his3-11,15 leu2 ura3 trp1 ade8 aim32::HIS3* [*pRS425 CYB2-AIM32 3XHA*]	This study
Δaim32 [p425]	MATα *his3-11,15 leu2 ura3 trp1 ade8 aim32::HIS3* [*pRS425*]	This study

WT [p425]	MATα *his3-11,15 leu2 ura3 trp1 ade8 rho+ mit+* [*pRS425*]	This study
Δaim32 [pSOD2-AIM32]	MATα *his3-11,15 leu2 ura3 trp1 ade8 aim32::HIS3* [*pRS424 SOD2-AIM32 3XHA*]	This study
Δaim32 [pSU9-AIM32]	MATα *his3-11,15 leu2 ura3 trp1 ade8 aim32::HIS3* [*pRS424 SU9-AIM32 3XHA*]	This study
Δaim32 [p424]	MATα *his3-11,15 leu2 ura3 trp1 ade8 aim32::HIS3* [*pRS424*]	This study
WT [p424]	MATα *his3-11,15 leu2 ura3 trp1 ade8 rho+ mit+* [*pRS424*]	This study
Δaim32 [pC213, 222S]	MATα *his3-11,15 leu2 ura3 trp1 ade8 aim32::HIS3* [*pRS316GPD-AIM32 C213, 222S 3XFLAG-PGK*]	This study
Δaim32 [pH249, 253A]	MATα *his3-11,15 leu2 ura3 trp1 ade8 aim32::HIS3* [*pRS316GPD-AIM32 H249, 253A 3XFLAG-PGK*]	This study
Δaim32 [pC213S]	MATα *his3-11,15 leu2 ura3 trp1 ade8 aim32::HIS3* [*pRS316GPD-AIM32 C213S 3XFLAG-PGK*]	This study
Δaim32 [pC222S]	MATα *his3-11,15 leu2 ura3 trp1 ade8 aim32::HIS3* [*pRS316GPD-AIM32 C222S 3XFLAG-PGK*]	This study

Table S3-1 Strains used in this study

Subcellular fractionation. Subcellular fractionation from spheroplasts was performed as previously described[22]. The fractions were separated by differential centrifugation and an equal

amount of each fraction was separated by SDS-PAGE followed by immunoblot analysis.

Sub-mitochondrial localization. Mitochondrial fractionation was performed as previously described[22]. For intact mitochondria, 300 μg of isolated mitochondria were incubated in 0.6 M sorbitol and 20 mM Hepes-KOH, pH 7.4. To generate mitoplasts, 300 μg of isolated mitochondria were incubated in 0.03 M sorbitol and 20 mM Hepes-KOH, pH 7.4. As indicated, 100 μg/ml of Proteinase K and 0.1% Triton-X-100 were added. Samples were centrifuged at 14,000 x g for 10 minutes to separate pellet (P) and supernatant (S). The supernatants were precipitated with 20% trichloroacetic acid and resuspended in SDS-sample buffer.

Mitochondrial purification and in vitro protein import assay. Mitochondria were purified from yeast cells grown in media with glucose or ethanol/glycerol[22]. Proteins for import studies were synthesized by the TNT Quick Coupled Transcription/Translation kits (Promega) in the presence of [35S] methionine. The radiolabeled precursor was incubated with isolated mitochondria and an import time course was performed. Non-imported radiolabeled protein was removed by treatment with 100 μg/ml trypsin for 15 minutes on ice and trypsin was inhibited with 200 μg/ml of soybean trypsin inhibitor for 30 min on ice. Samples were separated by SDS-PAGE and visualized using autoradiography.

Thiol trapping assay. For indirect thiol trapping assay, isolated mitochondria from the respective strains were treated with 150 mM mmPEG (22713 ThermoFisher, Waltham, MA) for 1 hour at room temperature in the dark. In control reactions, mitochondria were treated with either 20 mM DTT for 15 minutes at 65°C or with 50 mM IAA for 10 minutes at 30°C. Samples were analyzed by non-reducing SDS-PAGE.

Immunoprecipitation. 250ug mitochondria were purified, solubilized in lysis buffer (0.1% SDS, 50mM Tris HCl pH7.4, 150mM NaCl, 1 mM EDTA, 1% NP40, and 0.5 mM PMSF) for 30 minutes on ice. Lysate was centrifuged at maximum speed for 10 minutes to remove insoluble material. 10 μg lysate was removed from the supernatant to use as a reference for the total sample (T). The remaining was diluted to 0.5 μg/μl in buffer (50mM Tris HCl pH7.4, 150mM NaCl, 1 mM EDTA, 1% NP40, and 0.5 mM PMSF). Samples were incubated with 80 μl of ANTI-FLAG M2 affinity gel (Sigma Aldrich) for 4h at 4°C with rotation. After binding, 10 μg of lysate was removed as a reference for the material that did not bind (denoted flow-through, FT). The beads were then washed 3 times with buffer. Samples were eluted from beads with 10mM DTT (B). The samples collected throughout the experiment were separated by SDS-PAGE and analyzed by immunoblotting. For 2DGE analysis, samples were eluted in Laemmli SDS sample buffer with and without beta-mercaptoethanol.

SYPRO Ruby protein gel stain. PAGE gel was fixed twice in 100 ml fix solution (50% methanol and 7% glacial acetic acid) and stained with 60 ml SYPRO Ruby gel stain. After microwaved for 30' and agitated on shaker for three times, gel was transferred to a fresh container with wash solution (10% methanol and 7% glacial acetic acid) for 30 min, rinsed with water, and visualized using the Bio-Rad ChemiDoc MP imaging system.

2D- Diagonal gel electrophoresis (2DGE). Samples were resolved in the first dimension on a non-reducing SDS gel. Individual lanes isolated with a razor blade, were soaked in 1% (wt/vol) SDS, 1% (vol/vol) β-mercaptoethanol for 30 min at 50^0C, embedded in a 4% stacking gel, and resolved in the second dimension by SDS-PAGE.

Liquid chromatography- mass spectrometry analysis. The protein mixtures were reduced, alkylated, and digested by the sequential addition of trypsin and lys-C proteases. Afterwards, samples were desalted using Pierce C18 tips, eluted in 40% ACN, and dried and resuspended in 5% formic acid. Desalted samples were separated on C18 reversed phase (1.9 uM, 100A pores, Dr. Maisch GmbH) columns, packed with 25cm of resin in a 75uM inner diameter fused silica capillary. Digested peptides were fractionated online using a 140-minute water-acetonitrile gradient with 3% DMSO ionized using electrospray ionization by application of a distal 2.2kV. Ionized peptides were interrogated via tandem mass spectrometry (MS/MS) in a Thermo Orbitrap Fusion Lumos. For discovery acquisitions, Data-Dependent Acquisition (DDA) was utilized with an MS1 scan resolution of 120,000 and MS2 resolution of 15,000 and a cycle time of 3 seconds. Data analysis was performed using the Integrated Proteomics pipeline 2 (Integrated Proteomics Applications, San Diego, CA). MS/MS spectra were searched using the ProLuCID algorithm and peptide-to-spectrum matches (PSMs) were organized and filtered based on decoy database-estimated false discovery rate of <1% using the DTASelect algorithm. Database searching was performed using a Saccharomyces cerevisiae yeast database downloaded from Saccharomyces Genome Database (SGD) on 2-19-2016.

Antibodies. Most of the antibodies used in this work were generated by vendor Pacific Immunology from recombinant proteins in the Koehler laboratory and have been described previously. Other antibodies: anti-Cox-4, anti-Rip1-FeS, anti-Qcr10 and anti-Oxa1 (a gift of Dr. Rosemary Stuart, Marquette University, Milwaukee, WI), and horseradish peroxidase–conjugated secondary antibodies (Thermo Fisher Scientific).

References

1. Cardenas-Rodriguez, M., Chatzi, A. & Tokatlidis, K. Iron–sulfur clusters: from metals through mitochondria biogenesis to disease. *Journal of Biological Inorganic Chemistry* vol. 23 509–520 (2018).

2. Balsera, M. & Buchanan, B. B. Evolution of the thioredoxin system as a step enabling adaptation to oxidative stress. *Free Radical Biology and Medicine* vol. 140 28–35 (2019).

3. Kern, R., Malki, A., Holmgren, A. & Richarme, G. Chaperone properties of Escherichia coli thioredoxin and thioredoxin reductase. *Biochem. J.* **371**, 965–972 (2003).

4. Kranz, P. *et al.* PDI is an essential redox-sensitive activator of PERK during the unfolded protein response (UPR). *Cell Death Dis.* **8**, e2986 (2017).

5. Ang, S. K., Zhang, M., Lodi, T. & Lu, H. Mitochondrial thiol oxidase Erv1: Both shuttle cysteine residues are required for its function with distinct roles. *Biochem. J.* **460**, 199–210 (2014).

6. Neal, S. E. *et al.* Mia40 protein serves as an electron sink in the Mia40-Erv1 import pathway. *J. Biol. Chem.* **290**, 20804–20814 (2015).

7. Stegmaier, K. *et al.* Apd1 and Aim32 Are Prototypes of Bishistidinyl-Coordinated Non-Rieske [2Fe-2S] Proteins. *J. Am. Chem. Soc.* **141**, 5753–5765 (2019).

8. Hanschmann, E. M., Godoy, J. R., Berndt, C., Hudemann, C. & Lillig, C. H. Thioredoxins, glutaredoxins, and peroxiredoxins-molecular mechanisms and health significance: From cofactors to antioxidants to redox signaling. *Antioxidants and Redox Signaling* vol. 19 1539–1605 (2013).

9. Witte, C., Jensen, R. E., Yaffe, M. P. & Schatz, G. MAS1, a gene essential for yeast mitochondrial assembly, encodes a subunit of the mitochondrial processing protease. *EMBO J.* **7**, 1439–1447 (1988).

10. Yang, M., Jensen, R. E., Yaffe, M. P., Oppliger, W. & Schatz, G. Import of proteins into yeast mitochondria: the purified matrix processing protease contains two subunits which are encoded by the nuclear MAS1 and MAS2 genes. *EMBO J.* **7**, 3857–3862 (1988).

11. Mossmann, D., Meisinger, C. & Vögtle, F. N. Processing of mitochondrial presequences. *Biochimica et Biophysica Acta - Gene Regulatory Mechanisms* vol. 1819 1098–1106 (2012).

12. Yaffe, M. P. & Schatz, G. Two nuclear mutations that block mitochondrial protein import in yeast. *Proc. Natl. Acad. Sci. U. S. A.* **81**, 4819–4823 (1984).

13. Rowley, N. *et al.* Mdj1p, a novel chaperone of the DnaJ family, is involved in mitochondrial biogenesis and protein folding. *Cell* **77**, 249–259 (1994).

14. Qiu, X. B., Shao, Y. M., Miao, S. & Wang, L. The diversity of the DnaJ/Hsp40 family, the crucial partners for Hsp70 chaperones. *Cellular and Molecular Life Sciences* vol. 63 2560–2570 (2006).

15. Kubo, Y. *et al.* Mechanisms operate in the reactivation of heat-denatured proteins by the mitochondrial Hsp70/Mdj1p/Yge1p chaperone system. *J. Mol. Biol.* **286**, 447–464 (1999).

16. Westermann, B., Gaume, B., Herrmann, J. M., Neupert, W. & Schwarz, E. Role of the mitochondrial DnaJ homolog Mdj1p as a chaperone for mitochondrially synthesized and imported proteins. *Mol. Cell. Biol.* **16**, 7063–7071 (1996).

17. Ciesielski, G. L. *et al.* Nucleoid localization of Hsp40 Mdj1 is important for its function in maintenance of mitochondrial DNA. *Biochim. Biophys. Acta - Mol. Cell Res.* **1833**, 2233–2243 (2013).

18. Prip-Buus, C. *et al.* Role of the mitochondrial DnaJ homologue, Mdj1p, in the prevention of heat-induced protein aggregation. *FEBS Lett.* **380**, 142–146 (1996).

19. Nouailler, M. *et al.* Solution structure of HndAc: A thioredoxin-like domain involved in the NADP-reducing hydrogenase complex. *Protein Sci.* **15**, 1369–1378 (2006).

20. Sazanov, L. A. & Hinchliffe, P. Structure of the hydrophilic domain of respiratory complex I from Thermus thermophilus. *Science (80-.).* **311**, 1430–1436 (2006).

21. Koehler, C. M. *et al.* Tim9p, an essential partner subunit of Tim10p for the import of mitochondrial carrier proteins. *EMBO J.* **17**, 6477–6486 (1998).

22. Claypool, S. M., McCaffery, J. M. & Koehler, C. M. Mitochondrial mislocalization and altered assembly of a cluster of Barth syndrome mutant tafazzins. *J. Cell Biol.* **174**, 379–390 (2006).

Chapter 4: Cmc4 is an identified interactor of MIA pathway

4.1 Introduction

Proteins of mitochondrial intermembrane space (IMS) play many important roles including energy metabolism, lipid homeostasis, and metal ion homeostasis[1–4]. IMS proteins that lack an N-terminal targeting sequence are typically small cysteine-rich and imported by disulfide linkages through Mia40/Erv1 pathway[5]. Most of the class of proteins contain twin CX_3C motif or twin CX_9C motif that four cysteine residues form pairs each separated by either three or nine amino acids. The group of twin CX_3C motif contains small Tim proteins of Tim8, Tim9, Tim10, Tim12, and Tim13 function as chaperons to guide inner membrane proteins and are conserved from yeast to mammals and plants[6,7]. Proteins with twin CX_9C motif including Cmc1, Cmc2, Coa4, Cox11, Cox12, Cox17, Cox19, Cox23, and Pet191 are involved in the cytochrome c oxidase (COX) assembly[8–16]. Cox17 is well characterized as a copper chaperon[13,17]. Cmc2 interacts and works with Cmc1 to regulate copper delivery to COX and affect Sod1 level[9]. Coa4 (Cmc3) interacts genetically with *CYC1* and plays roles in COX assembly[10]. Besides, the function of additional proteins with twin CX_9C motif, Mic14, Mic17, and Cmc4 still remain unknown[18].

Studies of MIA pathway substrates will provide insights into the mechanism of redox regulation in IMS. A proteomic study of mass spectrometry analysis of disulfide partners with Mia40, Erv1, or Cmc1 was reported by Matt Maland, a previous member of the Koehler lab (Figure S4-1)[19]. His-tagged Mia40, Erv1, and Cmc1 were lysed and pulled down in a denature

condition in 8M urea, followed with trypsin digestion for mass spectrometry analysis. Among the potential binding candidates, Cmc4 was enriched in both Mia40, Erv1, and Cmc1 pull downs. The function of Cmc4 has not been studied before. A systematic analysis of twin CX_9C proteins found that unlike the deletions of *CMC2* and *CMC3*, no defects in respiration were found in mutant lacking *CMC4*[18]. Cmc4 contains the twin CX_9C motif that interacts with the MIA pathway.

4.2 Cmc4 interacts with Mia40 and Erv1

To confirm the interaction between Cmc1 and Mia40, and Erv1, we used a strain in which Cmc4 was tagged with a C-terminal FLAG tag (Cmc4-Flag). A fraction of Mia40 and Erv1 co-precipitated with Cmc4; as a control, the tested proteins were not detected in the untagged strain (Figure 4-1). Other MIA substrates Osm1 and Aim32 did not co-precipitated with Cmc4.

4.3 Cmc4 is not essential for mitochondrial protein import

To investigate whether Cmc4 plays a role in mitochondrial import pathway, we tested the ability of isolated mitochondria from Δ*cmc4* cells to import radiolabeled precursor proteins *in vitro* (Figure 4-2). As a control, protein import into isolated mitochondria from wild-type (WT) strain was examined. The import efficiency and kinetics of MIA substrate Cmc1 and TIM23 substrates Mia40 and Su9-DHFR were studied. The import of Cmc1 was not decreased in Δ*cmc4*. However, the import of Mia40 was modestly reduced by ~40% and Su9-DHFR was reduced by ~20%. To complement the import study, the steady-state level of mitochondrial proteins was determined by immunoblot analysis (Figure 4-3). In agreement with the reduced import Mia40, the abundance of Mia40 was diminished in the Δ*cmc4* strain. With the exception

of Tim13 and Cty c, the steady-state level of additional mitochondrial proteins in the MIA and respiratory complexes was not remarkedly changed. Thus, Cmc4 seems only moderately affect Mia40 protein import.

4.4 Discussion

Cmc4 localizes to the mitochondrial IMS and has twin CX_9C motif[18]. Cmc4 is conserved throughout eukaryotes and have homologs in fungi, plants, and animals including human (Figure 4-4). In this study, we confirmed the interaction of Cmc4 with Mia40 and Erv1. Sorting of twin CX_9C proteins has been shown to be facilitated by the MIA redox relay pathway[20]. Study has also shown that the import of Cmc4 does not require membrane potential, and high concentrations of reduced glutathione decreases the import of Cmc4[18]. Cmc4 very likely depends on the Mia40-Erv1 system for localization to the IMS of mitochondria. To assess the mitochondrial biogenesis of Cmc4, we prepared radiolabeled Cmc4 protein by *in vitro* translation; however, we were not successful with import into isolated mitochondria. Cells lacking CMC4 had modest defects in Mia40 import and decreased level. Further study should be done to investigate the redox within the MIA pathway that Cmc4 may play a role. Additional characterization of the Cmc4 import pathway should provide insights into the mechanism of redox regulation in IMS.

Most twin CX_9C proteins are crucial for respiration, particularly for the function of cytochrome *c* oxidase[8–16]. However, no defects in respiration were found in mutant lacking *CMC4*[18]. Deletion of protein Cmc4 did not alter the levels of cytochrome *c* oxidase proteins (Figure 4-3) or alter the enzyme activity[18]. Cmc4 may not be directly involved in the cytochrome

c oxidase biogenesis that defects in cytochrome *c* oxidase has been associated with lipid metabolism, heme biogenesis, and metal homogenesis[21–23]. Although there is limited knowledge about Cmc4, in the future, it will be exiting to unravel the function of this protein not only in yeast but also in higher eukaryotes.

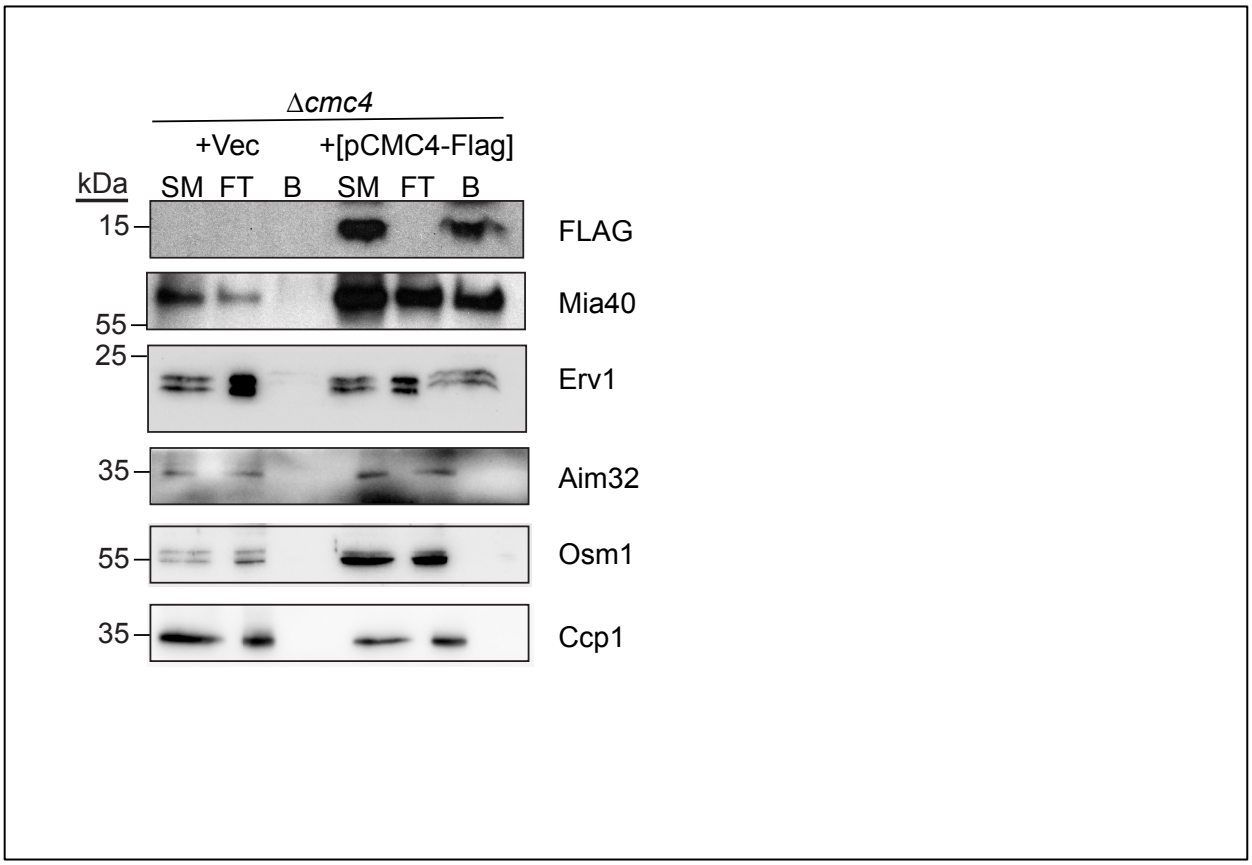

Figure 4-1 CMC4 interacts with Mia40 and Erv1. A FLAG tag was appended to the C-terminus of Cmc4 (Cmc4-FLAG) and transformed into Δ*cmc4*. As a control, empty vector was transformed into Δ*cmc4.* Mitochondria were solubilized in 1% digitonin. As a control, 20 µg of starting material (SM) was withdrawn, and 600 µg lysate was incubated with FLAG-resin. The resin was washed, and bound protein (B) was eluted. 20 µg of the flow-through fraction (FT) was also included. Samples were resolved by SDS-PAGE and analyzed by immunoblotting with specific antibodies against FLAG, Mia40, Erv1, Aim32, Osm1, and Ccp1.

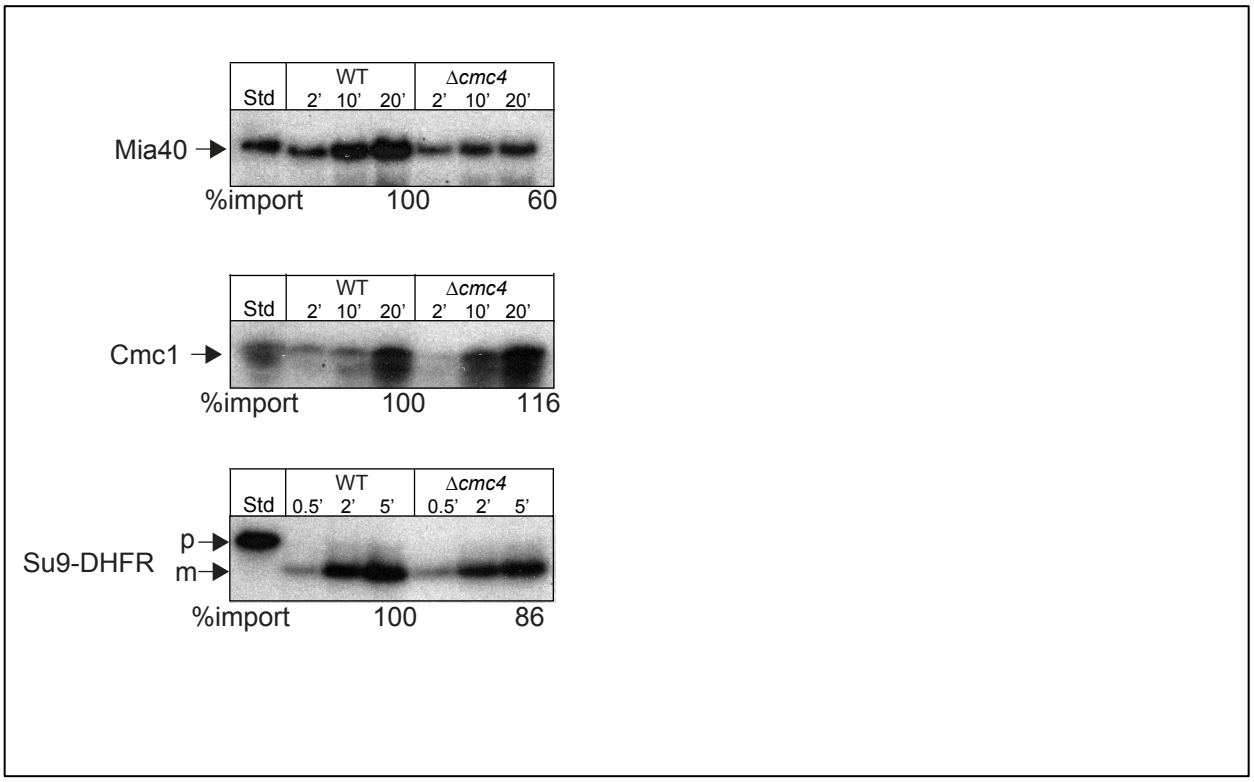

Figure 4-2 Protein import in Δ*cmc4* mutant. Radiolabeled Mia40, Cmc1, and Su9-DHFR were imported into WT and Δ*cmc4* mutant mitochondria in the indicated time course. Non-imported precursors were removed by protease treatment. The imported proteins were analyzed by SDS-PAGE and autoradiography. A 10% standard (Std) from the translation reaction was included. Import reactions were quantitated using Image J software; 100% was set as the amount of precursor that imported into WT mitochondria at the endpoint of the time course. A representative gel is shown. (n = 3).

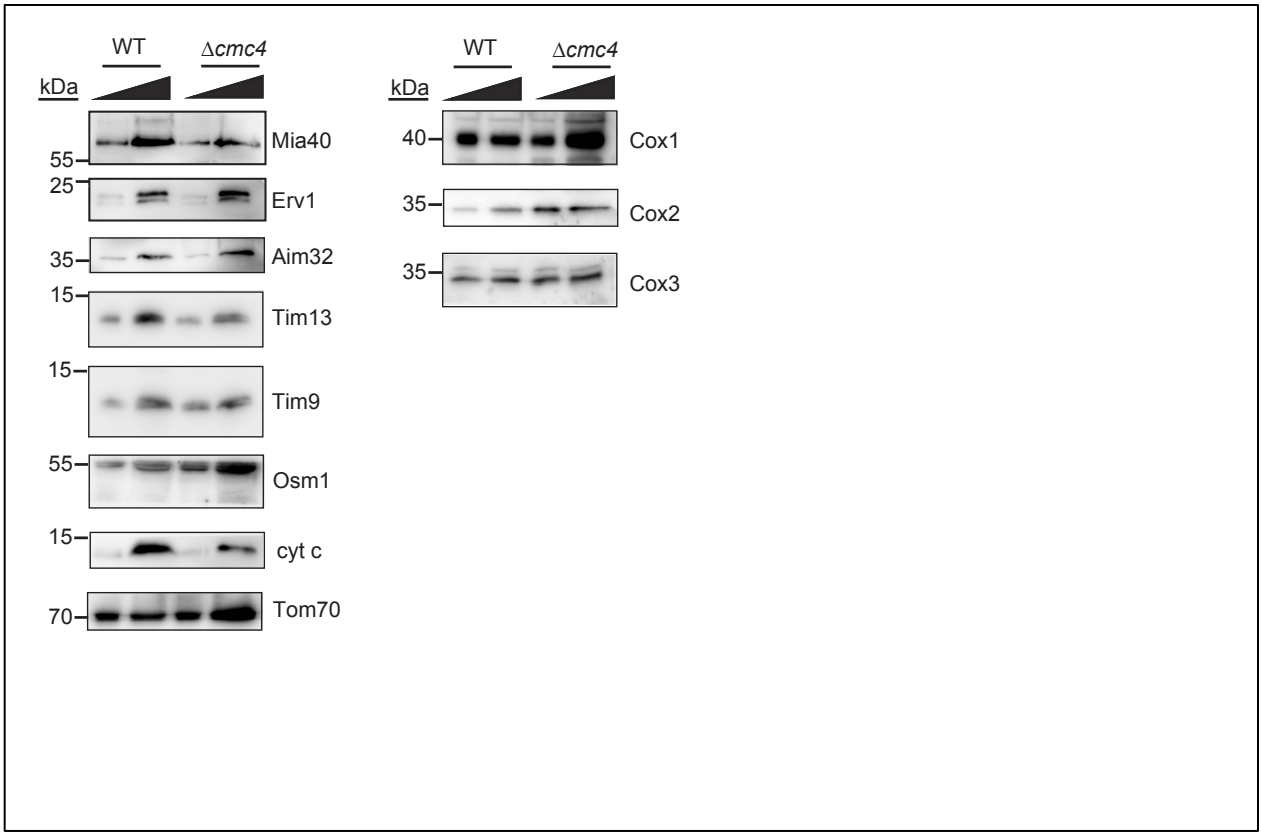

Figure 4-3 Protein levels in CMC4 knockout mutant. A systematic analysis of steady-state levels of mitochondrial proteins (50 and 100 μg) from the parent (WT) or Δ*cmc4* strain was performed by immunoblot with antibodies against the indicated mitochondrial proteins.

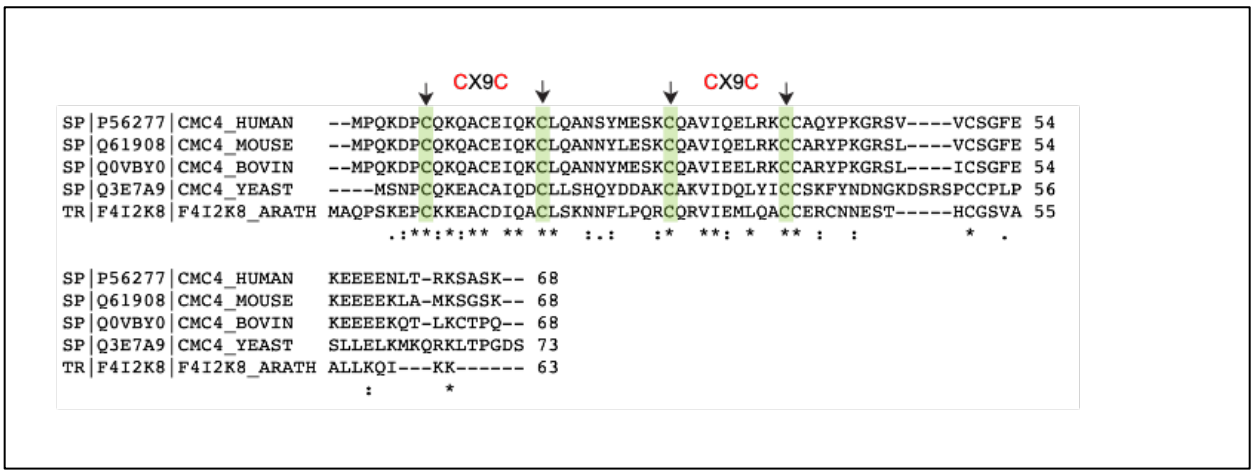

Figure 4-4 Cmc4 has conserved twin CX9C motif. Multiple sequence alignments of Cmc4 homologs.

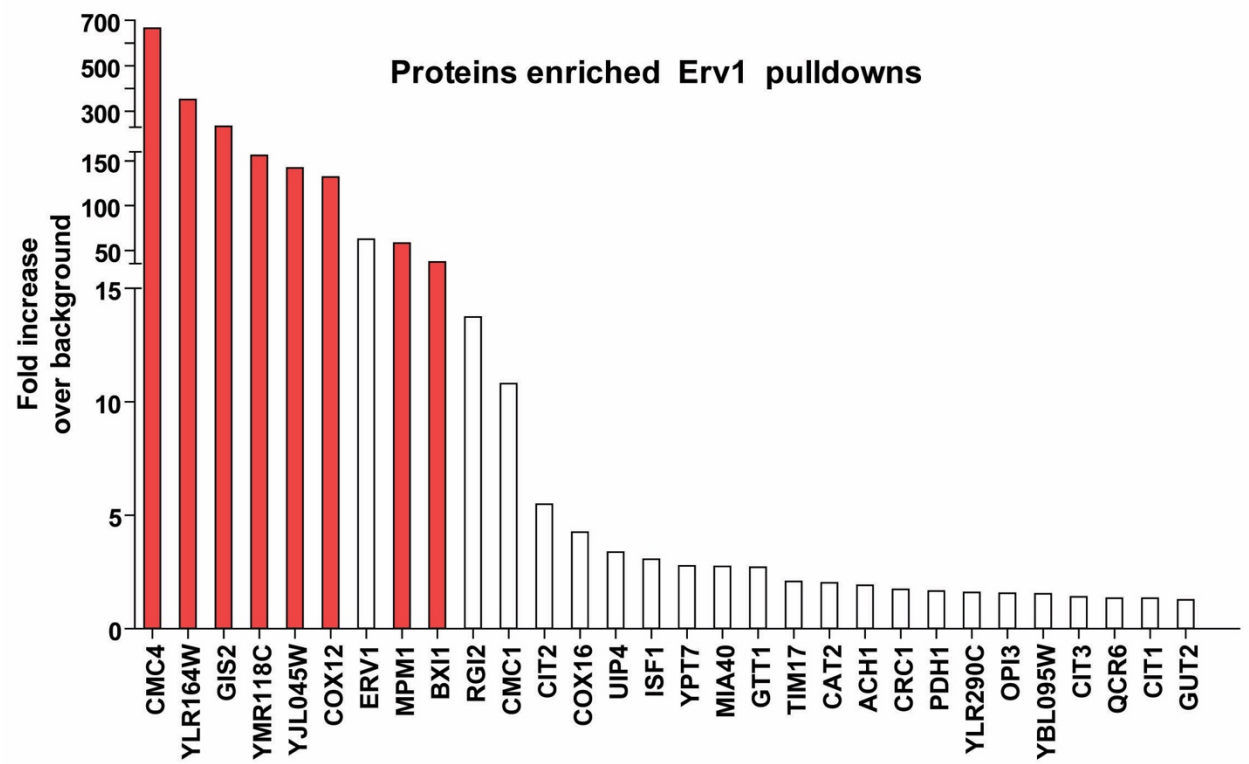
Proteins enriched Erv1 pulldowns
Fold increase over background
700
500
300
150
100
50
15
10
5
0
CMC4
YLR164W
GIS2
YMR118C
YJL045W
COX12
ERV1
MPM1
BXI1
RGI2
CMC1
CIT2
COX16
UIP4
ISF1
YPT7
MIA40
GTT1
TIM17
CAT2
ACH1
CRC1
PDH1
YLR290C
OPI3
YBL095W
CIT3
QCR6
CIT1
GUT2

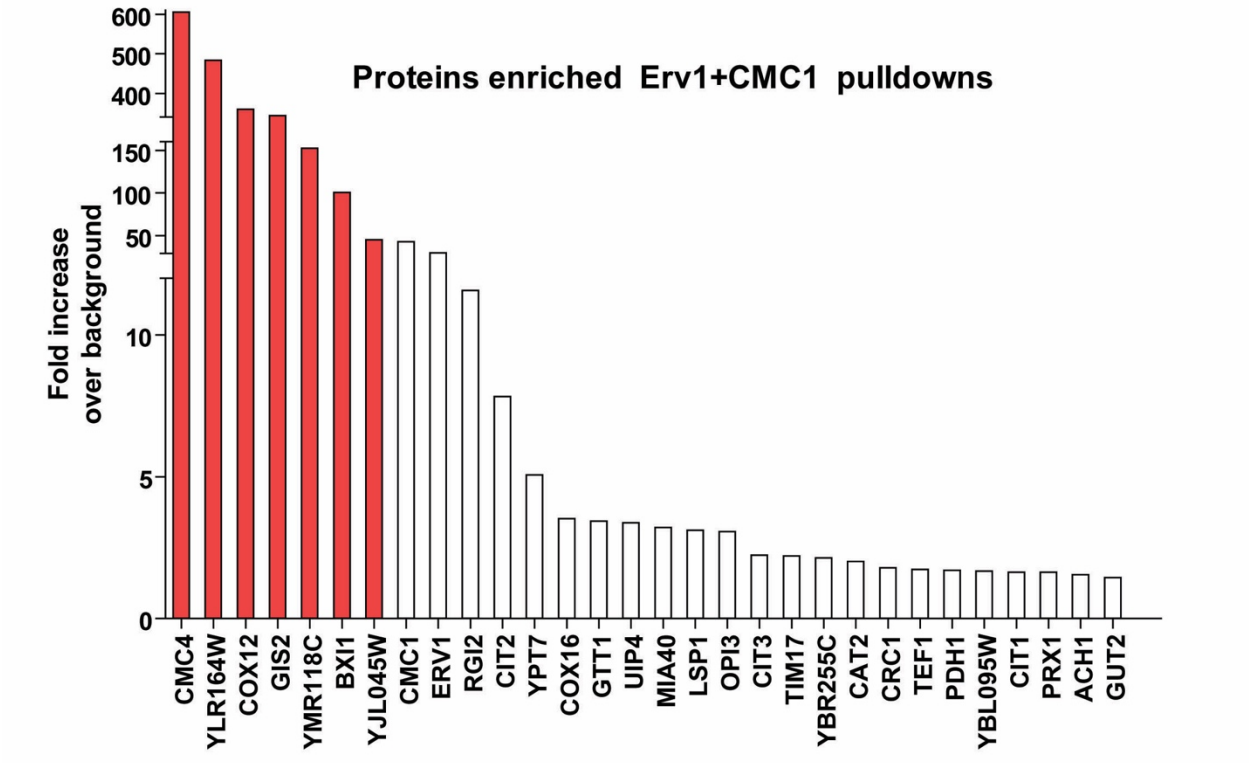
Proteins enriched Erv1+CMC1 pulldowns
Fold increase over background
600
500
400
150
100
50
10
5
0
CMC4
YLR164W
COX12
GIS2
YMR118C
BXI1
YJL045W
CMC1
ERV1
RGI2
CIT2
YPT7
COX16
GTT1
UIP4
MIA40
LSP1
OPI3
CIT3
TIM17
YBR255C
CAT2
CRC1
TEF1
PDH1
YBL095W
CIT1
PRX1
ACH1
GUT2

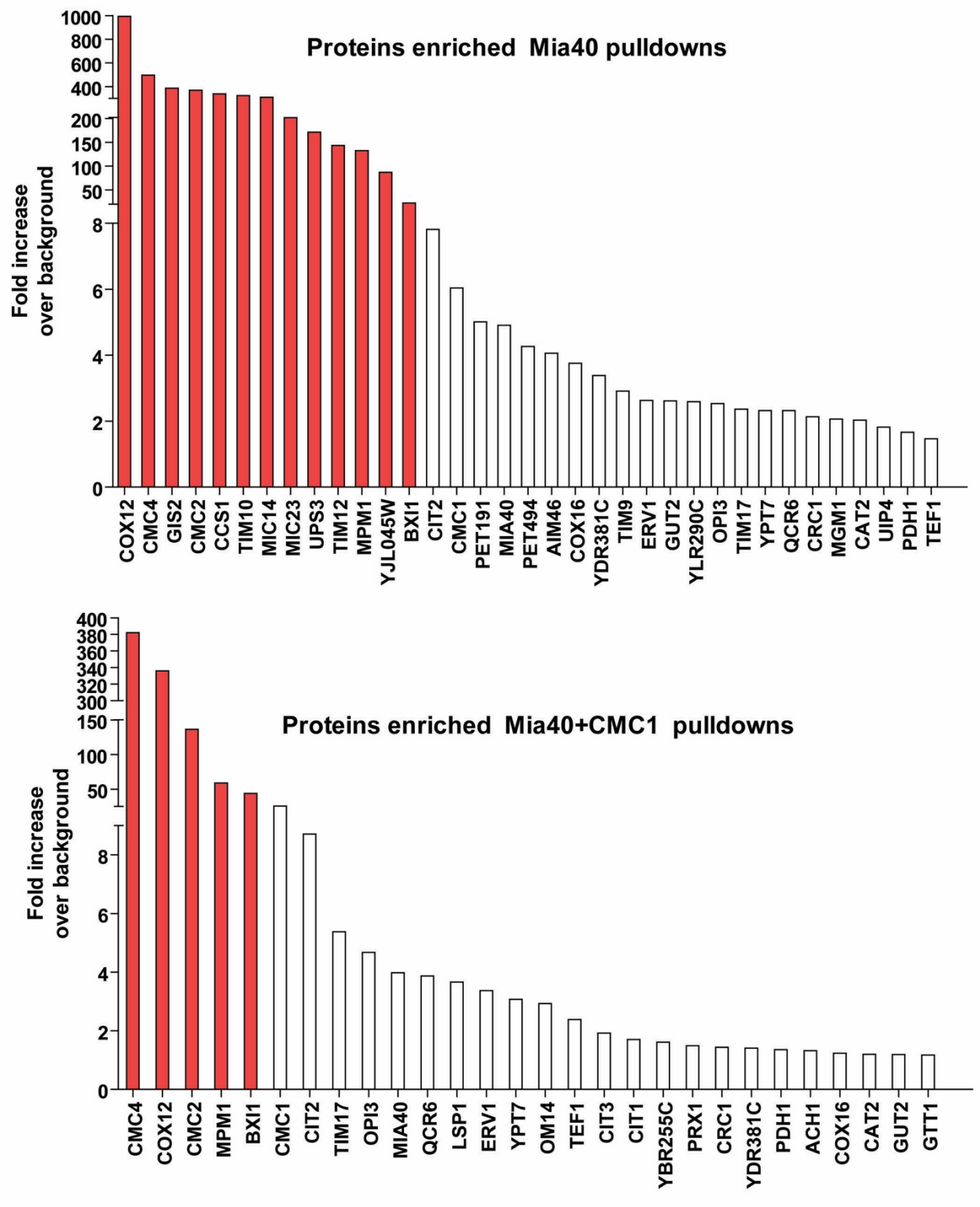
Proteins enriched Mia40 pulldowns
Fold increase over background
1000
800
600
400
200
150
100
50
8
6
4
2
0
COX12
CMC4
GIS2
CMC2
CCS1
TIM10
MIC14
MIC23
UPS3
TIM12
MPM1
YJL045W
BXI1
CIT2
CMC1
PET191
MIA40
PET494
AIM46
COX16
YDR381C
TIM9
ERV1
GUT2
YLR290C
OPI3
TIM17
YPT7
QCR6
CRC1
MGM1
CAT2
UIP4
PDH1
TEF1
Proteins enriched Mia40+CMC1 pulldowns
Fold increase over background
400
380
360
340
320
300
150
100
50
8
6
4
2
0
CMC4
COX12
CMC2
MPM1
BXI1
CMC1
CIT2
TIM17
OPI3
MIA40
QCR6
LSP1
ERV1
YPT7
OM14
TEF1
CIT3
CIT1
YBR255C
PRX1
CRC1
YDR381C
PDH1
ACH1
COX16
CAT2
GUT2
GTT1

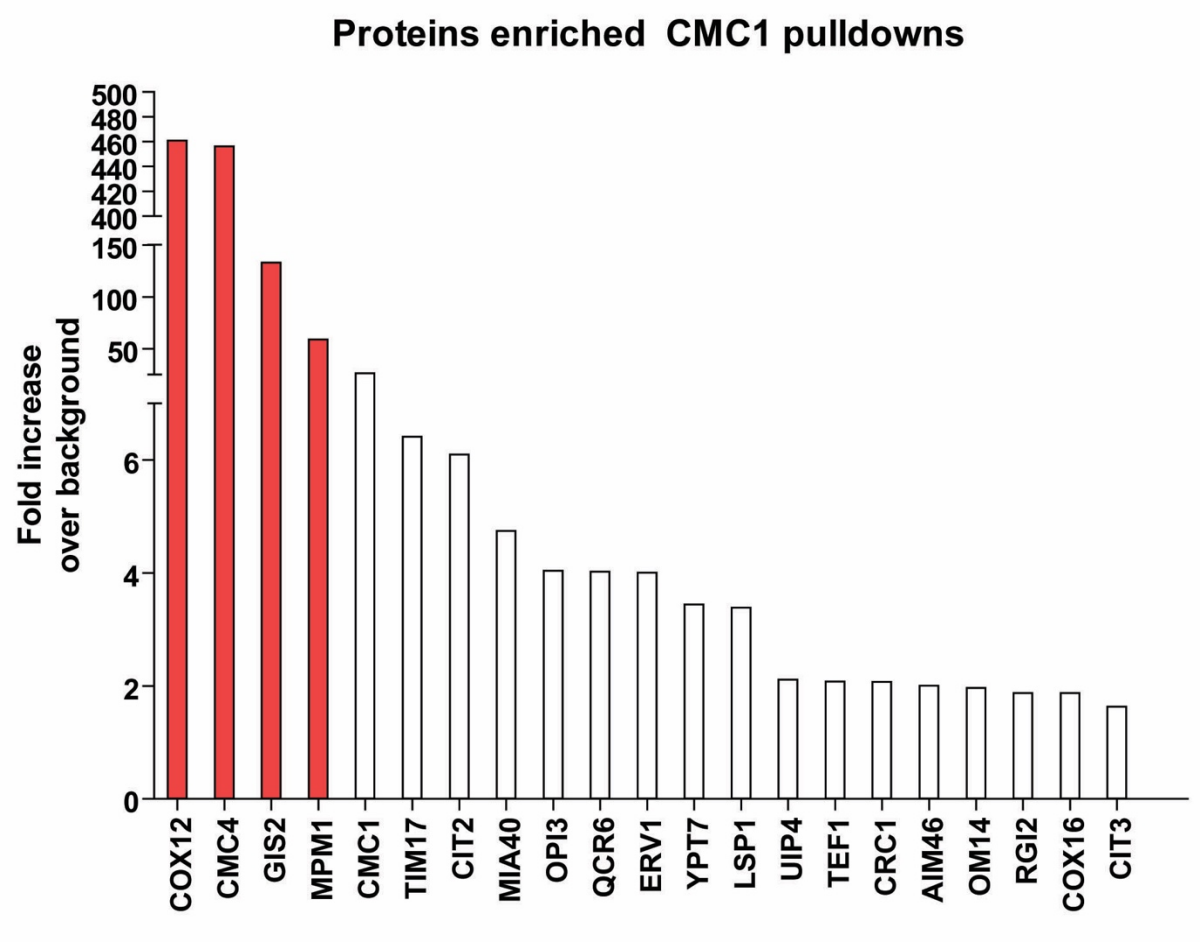

Figure 4S-1 Mass Spec analysis of disulfide partners with Mia40, Erv1, or Cmc1. WT, his-tagged Mia40 or Erv1were either mock treated or incubated with purified recombinant Cmc1. Disulfide interactions were trapped, mitochondria were lysed with 8M urea, and the complexes were isolated with Ni^{2+}-NTA affinity resin. Samples were digested with sequencing grade trypsin and subjected to mass spectrometry analysis. Bar graphs represent proteins that were enriched in each sample and reported by the fold change over the background. Red lanes represent proteins that had no detectable background so caution must be taken into account when comparing levels. *Figure included with permission from Matt Maland*[19].

Material and Methods

Plasmids and strains. Standard set of genetic and molecular techniques was used to generate the strains in this study.

Strain	Genotype	Source
BY4742	MATα *his3Δ1 leu2Δ0 lys2Δ0 ura3Δ0*	[24]
Δcmc4	MATα *his3Δ1 leu2Δ0 lys2Δ0 ura3Δ0 cmc4Δ::KAN*	This study
Δcmc4 [pCMC4-Flag]	MATα *his3Δ1 leu2Δ0 lys2Δ0 ura3Δ0 cmc4Δ::KAN* [*pRS316GPD-CMC4 3XFLAG-PGK: URA3*]	This study
Δcmc4 [Vec]	MATα *his3Δ1 leu2Δ0 lys2Δ0 ura3Δ0 cmc4Δ::KAN* [*pRS316: URA3*]	This study

Table 4-S1 Strains used in this study

Mitochondrial purification and in vitro protein import assay. Mitochondria were purified from yeast cells grown in media with glucose or ethanol/glycerol[25]. Proteins for import studies were synthesized by the TNT Quick Coupled Transcription/Translation kits (Promega) in the presence of [35S] methionine. The radiolabeled precursor was incubated with isolated mitochondria and an import time course was performed. Where indicated, the -Ψ was dissipated with 5 mM CCCP. Non-imported radiolabeled protein was removed by treatment with 100 μg/ml trypsin for 15 minutes on ice and trypsin was inhibited with 200 μg/ml of soybean trypsin inhibitor for 30 min on ice. Samples were separated by SDS-PAGE and visualized using autoradiography.

Immunoprecipitation. 400ug mitochondria were purified, solubilized in lysis buffer (1% digitonin, 50mM Tris HCl pH7.4, 150mM NaCl, 1 mM EDTA, and 0.5 mM PMSF) for 30 minutes on ice. Lysate was centrifuged at maximum speed for 10 minutes to remove insoluble

material. 10 µg lysate was removed from the supernatant to use as a reference for the total sample (T). The remaining was diluted to 0.5 µg/µl in buffer (50mM Tris HCl pH7.4, 150mM NaCl, 1 mM EDTA, 0.1% digitonin, and 0.5 mM PMSF). Samples were incubated with 20 µl of ANTI-FLAG M2 affinity gel (Sigma Aldrich) for 4h at 4°C with rotation. After binding, 10 µg of lysate was removed as a reference for the material that did not bind (denoted flow-through, FT). The beads were then washed 3 times with buffer. Samples were eluted from beads with 8M urea, 100mM Tris pH8.5 (B). The samples collected throughout the experiment were separated by SDS-PAGE and analyzed by immunoblotting.

Antibodies. Most of the antibodies used in this work were generated by vendor Pacific Immunology from recombinant proteins in the Koehler laboratory and have been described previously. Other antibodies: horseradish peroxidase–conjugated secondary antibodies (Thermo Fisher Scientific).

References

1. Erdogan, A. J. & Riemer, J. Mitochondrial disulfide relay and its substrates: mechanisms in health and disease. *Cell and Tissue Research* vol. 367 59–72 (2017).
2. Bihlmaier, K. *et al.* The disulfide relay system of mitochondria is connected to the respiratory chain. *J. Cell Biol.* **179**, 389–395 (2007).
3. LR, T. *et al.* Growth factor erv1-like modulates Drp1 to preserve mitochondrial dynamics and function in mouse embryonic stem cells. *Mol. Biol. Cell* **21**, (2010).
4. Lange, H. *et al.* An essential function of the mitochondrial sulfhydryl oxidase Erv1p/ALR in the maturation of cytosolic Fe/S proteins. *EMBO Rep.* **2**, 715–720 (2001).
5. Koehler, C. M., Beverly, K. N. & Leverich, E. P. Redox pathways of the mitochondrion. *Antioxidants and Redox Signaling* vol. 8 813–822 (2006).
6. Curran, S. P., Leuenberger, D., Schmidt, E. & Koehler, C. M. The role of the Tim8p-

Tim13p complex in a conserved import pathway for mitochondrial polytopic inner membrane proteins. *J. Cell Biol.* **158**, 1017–1027 (2002).

7. Gebert, N. *et al.* Assembly of the three small Tim proteins precedes docking to the mitochondrial carrier translocase. *EMBO Rep.* **9**, 548–554 (2008).

8. Horn, D., Al-Ali, H. & Barrientos, A. Cmc1p Is a Conserved Mitochondrial Twin CX9C Protein Involved in Cytochrome c Oxidase Biogenesis. *Mol. Cell. Biol.* **28**, 4354–4364 (2008).

9. Horn, D. *et al.* The conserved mitochondrial twin Cx9C Protein Cmc2 is a Cmc1 homologue essential for cytochrome c oxidase biogenesis. *J. Biol. Chem.* **285**, 15088–15099 (2010).

10. Bestwick, M., Jeong, M.-Y., Khalimonchuk, O., Kim, H. & Winge, D. R. Analysis of Leigh Syndrome Mutations in the Yeast SURF1 Homolog Reveals a New Member of the Cytochrome Oxidase Assembly Factor Family. *Mol. Cell. Biol.* **30**, 4480–4491 (2010).

11. Carr, H. S., George, G. N. & Winge, D. R. Yeast Cox11, a protein essential for cytochrome c oxidase assembly, is a Cu(I)-binding protein. *J. Biol. Chem.* **277**, 31237–31242 (2002).

12. LaMarche, A. E. P., Abate, M. I., Chan, S. H. P. & Trumpower, B. L. Isolation and characterization of COX12, the nuclear gene for a previously unrecognized subunit of Saccharomyces cerevisiae cytochrome c oxidase. *J. Biol. Chem.* **267**, 22473–22480 (1992).

13. Arnesano, F., Balatri, E., Banci, L., Bertini, I. & Winge, D. R. Folding studies of Cox17 reveal an important interplay of cysteine oxidation and copper binding. *Structure* **13**, 713–722 (2005).

14. Nobrega, M. P., Bandeira, S. C. B., Beers, J. & Tzagoloff, A. Characterization of COX19, a widely distributed gene required for expression of mitochondrial cytochrome oxidase. *J. Biol. Chem.* **277**, 40206–40211 (2002).

15. Barros, M. H., Johnson, A. & Tzagoloff, A. COX23, a homologue of COX17, is required for cytochrome oxidase assembly. *J. Biol. Chem.* **279**, 31943–31947 (2004).

16. Khalimonchuk, O. *et al.* Pet191 is a cytochrome c oxidase assembly factor in Saccharomyces cerevisiae. *Eukaryot. Cell* **7**, 1427–1431 (2008).

17. Horng, Y. C., Cobine, P. A., Maxfield, A. B., Carr, H. S. & Winge, D. R. Specific copper transfer from the Cox17 metallochaperone to both Sco1 and Cox11 in the assembly of yeast cytochrome c oxidase. *J. Biol. Chem.* **279**, 35334–35340 (2004).

18. Longen, S. *et al.* Systematic Analysis of the Twin Cx9C Protein Family. *J. Mol. Biol.* **393**, 356–368 (2009).

19. Maland, M. D. *UCLA UCLA Electronic Theses and Dissertations Title Dissecting*

Mitochondrial Redox-Regulated Protein Translocation Using Small Molecule Probes. https://escholarship.org/uc/item/1n4516dd (2016).

20. Gabriel, K. *et al.* Novel Mitochondrial Intermembrane Space Proteins as Substrates of the MIA Import Pathway. *J. Mol. Biol.* **365**, 612–620 (2007).

21. Horn, D. & Barrientos, A. Mitochondrial copper metabolism and delivery to cytochrome C oxidase. *IUBMB Life* vol. 60 421–429 (2008).

22. Ostrander, D. B., Zhang, M., Mileykovskaya, E., Rho, M. & Dowhan, W. Lack of mitochondrial anionic phospholipids causes an inhibition of translation of protein components of the electron transport chain: A yeast genetic model system for the study of anionic phospholipid function in mitochondria. *J. Biol. Chem.* **276**, 25262–25272 (2001).

23. Tzagoloff, A. & Dieckmann, C. L. PET genes of Saccharomyces cerevisiae. *Microbiological Reviews* vol. 54 211–225 (1990).

24. Brachmann, C. B. *et al.* Designer deletion strains derived from Saccharomyces cerevisiae S288C: A useful set of strains and plasmids for PCR-mediated gene disruption and other applications. *Yeast* **14**, 115–132 (1998).

25. Claypool, S. M., McCaffery, J. M. & Koehler, C. M. Mitochondrial mislocalization and altered assembly of a cluster of Barth syndrome mutant tafazzins. *J. Cell Biol.* **174**, 379–390 (2006).

Chapter 5: Using A Small Molecule to Investigate Mitochondrial Disulfide Relay System in Human Pluripotent Stem Cells

5.1 Introduction

Human stem cells have potential in regenerative medicine because of their ability to self-renew and to differentiate into every cell type[1]. Human embryonic stem cells (hESCs) are derived from embryos and found during the early stages of development before the commitment to form particular tissues of body[2]. hESCs are pluripotent that they are able to grow into derivatives of the three primary germ lineages: ectoderm, mesoderm, and endoderm[3]. Pluripotency differentiates hESCs from adult stem cells that are multipotent found in adult body and can produce limited mature cell types of associated tissue lineage. Because of pluripotency and capacity for self-renewal, hESCs therapies have been proposed for regenerative medicine and tissue replacement.

Human induced pluripotent stem cells (iPSCs) share similar properties with hESCs. Differentiated somatic cells are reprogrammed into a pluripotent embryonic stem cell-like state by retroviral mediated expression of specific transcription factors of Oct4, Sox2, Klf4, and c-Myc[4]. The use of iPSCs for the generation of therapeutic cells for cell replacement therapy may avoid the requirement of post-transplant immune suppression because iPSCs can be generated directly from the transplant recipient, therefore be genetically identical to the patient. Because iPSCs avoid many of ethical concerns associated with origin of cells, they have great potential in regenerative medicine. However, methods for reprogramming are not completely efficient and

there are concerns about immunogenicity of cells differentiated from iPSCs[5].

Despite the significant progress in establishing conditions to reproducibly differentiate hPSCs into various functional cell types of therapeutic value, the differentiation process is rarely complete with some undifferentiated hPSCs remaining among the differentiated derivatives. Because embryonic stem cells have the ability to form noncancerous tumors called teratomas[6], tumor formation is a major safety concern in the use of human embryonic stem cell when differentiated lineages contaminated with hPSCs are transplanted into patients. Eliminating undifferentiated pluripotent stem cells from a differentiated cell lineage is the challenge for developing transplantation treatment.

Currently, methods to remove undifferentiated hPSCs from differentiated cell pools are extremely limited and difficult to implement. One method has relied on a cytotoxic antibody specific for a surface marker on hESCs and kills undifferentiated human embryonic stem cells via oncosis[7]. However, this approach is limited because not all hPSCs display this marker and the cells may require sorting. Another concern is immune responses to foreign proteins if used as a treatment *in vivo*. A second method relies on introduction of a suicide gene into a genetic locus that is highly expressed in hPSCs but not the differentiated derivatives[8]. The thymidine kinase (TK) and ganciclovir (GCV) system is an example of current application of suicide genes, which is a drug therapy with GCV that targets cells expressing specific TK enzymes[9]. However, there are concerns with using retrovirus and lentivirus with risk of harmful effects. Moreover, this approach requires additional genetic manipulation of the hPSCs, which is not desirable. Based on the aforementioned shortcomings, a new approach is needed to eliminate tumorigenic potential

from candidate cellular therapies. Sorting schemes that rely on biomarkers are imperfect and sorting desirable cells in the mixture to remove the potentially harmful ones may negatively impact their function and clinical efficacy.

From preliminary results, we have found Erv1/ALR is an unexpected pro-survival molecule in hPSCs. Surprisingly, the small molecule MitoBloCK-6 (MB6) selectively induces apoptosis in hPSCs but not their differentiated progeny lineages[10]. The advantage of this small molecule probe is that it can be reversibly incubated with cells to instantly modulate the pathway, in contrast to complementary RNAi approaches that take several days. MB6 inhibits Erv1/ALR oxidative activity and attenuates the redox regulated mitochondrial intermembrane space assembly (MIA) pathway in mitochondria. This pathway is thought to be essential for viability and we were surprised when MB6 treatment (up to 100 μM) in a variety of differentiated cell lineages [cancer cell lines HEK293, HeLa, COS and primary NHDFs] had no inhibitory effect on growth or mitochondrial morphology. In contrast, hPSCs died when treated with 10-20 μM MB6. However, after 4 days differentiation with retinoic acid, the cells were no longer sensitive to MB6. Thus, the data suggests an unexpected role of ALR in hPSCs survival and MB6 is a small molecule reagent that can regulate this key function. In this chapter, we explore the mechanism of MB6 induced human pluripotent stem cell apoptosis. We hypothesize that the variation in sensitivity among stem cells of differentiated progeny lineages and pluripotency states is mediated by different protein interactions. Determine the mechanism for pluripotent-state specific death will help enable MB6 as a potential agent for removing hPSCs that fail to differentiate into desired cell types, furthering clinical applications in cell therapeutics.

5.2 Determine MB6 sensitivity in a wide-range pluripotent and differentiated cells

Previous study had tested MB6 with HSF1 hESCs. To characterize MB6 specificity in a wide range of cell types, we have investigated hESCs, iPSCs, and their differentiated progeny. Pluripotent cells, H9 hESCs and hIPS2 iPSCs, were treated with 20 μM MB6 for different time points (Figure 5-1). Downstream events in apoptosis, caspase-3 cleavage was measured with flow cytometry (Figure 5-1A, B) and poly ADP-ribose polymerase (PARP) cleavage was analyzed from immunoblotting (Figure 5-1C, D). Quantification of caspase-3 and PARP cleavage indicated that 20 μM MB6 induces apoptosis in H9 and hIPS2 after 6 hours treatment which is similar with the addition of actinomycin D, a known apoptosis inducer. Control treatment with 1% DMSO did not initiate apoptosis.

MB6 sensitivity was also tested on early differentiated germ lineages. H9 hESCs were differentiated to neutral ectoderm for 5 or 10 days (Figure 5-2). Cells were treated with 20μM MB6 for different timecourses and PARP cleavage were quantified from immunoblotting. As predicted, 5-day differentiated neural ectoderm gained resistance to MB6 compare to undifferentiated H9 cells. 10-day differentiated neural ectoderm were no longer sensitive to MB6 which is same as control HEK293T cell. Caspase-3 cleavage was also analyzed by flow cytometer of pluripotent H9 and differentiated neural ectoderm (Figure 5-2B). Differentiated neural ectoderm required longer MB6 treatment to initiate apoptosis than H9 cells. 5-day differentiated neural ectoderm is less sensitive to MB6 than 3-day neural ectoderm. To compare between germ lineages, 3-day and 5-day differentiated mesoderm and ectoderm were treated

with 20 μM MB6 for 6 or 12 hours (Figure 5-3). Quantification of PARP cleavage showed that ectoderm was less sensitive to 20 μM MB6 treatment compared to undifferentiated cells. Interestingly, 3-day and 5-day differentiated mesoderm had similar MB6 sensitivity as undifferentiated pluripotent cells. As ectoderm, 5-day differentiated mesoderm is less sensitive to MB6 than 3-day mesoderm. In sum, different pluripotent cell lines of hESCs and iPSCs do not impact MB6 sensitivity but length of differentiation changes the sensitivity that the longer differentiation results in less sensitivity to MB6. Differences in sensitivity to MB6 were observed between germ lineages from cells that were induced to differentiate to early neural ectoderm and mesoderm.

In order to define the mechanism of action of MB6 on hPSCs, ALR expression has been decreased by shRNA approaches to generate ALR knockdown (KD) UCLA1 hESC and hIPS2 cell lines (Figure 5-4A). ALD KD cells are maintained in hypoxia condition (2% O_2). Cells in normoxia with ALR KD begin to differentiation with reduced OCT4 within 24 hours (data not shown). Mitochondrial membrane potential and morphology are unchanged in ALD KD cells by measuring TMRE fluorescence intensity (Figure S5-1). As predicted, ALR KD cells died by apoptosis upon MB6 treatment (Fig 5-4B, C) and differentiated lineages showed resistance to MB6 when ALR is knocked down.

5.3 MB6 treatment with elevated ROS levels in hPSCs

hPSCs are inherently glycolytic and low oxidative phosphorylation (OXPHOS) maintain low reactive oxygen species (ROS) levels[11]. Studies showed elevation in ROS can regulate stem cell commitment and differentiation[12]. Maintaining low ROS levels is required to sustain self-

renew capacity. Here, we hypothesized that MB6 increases levels of ROS production by disrupting redox relay pathway, contributing to hPSCs cell apoptosis. To evaluate oxidative level, fluorescence microscopy of dihydroethidium (DHE) staining[13] of UCLA1 hESCs and ALR KD cells were analyzed (Figure 5-5). A small increase level of ROS was observed in cells treated with MB6 compared to untreated cells. Interestingly, ALR KD in cells caused ROS accumulation and elevated ROS levels with MB6 treatment. Further studies should test on differentiated cells since they have better ROS protective mechanisms.

To test if MB6 induced cell apoptosis could be protected from antioxidant, general antioxidant N-acetyl-L-cysteine (NAC)[14] and mitochondria-targeted ROS scavenger MitoTempo (M-T)[15] were applied (Figure 5-6). Same as MB6 treated pluripotent cells and differentiated mesoderm, addition of antioxidants still resulted in PARP cleavage and apoptosis. Antioxidant treatments did not recue MB6-induced stem cell apoptosis. Although MB6 increased ROS levels, it is unlikely ROS is the primary driver of MB6 induced apoptosis. However, we cannot exclude that MB6 induced apoptosis lead to ROS.

5.4 Disulfide relay system does not contribute to respiration in hPSCs

The MIA pathway passes electrons to cytochrome *c* that the disulfide relay system could be feeding electrons into the electron transport chain (ETC) [16]. We hypothesized that MB6 treatment could affect the respiration in hPSCs. To examine the ETC, the oxygen consumption rate (OCR) was measured with hPSCs treated with MB6 or DMSO (Figure 5-7A, B). MB6 did not affect basal respiration, maximal respiration, or proton leak that there was no effect on respiration. Note that respiration is reduced in hPSCs compared to differentiated counterparts[17]. Furthermore, to

test that electron donated from MIA to Complex IV of ETC causing respiration independent of Complex I-III, a mitochondrial stress test during which the ETC is uncoupled from ATP synthase and Complex I and III are inhibited (Figure 5-7C, D). However, if the disulfide relay system is feeding electrons into Complex IV, it would not be inhibited by a Complex I or III inhibitor. Therefore, a Complex IV inhibitor, azide, was used at the end of the assay which may cause a change in OCR due to inhibiting the disulfide relay system. No change in OCR was observed after azide treatment which suggests that the disulfide relay system is not contributing to respiration in hPSCs. This was performed in cells pretreated with DMSO or MB-6 and no difference was seen between the two, which provides further support for the conclusion that the disulfide relay system is no contributing to respiration.

5.5 Decreased disulfide interactions in ALR-knockdown pluripotent stem cells

Decreased protein levels in ALR-KD hPSCs have been detected from immunoblotting (Figure 5-8A). MIA pathway protein Mia40 was expected to be lower in the ALR-KD cells. ALR has been suggested to maintain murine ESC pluripotency through modulation of the mitochondrial fission factor Drp1[18], and we found Drp1 level decreased in ALR-KD cells. Interestingly, the expression of MICU1, the key regulator of mitochondrial calcium uniporter (MCU), is significantly reduced in ALR-KD cells. Level of MCU is also reduced in KD cells (data not shown). MICU1 works with MICU2 together to form disulfide-linked heterodimer to modulate MCU[19].

To test if disulfide interactions have been disrupted when knockdown ALR levels in hPSCs, isolated mitochondria from wild type (WT) and ALR KD UCLA1 cells were examined on 2D-

Diagonal gel electrophoresis (2D-DGE) followed by Coomassie stain (Figure 2-8B) or immunoblotting (Figure 5-8C). The immunoblotting of 2D-DGE highlighted several redox statuses of proteins. Coomassie stain showed that WT UCLA1 mitochondria has more off-diagonal proteins, meaning higher molecular disulfide interactions comparing to the ALR-KD.

5.6 Discussion

Despite the potential use of hPSCs into various functional cell types of therapeutic value, the current risk presents the teratoma formations when differentiated lineages contaminated with hPSCs are transplanted into patients. Current methods to remove undifferentiated hPSCs from differentiated pools are limited and difficult to implement. The small molecule inhibitor, MitoBloCK-6 (MB6), that takes the advantage by selectively inducing apoptosis in hPSCs can be a potential method for the selective removal of hPSCs[10]. MB6 selectively inhibits the Mia40/Erv1(ALR) redox-mediated import pathway of mitochondria and dissociates cytochrome *c* from ALR in mitochondria to cause release, which activates caspase-dependent apoptosis exclusively in hPSCs. Here we focus on the mechanism through which MB6 selectively induces apoptosis in hPSCs and the pro-survival role of ALR in hPSCs during apoptosis and differentiation processes.

In this study, we have evaluated the cell death kinetics and the effectiveness of MB6 treatment on hPSCs and early differentiated germ lineages. A wide range of cell types were tested to conclude that 20 μM MB6 treatment for 6 hours was able to effectively and selectively induce apoptosis in hPSCs. Differences in sensitivity to MB6 were observed between germ lineages from cells that were induced to differentiate into early neural ectoderm and mesoderm.

Studies have shown that early ectoderm differentiation requires maintenance of glycolytic flux while there is a metabolic switch from glycolysis towards oxidative phosphorylation (OXPHOS) during differentiation into the mesoderm and endoderm linages[20,21]. We have observed that early differentiated mesoderm has similar sensitivity to MB6 as undifferentiated hPSCs. However, early differentiation apoptotic assays have yet to be done on directed early endoderm differentiation following MB6 treatment. The comparison to mesoderm differentiation with the endoderm lineage which undergoes a similar metabolic switch will provide more insight to the differences in sensitivity to MitoBloCK-6 treatment between lineages. Thus, during differentiation the increase of OXPHOS and changes in mitochondrial morphology that occur may be dependent on the ALR-dependent disulfide relay system of the IMS. It will be important to determine if there are metabolic changes when ALR is knocked down in hPSCs. We predict that ALR-KD hPSCs with impaired mitochondrial protein import will experience difficulties in mesodermal and endodermal differentiation without impairment in ectodermal differentiation. Therefore, we suggest that cell fate determining lineage specific metabolic switching is dependent on activity of the ALR-dependent mitochondrial disulfide relay system.

The ALR-dependent mitochondrial disulfide relay system is required for the import of cysteine rich proteins into the IMS. ALR knockdown stem cells maintain pluripotency in hypoxia but have decreased protein levels of Mia40, calcium transport MCU and regulator MICU1. MICU1, also as CBARA1, plays a role in stemness and proliferation of human embryonic stem cells[22]. CBARA1 expression is suppressed when stem cell is stimulated to differentiation. In addition, the disulfide dimerization of MICU1 and MICU2 is formed facilitated by Mia40 and

associates with MCU to control Ca^{2+} uptake of mitochondria[19]. Thus, ALR plays a role in stem cell differentiation by controlling calcium signaling. Considering that ALR KD cells maintains in hypoxia while increase respiration capacity and differentiation in normoxia and reduced Mia40 and MICU1, Ca^{2+} flux may be a trigger for differentiation and respiration is required. For future study, Ca^{2+} imaging can be used to examine Ca^{2+} flux in wild type and ALR-KD cells and during differentiation processes. Based on the oxygen consumption rate (OCR) measurements, it is concluded that ALR-Mia40 redox relay system is working in low respiring pluripotent stem cells and is not appreciably contributing electrons to electron transport chain (ETC) in order to maintain low respiration. However, respiration of ALR KD cells and early differentiated lineages should also be studied. In sum, our data suggests that ALR redox relay system controls Ca^{2+} flux controlling stem cell differentiation.

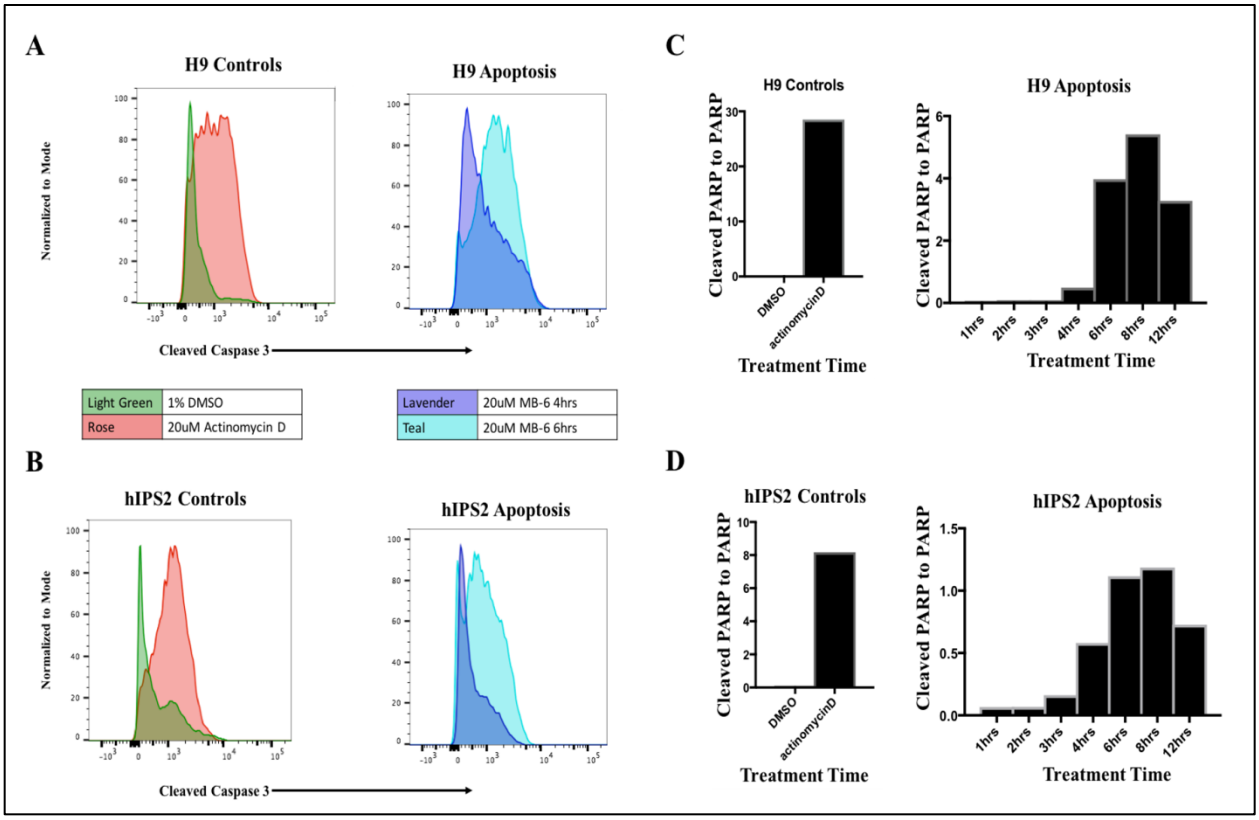

Figure 5-1 MB6 induces apoptosis in pluripotent stem cells. (A) Flow cytometry analysis of caspase 3 cleavage in H9 cells treated with 20 µM MB6 for 4 (lavender) and 6 hours (teal). As a positive control, apoptosis was induced in cells by treatment with 20 µM actinomycin D for 6 hours (rose). 1% DMSO was used as vehicle control (light green). (B) The same flow cytometry analysis was performed as in (A) with hIPS2 cells. (C) Ratio of cleaved PARP/PARP of H9 cells treated with 20 µM MB6 for 1, 2, 3, 4, 6, 8, and 12 hours, 20 µM actinomycin D, or 1% DMSO quantified from immunoblotting. (D) As in (C), hIPS2 cells were analyzed.

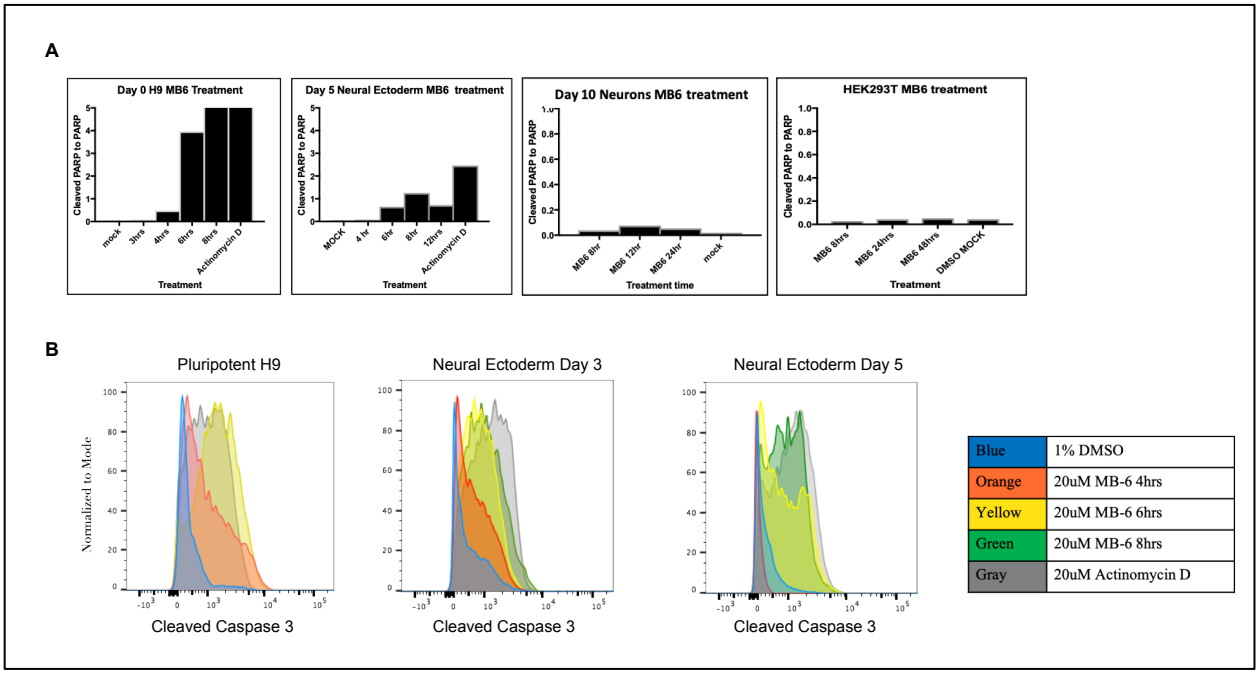

Figure 5-2 Neural ectoderm shows varied sensitivity to MB6. (A) Ratio of cleaved PARP/PARP of pluripotent H9 cells, H9 cells differentiated to neural ectoderm for 5 and 10 days, and HEK293T cells treated with 20 µM MB, 20 µM actinomycin D, or 1% DMSO mock. Quantification was analyzed from immunoblotting. (B) Flow cytometry analysis of caspase 3 cleavage in pluripotent H9 cells and cells differentiated to neural ectoderm for 3 and 5 days and treated with 20 µM MB6 for 4, 6, and 8 hours, 20 µM actinomycin D, or 1% DMSO.

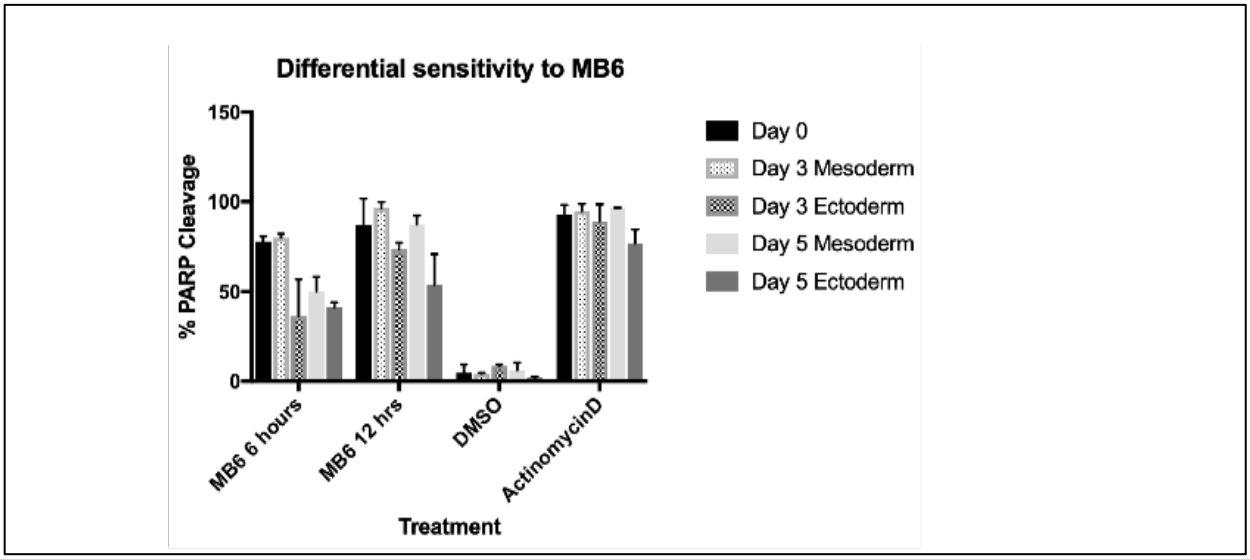

Figure 5-3 Varied MB6 sensitivity in differentiated lineages. Percentage of cleaved PARP/PARP of pluripotent H9 cells differentiated to ectoderm or mesoderm for 3 and 5 days treated with 20 μM MB6 for 6 and 12 hours, 20 μM actinomycin D, or 1% DMSO quantified from immunoblotting.

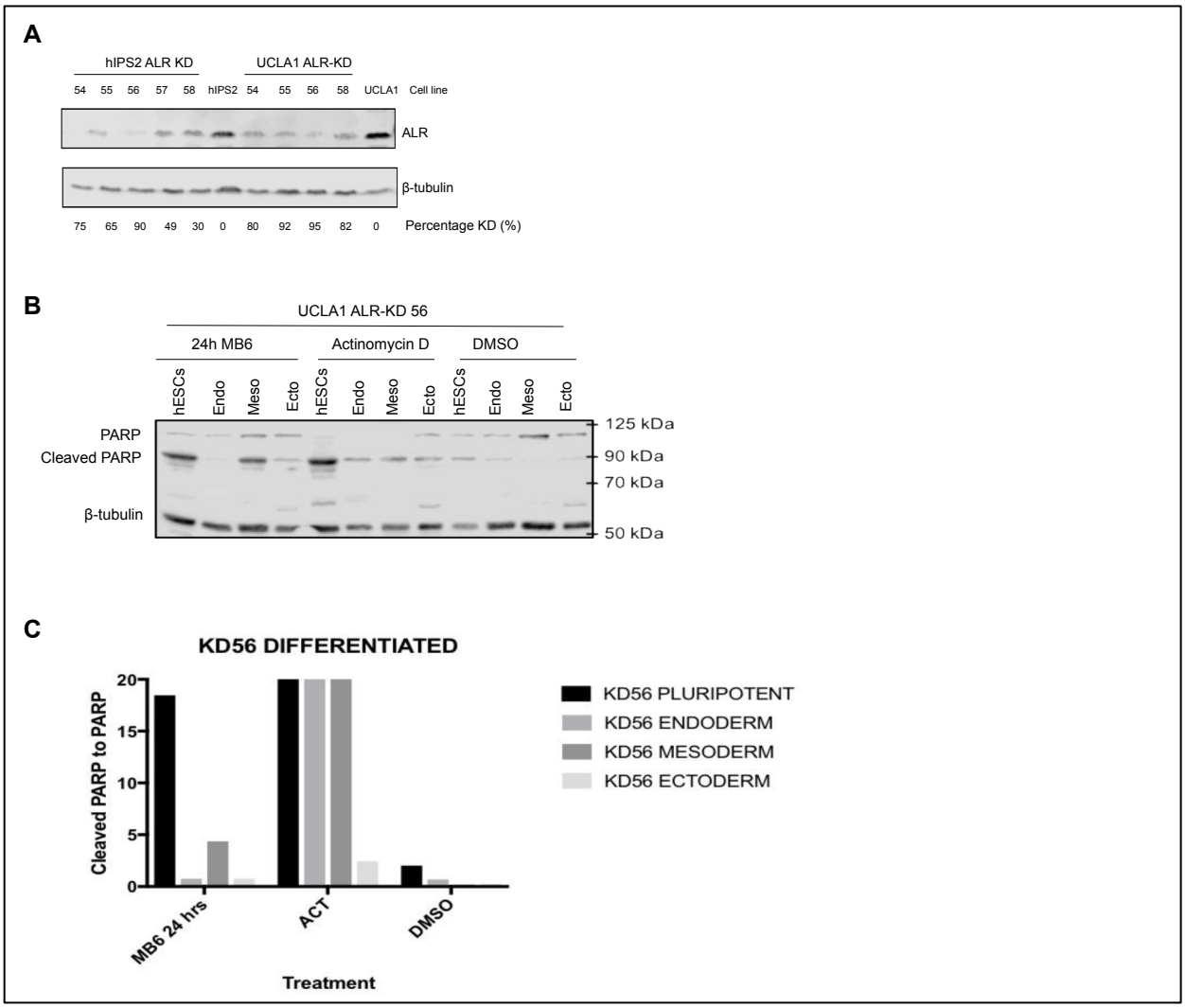

Figure 5-4 MB6 sensitivity in ALR knockdown cells. (A) Immunoblot of ALR protein levels in hIPS2 ALR-knockdown (KD) cell lines (54, 55, 56, 57, 58) and UCLA1 hESC ALR-KD cell lines (54, 55, 56, 58). β-tubulin was included as loading control. (B) Immunoblot of PARP in UCLA1 hESC ALR-KD 56 cell line and differentiated endoderm, mesoderm, or ectoderm treated with 20 μM MB6, 20 μM actinomycin D, or 1% DMSO for 4 hours. β-tubulin was included as loading control. (C) Quantification of cleaved PARP/PARP ratio from (B).

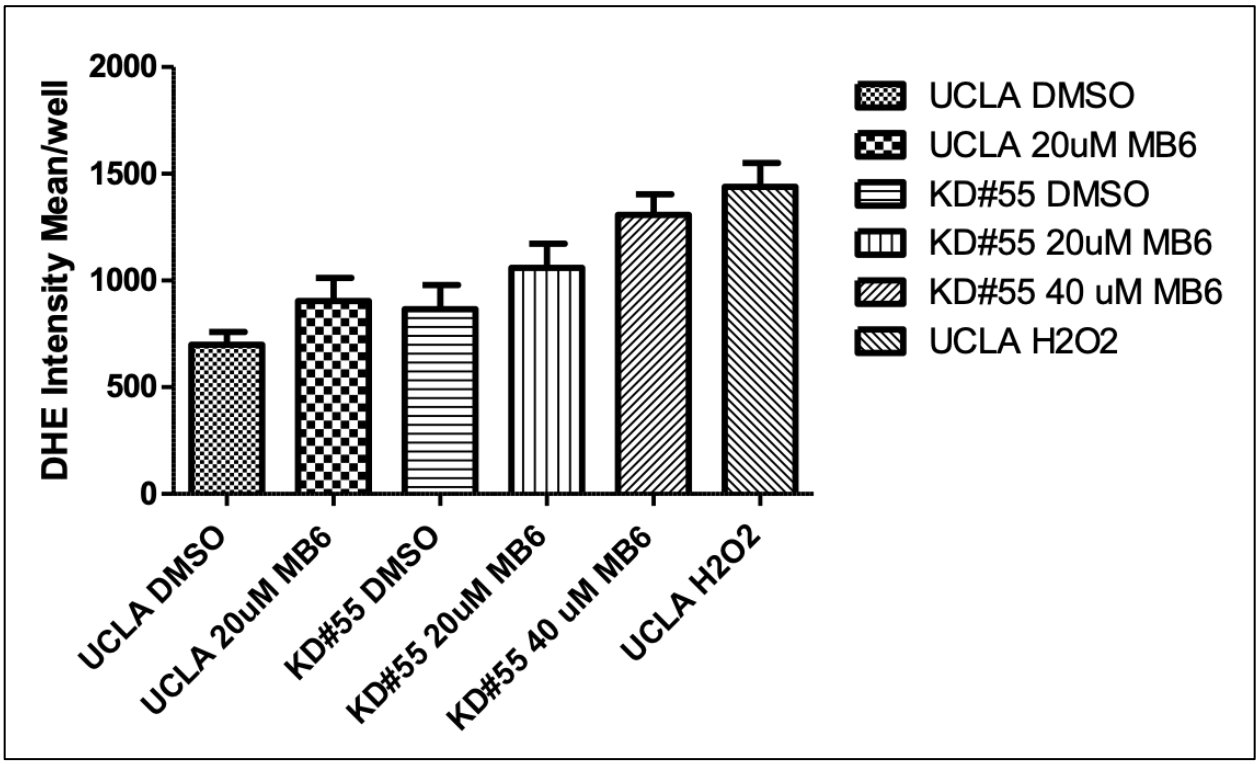

Figure 5-5 MB6 induced ROS level in ALR knockdown hPSCs. UCLA1 hESCs and ALR KD #55 cells were treated with 20 or 40 μM MB6 for 4 hours. 1% DMSO was used as vehicle control. As a positive control, UCLA1 were treated with H_2O_2. Cells were incubated with 30μM dihydroethidium (DHE) for 1 hour at 37 °C. Cells were imaged after replacing staining solutions with growth media. Red fluorescence intensity was quantified by using ImageJ.

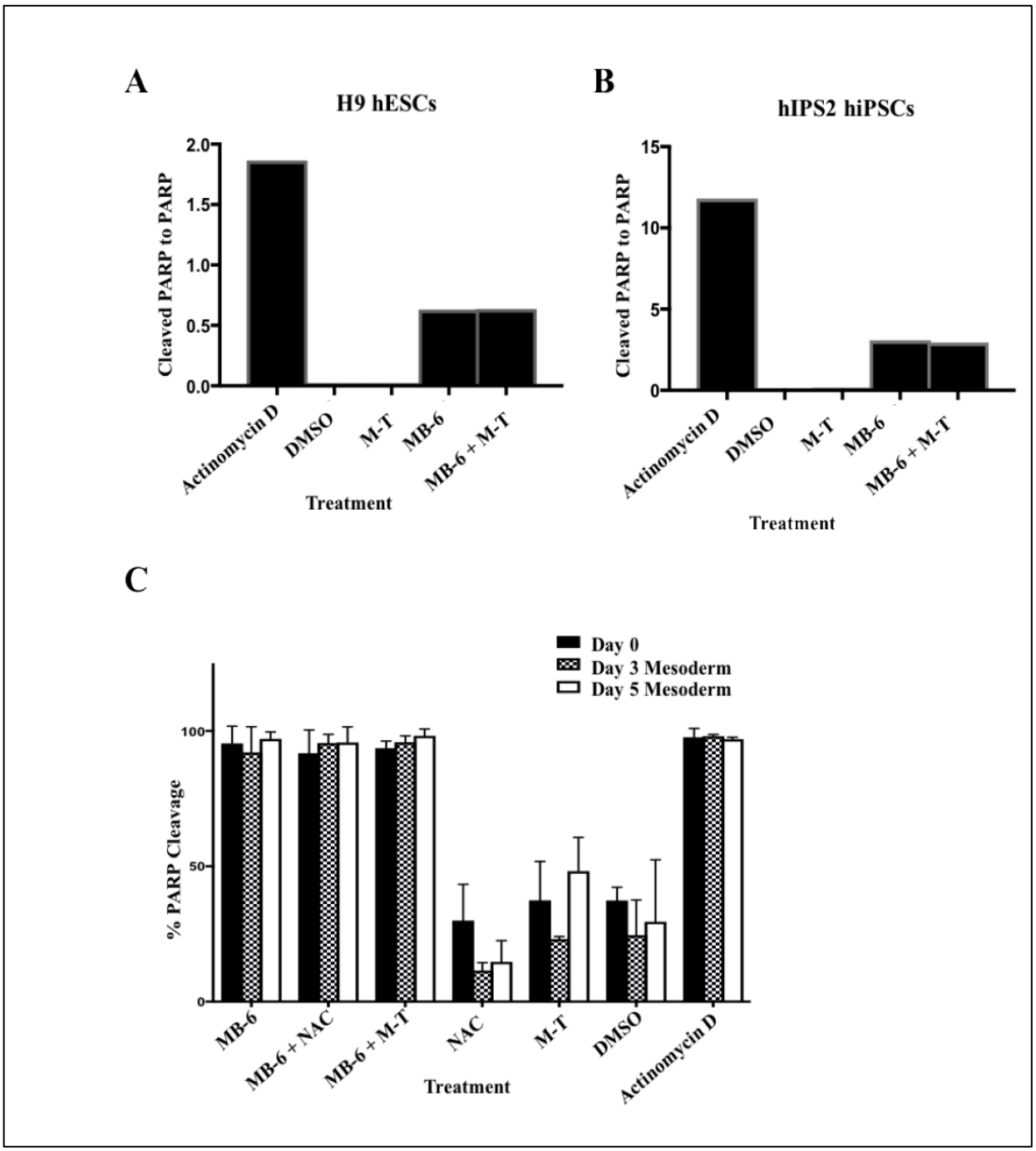

Figure 5-6 No MB6 rescue with addition of antioxidant. (A) Ratio of cleaved PARP/PARP of H9 cells treated with 20 μM actinomycin D, vehicle control 1% DMSO, 20 μM MitoTempo (M-T), and 20 μM MB6 for 4 hours. Quantification was analyzed from immunoblotting. (B) As in (A), quantification of cleaved PARP/PARP of hIPS2 cells. (C) Percentage of cleaved

PARP/PARP of pluripotent UCLA1 cells and differentiated 3-day and 5-day mesoderm treated with 20 μM actinomycin D, vehicle control 1% DMSO, 20 μM MitoTempo (M-T), 1mM N-acetyl-L-cysteine (NAC), and 20 μM MB6 for 4 hours. Quantification was analyzed from immunoblotting.

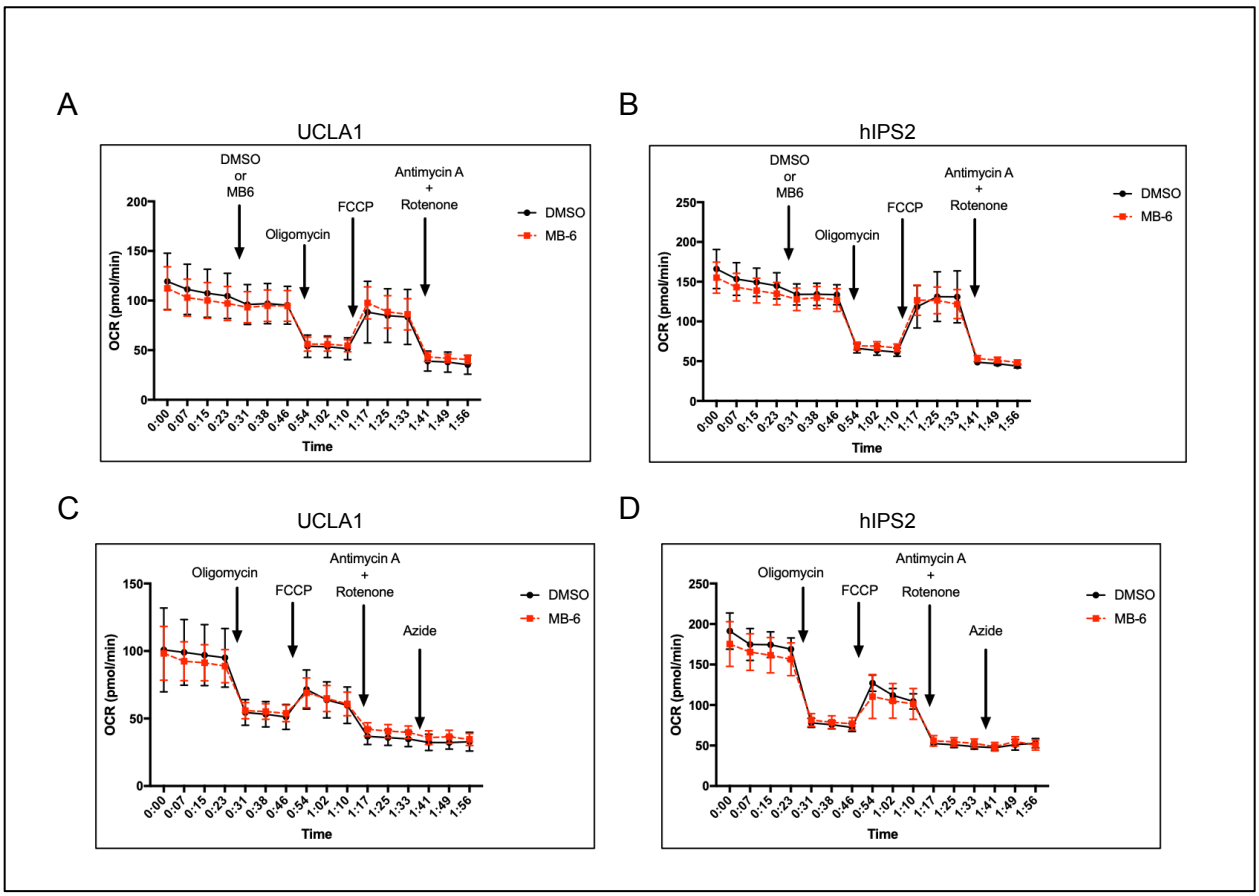

Figure 5-7 Disulfide relay system does not contribute to respiration in hPSCs. (A) Oxygen consumption rate (OCR) in UCLA1 hESCs treated with 20 μM MB6 or vehicle control 1% DMSO. (B) OCR in hIPS2 as in (A). (C) As in (A), complex IV inhibitor, azide was added at the end of the assay. (D) As in (B), complex IV inhibitor, azide was added at the end of the assay.

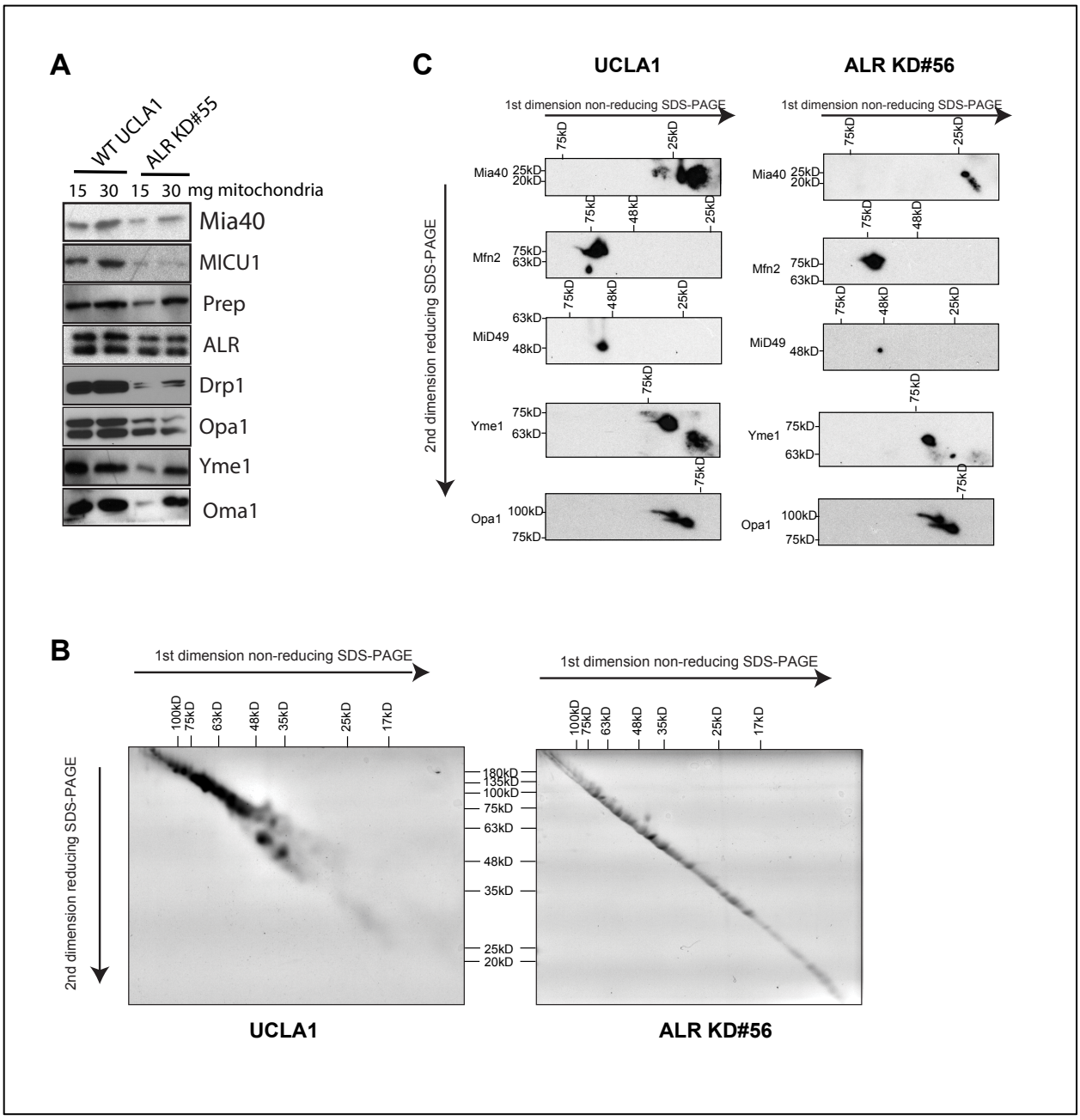

Figure 5-8 Decreased disulfide interactions in ALR-knockdown pluripotent stem cells. (A) Immunoblot of protein levels of mitochondria were isolated from wild type (WT) UCLA1 and ALR knockdown (KD) #55 cells. (B) 50ug isolated mitochondria from WT UCLA1 and ALR KD#56 cells were prepared without reducing agent and loaded on SDS-PAGE in non-reducing condition. Gels were incubated with reducing agent before running on second SDS-PAGE in

reducing condition followed by coomassie stain (B) or immunoblotting (C).

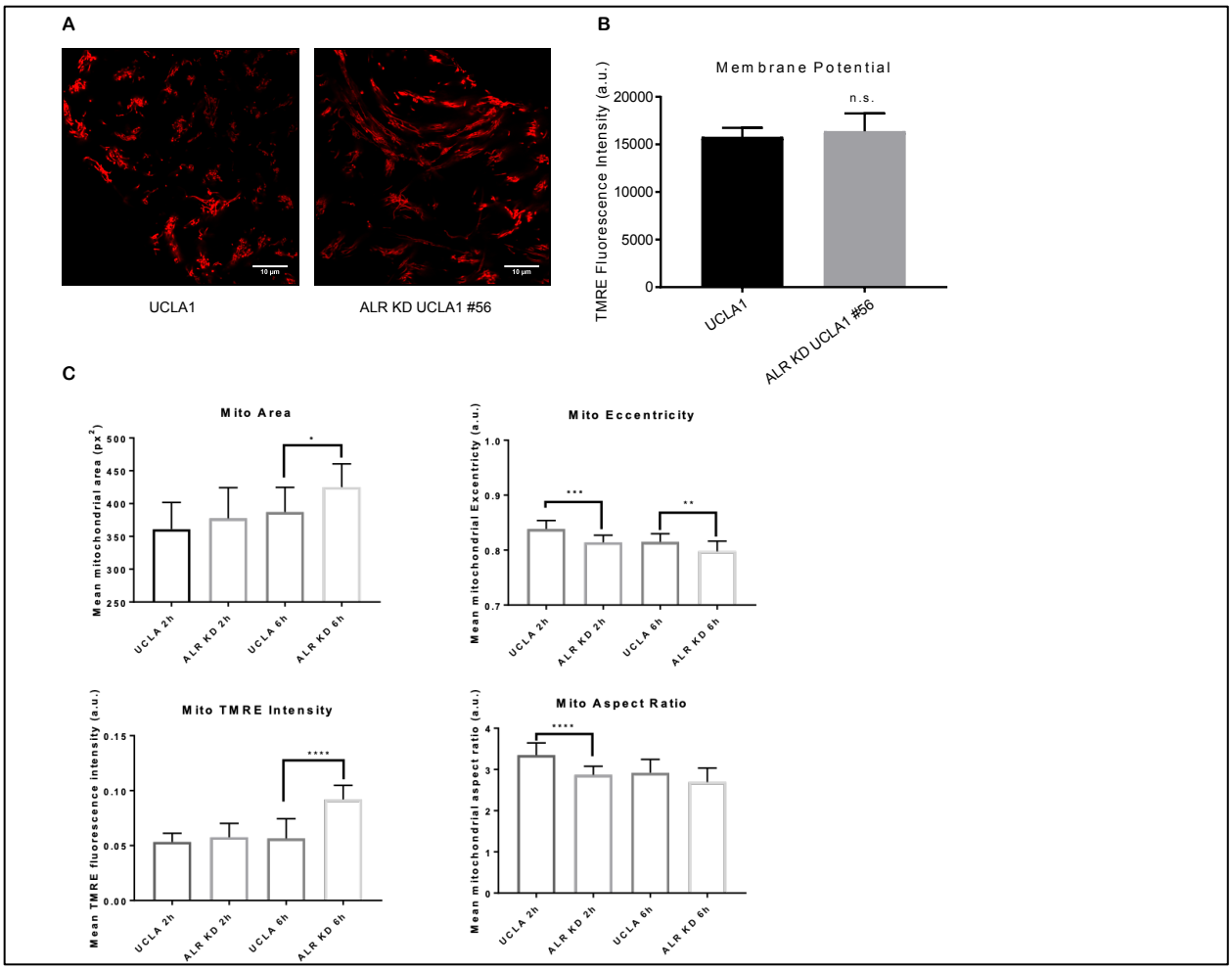

Figure S5-1 Mitochondrial membrane potential and morphology in hPSCs and ALR KD cells. (A) Live-cell super-resolution confocal imaging of UCLA1 and ALR KD UCLA #56 cells. Cells were stained membrane potential sensitive dye TMRE (red). Scale bar = 10 µm. (B) Quantification of TMRE mean fluorescence intensity from images shown in (A). ns $P > 0.05$ by Student's t-test. (C) Quantification of TMRE of UCLA1 and ALR KD UCLA #56 cells and hours of differentiation. Mitochondrial membrane potential, area, and morphology are quantified and analyzed.

Material and Methods

Cell Culture. hESCs (UCLA1, UCLA9, Line H1, Line H9, HSF-1) and hiPSCs (hIPS2, hIPS9) were passaged with Gentle Cell Dissociation Reagent (Stem Cell Technologies) onto feeder-free Matrigel (Thermo Fisher) in mTeSR1 (Stem Cell Technologies) or essential-8 (Thermo Fisher) medium and were maintained in hypoxic conditions (2-5%). HEK 293T were cultured on DMEM medium (10% FBS, 1% glutamax, 1% non-essential amino acids and 1% sodium pyruvate).

Lentivirus-mediated shRNA Knockdown. pLKO.1 vectors containing shRNA targeting SDHA RNA transcripts were purchased from Sigma-Aldrich (TRCN000028085 (shSDHA#1), TRCN000028043 (shSDHA#2), and TRCN000028093 (shSDHA#5). Vectors were transfected along with packaging vectors pCMV-dR8.9 and pCMV-VSVG into cells using Fugene HD (Promega). The next day sodium butyrate was added for 8h followed by addition of fresh media. To harvest lentivirus, media was collected 48h and 72h after transfection. Virus was concentrated using a Lenti-X Concentrator (Clontech) and suspended in OptiMEM (Life Technologies). For hESC transduction, colonies on matrigel were transduced with 25 µl of 1×107 TU/ml of viral particles and 7 µg/ml polybrene for 8h on day 1. Transduction was repeated on days 2, 4, and 5. Selection with 1µg/ml puromycin started on days 7-10 post first transduction.

Ectoderm, Mesoderm, and Endoderm Differentiation. hPSCs were incubated at room temperature for 15 minutes in Gentle Cell Dissociation Reagent (Stem Cell Technologies). With the addition of 10 µm ROCK inhibitor (Y-27632, BioPioneer) 2 x 105 cells/well were plated on a six-well plate with mTeSR1. For neural ectoderm differentiation, on the day after plating, daily

media was replaced with RPMI 1640 (Thermo Fisher) supplemented with 2% B27 supplement (Life Technologies), 1% N-2 supplement (Thermo Fisher), 10 μM SB431542 (Stemgent), 0.2 μM Dorsomorphin (Stemgent), 1% glutamax, and 1% MEM non-essential amino acids (Thermo Fisher). For mesoderm differentiation, protocol described in the STEMdiff™ Mesoderm Induction medium (Stem Cell Technologies) was followed. Endoderm differentiation was performed as previously described (D'Amour et al., 2005). Briefly, media was changed 1 day after plating (on day 0) to RPMI supplemented with 0.1% FBS (Omega), 1% glutamax (Life Technologies), and 100ng/ml Activin A (Life Technologies). Two days after plating (day 1), the concentration of FBS in the medium was increased to 2%. Treatment with NPA, dm-aKG, dms, FCCP, oligomycin, AOA, cyclo, or DCA was started on day 0 of differentiation and maintained in culture medium until cells were collected for analysis.

Flow Cytometry Analysis. Cells were incubated at room temperature for 15 minutes in Gentle Cell Dissociation Reagent (Stem Cell Technologies) then transferred into a conical vial. Cells were then centrifuged at 300 × g for 5 minutes at 4 C followed by wash with PBS. Supernatant was removed and pellet resuspended in BD Perm/Fix Buffer (BD Bioscience). Cells were incubated for 15 min on ice followed in BD Perm/Wash Buffer (BD Bioscience) with conjugated antibody for 45 min. Cells were then washed with 1BD Perm/Wash Buffer and resuspended in ice cold FACS buffer. Flow data collection was performed on either an LSRFortessa (BD Bioscience). Data analysis was done with FlowJo software (Treestar).

Mitochondria Isolation. Cells were collected and homogenized in 20 mM HEPES pH 7.6, 220 mM mannitol, 70 mM sucrose, 2 mg/ml BSA, and 0.5 mM PMSF. Lysates were dounced with

Teflon douncer. Homogenates were centrifuged at 770 x g at 4ºC for 5 minutes. Post-nuclear supernatants were centrifuged at 10,000 x g for 10 minutes to obtain mitochondria pellets. Pellets were further washed with homogenization buffer without BSA. Protein concentrations were determined using BCA assay (Thermo Scientific).

DHE Staining. Cells were washed with growth media without phenol red and incubated with 30 μM fluorescent dye dihydroethidium (DHE, Thermo Fisher Scientific) in a 37 °C, CO_2 incubator for 1 hour. Staining solution was replaced with growth media without phenol red before imaging. Digital images were captured, and the red fluorescence intensity was quantified by using NIH ImageJ software. ROS levels are expressed as the rate of DHE oxidation in %/sec normalized to the unoxidized probe.

Seahorse Measurement. Oxygen consumption rate (OCR) was performed as previously described[23]. hPSCs were plated onto an XF24 microplate (Seahorse Bioscience) at 105 cells/well or 106 cells/well with 10 μM Y-27632 (BioPioneer). The next day, 1h prior to the assay, the medium was changed to XF Media (Seahorse Bioscience) supplemented 17.5 mM glucose. Cell metabolic rates were measured using an XF24 Extracellular Flux Analyzer (Seahorse Bioscience). Basal respiration was determined by quantifying OCR prior to and after the addition of 1 μM rotenone (Sigma) and 1 μM antimycin A (Sigma).

Fluorescence Confocal Microscopy. To measure membrane potential, cells were incubated with 15 nM Tetramethylrhodamine Ethyl Ester Perchlorate (TMRE) (Thermo Fisher Scientific, Roskilde, Denmark) for 1 h. Cells were imaged in presence of TMRE in regular culture media. Image analysis was performed in ImageJ.

2D- Diagonal gel electrophoresis. Mitochondria (5 mg/ml) were solubilized with 20 mM Hepes-KOH, pH 7.4, 10% glycerol, 50mM NaCl, 1mM EDTA, and 2.5 mM MgCl2 supplemented with 1% (w/v) digitonin and protease inhibitors. Lysates were resolved in the first dimension on a non-reducing SDS gel. Individual lanes isolated with a razor blade, were soaked in 1% (wt/vol) SDS, 1% (vol/vol) β-mercaptoethanol for 30 min at 50^{o}C, embedded in a 4% stacking gel, and resolved in the second dimension by SDS-PAGE.

References

1. Angelos, M. G. & Kaufman, D. S. Pluripotent stem cell applications for regenerative medicine. *Current Opinion in Organ Transplantation* vol. 20 663–670 (2015).
2. Chatterjee, T., Sarkar, R. S., Dhot, P. S., Kumar, S. & Kumar, V. K. Adult stem cell plasticity: Dream or reality? *Med. J. Armed Forces India* **66**, 56–60 (2010).
3. Odorico, J. S., Kaufman, D. S. & Thomson, J. A. Multilineage Differentiation from Human Embryonic Stem Cell Lines. *Stem Cells* **19**, 193–204 (2001).
4. Takahashi, K. & Yamanaka, S. Induction of Pluripotent Stem Cells from Mouse Embryonic and Adult Fibroblast Cultures by Defined Factors. *Cell* **126**, 663–676 (2006).
5. Csobonyeiova, M., Polak, S., Koller, J. & Danisovic, L. Induced pluripotent stem cells and their implication for regenerative medicine. *Cell and Tissue Banking* vol. 16 171–180 (2015).
6. Fujikawa, T. *et al.* Teratoma formation leads to failure of treatment for type I diabetes using embryonic stem cell-derived insulin-producing cells. *Am. J. Pathol.* **166**, 1781–1791 (2005).
7. Tan, H. L., Fong, W. J., Lee, E. H., Yap, M. & Choo, A. mAb 84, a cytotoxic antibody that kills undifferentiated human embryonic stem cells via oncosis. *Stem Cells* **27**, 1792–1801 (2009).
8. Jung, J. *et al.* Ablation of tumor-derived stem cells transplanted to the central nervous system by genetic modification of embryonic stem cells with a suicide gene. *Hum. Gene Ther.* **18**, 1182–1192 (2007).
9. Cheng, F. *et al.* Protecting against wayward human induced pluripotent stem cells with a

suicide gene. *Biomaterials* **33**, 3195–3204 (2012).

10. Dabir, D. V. *et al.* A small molecule inhibitor of redox-regulated protein translocation into mitochondria. *Dev. Cell* **25**, 81–92 (2013).

11. TeSlaa, T., Setoguchi, K. & Teitell, M. A. Mitochondria in human pluripotent stem cell apoptosis. *Semin. Cell Dev. Biol.* **52**, 76–83 (2016).

12. Liang, R. & Ghaffari, S. Stem cells, redox signaling, and stem cell aging. *Antioxidants Redox Signal.* **20**, 1902–1916 (2014).

13. Wang, Q. & Zou, M. H. Measurement of reactive oxygen species (ROS) and mitochondrial ROS in AMPK knockout mice blood vessels. in *Methods in Molecular Biology* vol. 1732 507–517 (Humana Press Inc., 2018).

14. Effects of N-acetylcysteine on acetaminophen covalent binding and hepatic necrosis in mice - PubMed. https://pubmed.ncbi.nlm.nih.gov/3973835/.

15. Trnka, J., Blaikie, F. H., Smith, R. A. J. & Murphy, M. P. A mitochondria-targeted nitroxide is reduced to its hydroxylamine by ubiquinol in mitochondria. *Free Radic. Biol. Med.* **44**, 1406–1419 (2008).

16. Bihlmaier, K. *et al.* The disulfide relay system of mitochondria is connected to the respiratory chain. *J. Cell Biol.* **179**, 389–395 (2007).

17. Zhang, J. *et al.* UCP2 regulates energy metabolism and differentiation potential of human pluripotent stem cells. *EMBO J.* **30**, 4860–4873 (2011).

18. Todd, L. R. *et al.* Growth Factor ero1-like Modulates Drp1 to Preserve Mitochondrial Dynamics and Function in Mouse Embryonic Stem Cells. *Mol. Biol. Cell* **21**, 1225–1236 (2010).

19. Petrungaro, C. *et al.* The Ca2+-dependent release of the Mia40-induced MICU1-MICU2 dimer from MCU regulates mitochondrial Ca2+ uptake. *Cell Metab.* **22**, 721–733 (2015).

20. Zhang, J. *et al.* Metabolism in Pluripotent Stem Cells and Early Mammalian Development. *Cell Metab.* **27**, 332–338 (2018).

21. Lu, V. *et al.* Mitochondrial metabolism and glutamine are essential for mesoderm differentiation of human pluripotent stem cells. *Cell Res.* **29**, 596–598 (2019).

22. Chen, K. *et al.* CBARA1 Plays a Role in Stemness and Proliferation of Human Embryonic Stem Cells. *PLoS One* **8**, 1–8 (2013).

23. Zhang, J. *et al.* Measuring energy metabolism in cultured cells, including human pluripotent stem cells and differentiated cells. *Nat. Protoc.* **7**, 1068–1085 (2012).

Appendices

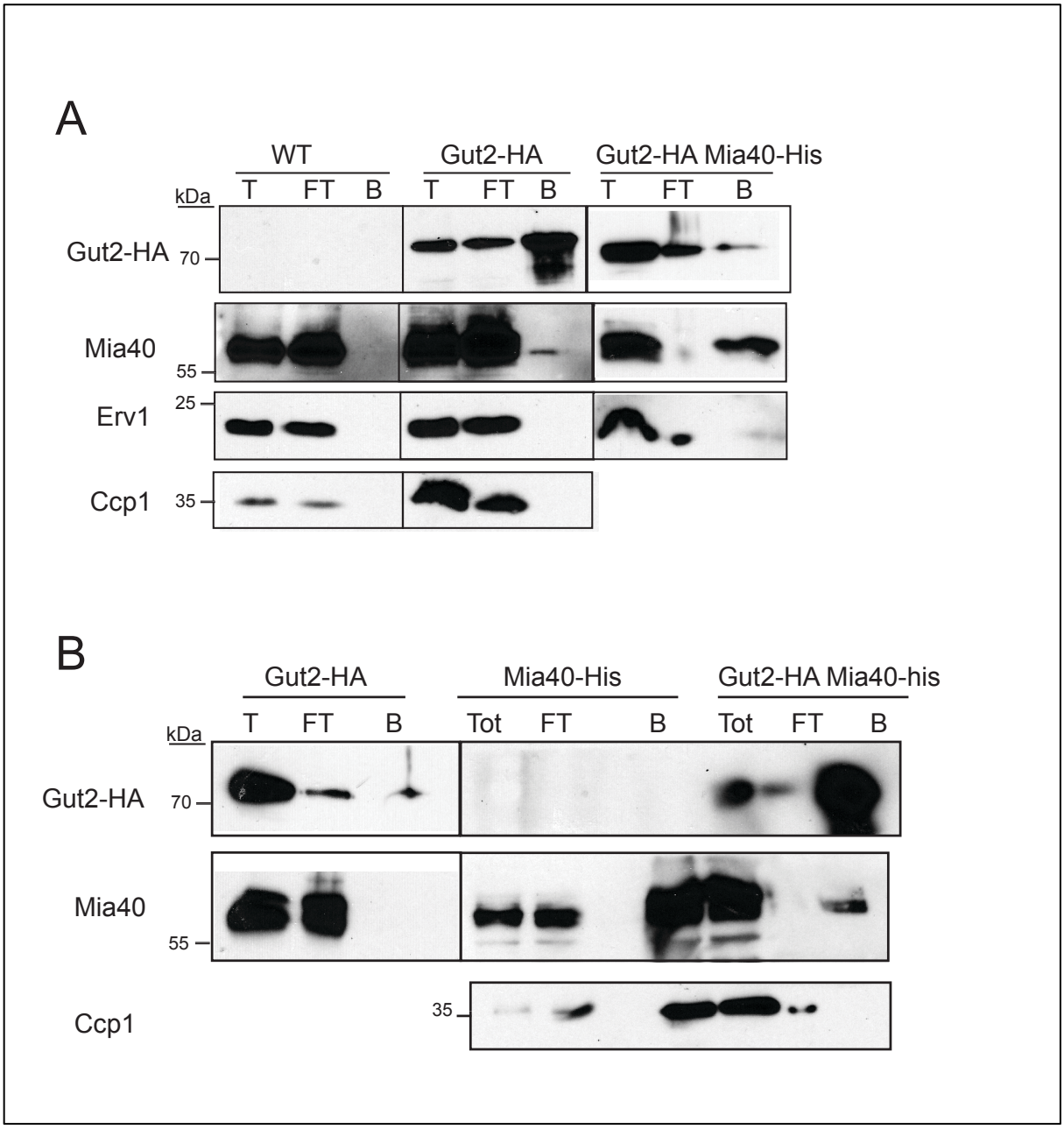

Appendix A. Gut2 binds to Mia40. (A) Mitochondria from WT, a strain expressing a C-terminal HA tagged Gut2 (Gut2-HA), or a strain expressing both C-terminal HA tagged Gut2 and C-terminal His tagged Mia40 (Gut2-HA Mia40-His) were solubilized in 1% digitonin. As a

control, 25 µg of total extract (T) was withdrawn, and 500 µg lysate was incubated with anti-HA magnetic beads. The beads were washed, and bound protein (B) was eluted. 25 µg of the flow-through fraction (FT) was also included. Samples were resolved by SDS-PAGE and analyzed by immunoblotting with specific antibodies against HA, Mia40, Ccp1, Erv1, and Ccp1. (B) As in (A), except that mitochondria from a strain expressing a C-terminal histidine tagged Mia40 (Mia40-His) was also included. Lysate was incubated with Ni^{2+}-agarose beads.